Study of Morphology Effect on Polydopamine-based Adsorbents for Dye Removal

by

Haotian Wu

A dissertation submitted to the Graduate Faculty of
Auburn University
in partial fulfillment of the
requirements for the Degree of
Doctor of Philosophy

Auburn, Alabama
December 10, 2022

Keywords: Polydopamine, Adsorbents, Morphology,
Dye Removal, Adsorption Performance

Approved by

Dr. Edward Davis, Chair, Associate Professor, Department of Materials Engineering
Dr. Bart Prorok, Professor, Department of Materials Engineering
Dr. Pengyu Chen, Associate Professor, Department of Materials Engineering
Dr. Xinyu Zhang, Professor, Department of Chemical Engineering
Dr. Bryan Beckingham, Associate Professor, Department of Chemical Engineering

Abstract

Dyes are one of the most hazardous materials in industrial wastewater, which poses severe problems to the humans and ecosystem. Adsorption is a promising technique for dye removal because of its low cost, high efficiency, and facile operation. With the rapid development of nanotechnology, micro/nano-scale functionalized polymers have been developed as adsorbents for the remediation of dye-contained water.

Polydopamine (PDA) is a mussel inspired synthetic eumelanin polymer, which could be obtained by a facile self-polymerization of dopamine (DA) at room temperature in alkaline condition. It has received tremendous attention due to its striking properties, such as adhesion capability, high reactivity, photothermal conversion capability and biocompatibility. These properties make PDA a promising material that is widely applied in biological, energy, environmental and catalyst fields. Owing to its strong adhesion property and presence of abundant catechol, amine, and imine functional groups, which are conducive to binding metal ions, organic molecules and functional polymers, PDA has been considered as a promising candidate for wastewater remediation. However, the adsorption capacity of PDA-based adsorbent is too low to meet the demand for practical application due to the presence of different types of dyes in co-contaminated wastewater. Additionally, controllable morphology of PDA could be achieved by varying synthesis approaches, which results in different surface properties. Therefore, morphology can affect the adsorption performance and mechanism of PDA-based adsorbents. Accordingly, the main objectives of this work are constructing PDA-based adsorbent for dye removal with good adsorption performance and investigating the morphology effect on PDA-based adsorbents.

In the first project (Chapter 2), PDA-based adsorbents with different morphology, including nanotubes, hollow spheres, and mesoporous structures were prepared by utilizing the self- polymerization of DA, co-precipitation of magnetic particles, and the crosslinking reactions with polyethyleneimine (PEI). The obtained adsorbents

exhibited desirable morphology with good magnetic properties with the high saturation magnetization value of 28.9 emu g^{-1} and large specific surface area of 158.1 m^2 g^{-1}.

The second project (Chapter 3) exploits the promising application of these adsorbents obtained in Chapter 2 for dye remediation. Methylene blue (MB) and methyl orange (MO) are used as two model dyes. The kinetics study showed the adsorption dynamics conforms pseudo-second-order kinetics model. And the dye adsorption equilibrium data were fitted well to Freundlich isotherm model for two dyes. Besides, the prepared adsorbents exhibited a good adsorption capacity for MB and MO with maximum adsorption capacity of 156.2 and 255.7 mg g^{-1}, respectively. The thermodynamic study indicated that the adsorption process of cationic and anionic dyes onto the prepared adsorbents were spontaneous and endothermic. Moreover, these adsorbents exhibited excellent regeneration properties after five adsorption/desorption cycles for both cationic and anionic dyes.

To the best of our knowledge, very few studies have been reported to develop PDA-based adsorbents with desirable adsorption performance for both cationic and anionic dyes. The PDA-based adsorbents prepared in this work possessed good adsorption capacity for both cationic and anionic dyes, which also can be quickly magnetic separated and regenerated, showing the potential applications for dye remediation.

Acknowledgements

I owe immense gratitude to those who have helped me during my time at Auburn University.

First and foremost, I would like to express my deepest respect and gratitude to my advisor Dr. Edward Davis for his guidance, support, and encouragement throughout my PhD study. Without him, this dissertation would not be possible. I am also grateful to my committee members, Dr. Bart Prorok, Dr. Pengyu Chen, and Dr. Xinyu Zhang for their valuable advice, insightful comments, and inputs on my research. I would also like to thank Dr. Beckingham for serving as my university reader.

I would like to thank Dr. Michael Miller, Dr. Cheryl Colquhoun, Mr. Steve Moore, Dr. Martin Mougrial, and Delaney Clouse for providing guidance on sample characterization.

I would like to thank my lab mates, Yuzhe Sun and Leyton Janowsky for their help and support in lab. Thanks to my friends, Tong Sheng, Chennan Xue, Chengyun Miao, Qifan Zeng, Mingyu Qiao, and Yuan Tian, for offering me help during my time at Auburn.

At last, I am very grateful to my parents Yanlong Wu and Yingjie Ma for their endless love, support, and encouragement throughout these years.

List of Figures

List of Tables

List of Abbreviations

DA	Dopamine
PDA	Polydopamine
PEI	Polyethyleneimine
HNT	Halloysite Nanotube
PDA-NT	Polydopamine Nanotube
HPDA	Hollow Polydopamine
MPDA	Mesoporous Polydopamine
MB	Methylene Blue
MO	Methyl Orange
TMB	1,3,5-Trimethylbenzene
DI	Deionized
NPs	Nanoparticles
MNPs	Magnetic Nanoparticles
FT-IR	Fourier Transform Infrared Spectroscopy
TEM	Transmission Electron Microscopy
VSM	Vibrating Sample Magnetometer
DLS	Dynamic Light Scattering
BET	Brunauer-Emmett-Teller
UV-Vis	Ultraviolet-Visible
PFO	Pseudo-first-order
PSO	Pseudo-second-order

Table of content

1. Chapter 1 Introduction

Water connects every aspect of life, so it is one of the most essential goals to get a dependable access to clean water source, which remains a major global challenge. Due to the massive development of modern economy, the expansion of cities, industries, and the growth of population, the wastewater quantity is increasing at equal proportion. However, the current water and wastewater treatment infrastructure are reaching their utmost to meet the demand of both human and environment for sufficient clean water. Thus, the remediation of dye-containing water urgently calls for developing upgrading water treatment approaches.

Among the polluters of fresh water, various dyes which are widely used in industrial field, such as textiles, food, pharmaceutical, printing, rubber and plastics, posing one of the major contributors to wastewater sources due to massive discharge of wastewater.[1] From the data reported, more than 100,000 commercial dyes are known with an annual production of over 7×10^5 tons per year and about 100 tons per year of dyes are discharged into water streams.[2] Besides, the water-soluble colorants are more than unaesthetic, as they are harmful to ecologies, biological organisms due to mutagenic and teratogenic effect and cause serve damage to human health including kidney, central nerve and reproductive system, carcinogenic, mutagenic and allergic effects. [3]

Due to both environmental and health concerns about the dye-laden water, research interests in developing technologies via physical, chemical, and biological approaches for the remediation of dye-containing effluents have been increasing in these years. And some of these technologies have already been applied in practical industrial wastewater treatment. Ultrafiltration,[4] nanofiltration, [5] and reverse osmosis[6] are most commonly used filtration technologies in dye removal. While the lack in reusability of membrane, and high energy consumption due to the high pressure applied in filtration process leads to high costs.[7] For electrochemical treatments,[8] much higher consumption of electricity will result in high costs. Oxidation utilize substances with

strong oxidizing capabilities, such as hydrogen peroxide,[9] Fenton's reagent, [10] and ozone[11] to achieve the degradation of dye. However, the undesirable or toxic byproducts will form during the degradation process limits its application. Major drawback of the above technologies is the high costs. Compared to the strategy mentioned above, adsorption has gotten a lot of attention due to its superiorities, such as low cost, highly-efficiency against wide range of pollutants, lower toxic byproducts formation, facile design and ease in operating. Which utilize adsorbents to grasp the water-soluble contaminant, including dyes in industrial wastewater.

Nanotechnology, since it was first proposed in 1959, has drawn tremendous interest on the development and application of nanomaterials. The advances in nanotechnology arrived in the past decades create opportunities for applying nanomaterials in water remediation due to their large surface area and high reactivity. However, conventional separation methods such as filtration and high-speed centrifugation are time-consuming and uneconomical for the separation of nano-sorbents. Therefore, magnetic nanoparticles were introduced to overcome these problems since they could be easily separated from the water after adsorption by the applied magnetic field, which has been proved to be an easy and economical approach.[12] Recently, mussels inspired polydopamine (PDA) has attracted strong interest as a biomimetic polymer and a universal surface modification agent for various materials with a broad range of applications,[13,14] PDA-incorporated hybrid nanoparticles have already been developed as nano-adsorbents for dye removal.[15,16]

In view of various adsorbents have been developed and applied in adsorption technique to remove dye stuff in wastewater, the introduction will be divided in the following two sections. At first, the mechanism of adsorption and the recent development of adsorbents will be reviewed. Then, the application of polydopamine materials in dye removal is introduced.

1.1 Adsorption

Adsorption is a mass transfer process and the substances would assemble around the interface of the two similar or different phases, and in dye removal process it is

usually solid-liquid systems, the adsorbents could provide adsorption sites for the adsorbate (dye stuff molecules) to accumulate on their surface, once the adsorption sites is saturate for no more adsorbate to adsorb or all the dye molecules have already been adsorbed, it will reach a dynamic equilibrium. Adsorption is an exceptional dye removal technique among diverse dye methods in terms of its capability to remove almost all kinds of dye stuff[17-19] in wastewater effluent and easy in operation. Moreover, no pretreatment is need and it could be employed as post-treatment in some cases to achieve the completely elimination of residue dye stuff after using other dye removal methods. Besides, there is no generation of toxic or hazardous by-product or residues after adsorption process.[18,20] The adsorption of dyes on adsorbents mainly attribute to electrostatic, π-π interactions, van der Waals forces, hydrogen boding, hydrophobic, and acid-base reactions.[21] The critical obstacle of adsorption technique is that this method requires adsorbents which may of high cost, so developing economical and efficient adsorbents is highly considered.

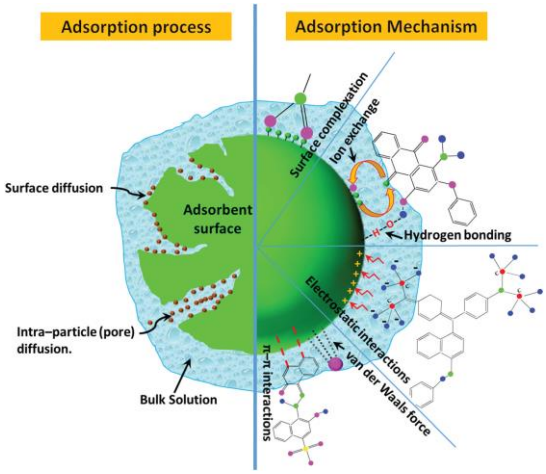

Figure 1.1 Adsorption process and mechanisms for dye removal.[21]

1.1.1 Key factors for adsorption of dye

Many factors affect adsorption of dye such as solution pH, temperature, initial dye concentration and dosage of adsorbents. In terms of practical application, optimizing these factors is conducive to the development of adsorbents for industrial-scale dye-laden wastewater treatment, all these factors effect will be discussed below.

1.1.1.1 PH

The solution pH play an important role in the adsorption process, as the variation of pH will result in the change in surface properties of adsorbents and the degree of ionization of adsorptive molecule.[22] Normally, low pH will benefit the removal efficiency for anionic dye and higher pH will promote the removal of cationic dyes.[23] The point of zero charge (pH_{pzc}) is a necessary parameter to study the adsorption mechanism and the adsorption ability. When pH is above $pH_{pzc,}$ cationic dye adsorption is preferred because of the existence of functional groups such as -OH. In contrast, when pH is below pH_{pzc}, anionic dye adsorption is preferred due to the positively charged surface of adsorbents.[24]

1.1.1.2 Initial dye concentration

The influence of initial dye concentration is also related to the number of adsorption sites on the surface which have common effect on the adsorption kinetic. Generally, when there are redundant adsorption sites on the surface of adsorbents, increasing initial dye concentration will enhance the driving force of mass transfer and thus the removal percentage will increase. However, if the adsorption sites on the surface of adsorbents are saturated, the removal percentage would decrease with increase of initial dye concentration.[25]

1.1.1.3 Temperature

Temperature is usually studied to determine the adsorption process is exothermic or endothermic.[25]If the interactions between dye molecule and the adsorption sites of adsorbents decrease with increasing temperature, the adsorption is an exothermic process.[26] Whereas, if the adsorption percentage increase with temperature, the adsorption is an endothermic process, as increasing temperature will accelerate the motion of dye molecule and facilitate the interaction between dye molecules and active sites.[27]

1.1.1.4 Dosage of adsorbents

Normally, when increasing the mass of adsorbents, the removal efficiency will increase since more adsorption sites are provided. The minimum demand of adsorbents required for the removal of dyes will be determined by studying thew amount effect of adsorbents. And then, the adsorbent could be evaluated in view of economical application in practical dye removal process.[23]

1.1.2 Adsorbents developed for dye removal

At present, various adsorbents such as activated carbon, bio-sorbents, agriculture/industrial waste, clays polymer-based adsorbents, and nanomaterials have been reported in applying as adsorbents for the dye removal in many works.

1.1.2.1 Activated carbon

Activated carbon is one of the most widely used and well-known adsorbents for wastewater treatment. The high removal efficiency of activated carbon for various dyes allows it to be a good candidate as adsorbents.[7] While, there are some drawbacks that limit its application, such as the cost is high, difficult to regenerate[28,29] and ineffective and show poor selectivity for vat dyes.[30] In this case, many novel adsorbents were developed as alternatives for dye removal application, which will be briefly introduced in the following part.

1.1.2.2 Bio-sorbents

Chitosan (CS) and derives have been developed as adsorbents mainly due to two excellent advantages, one is its low cost since it is abundant exist in natural, another is its outstanding chelation behavior. Due to the numerous exist functional groups such as amino and hydroxyl, and the advantages of hydrophilic, biocompatible and biodegradable properties allowing chitosan to be a promising adsorbent for dye removal. The adsorption of dyes is realized the protonation of amino group on the surface which could bind cationic dye via electrostatic interaction. However, there still drawbacks that limits its application in practical applications, such as many chitosan-based adsorbents

could not be used in acidic condition, weak mechanical properties. Thus, some modification strategies have been done to solve these problems.

Guo[31] reported the CS-PDA aerogels that prepared via DA polymerization and glutaraldehyde as crosslinking agent. Most noteworthy is using the free-drying method to treat the chitosan bead, which could significantly increase the surface area and the pore size is higher after the introduction of PDA. Besides, surface modification of aerogels with glutaraldehyde could enhance the stability and acid resistance of aerogels. As the hydroxyl and amine groups existing on CS-PDA could easily protonated in water and generate strong electrostatic interaction with negatively charged dye molecules. And the adsorption capacity of methyl blue (MB) and rhodamine b (RB) were tested to be 734.4 and 495.3 mg g^{-1}. Halloysite nanotubes (HNTs) was also introduced into chitosan to enhance the mechanical property, Peng[32] developed CS-HNTs hydrogel beads by dropping and pH-precipitation method, the thermal stability, adsorption efficiency and adsorption capacity are significantly enhanced comparing with pure CS beads And the reusability of the bead could be realized via desorbing by NaOH and acetone.

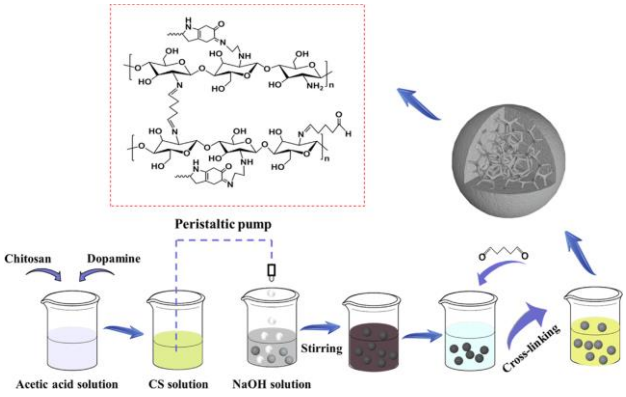

Figure 1.2 The preparation of PDA-modified-chitosan aerogel. [31]

Cyclodextrins (CDs) are another widely used bio-sorbent for dye removal. Due to the hydrophobic cavity, it could trap molecules with certain polarity and size through host-guest interactions.[33] Wang[34] prepared Fe_3O_4/β-CD/GO nanocomposites which were used in the removal of malachite green, this adsorbent exhibits excellent

adsorption ability and regeneration properties, as the adsorption capacity of 990.10 mg g^{-1} at 45°C and pH 7, and the capacity could still retain at 80% after five cycles.

1.1.2.3 Agricultural solid wastes

As agricultural solid wastes are abundant exist around the world and they generally contain numerous functional groups such as hydroxyl, amino, carboxyl which could allow them to interact with dye molecules via hydrogen bonding and ion exchange. Sawdust and bark, which are by-product of wood and timber industry have already been reported as adsorbents for dye removal.

Khan prepared Fe_2O_3/chitosan-bamboo sawdust composites, and the capacity of acid dye bromothymol blue could reach 217.39 mg g^{-1} in only 30 min and could be magnetically recovered. Ozacar[35] utilized pine sawdust to remove metal complex dyes, after some simple pretreatment such as boil, wash and sieved, the pine sawdust show good adsorption capacity which are 290.3 and 398.8 mg g^{-1} for metal complex blue and metal complex yellow. Demarchi[36] reported the removal of three cationic dyes including methylene blue (MB), crystal violet (CV) and RB from aqueous solution by a bark generated through medicinal plant processing. The maximum adsorption capacities were calculated to be 89.5, 69.4 and 211.5 mg g^{-1} respectively.

1.1.2.4 Industrial by-products

Many industrial by-products such as metal hydroxide sludge, fly ash and red mud are low cost and abundant available, which could be used as substitutes for the replacement of costly conventional adsorbents.

Metal hydroxide sludge is a kind of industrial by-product contains metal hydroxides and salts, which are used as adsorbents for dyes through ion exchange. Gunes[37] investigated an industrial waste sludge including Al(III) hydroxides to adsorb reactive dye reactive blue 222, and many parameters have been studied, the amount of dye adsorbed increased with agitation time and reach equilibrium in 90 min. The adsorption capacity was calculated to be 18.38 mg g^{-1} according to the Langmuir model. Fly ash is industrial wastes that generated in large amount during the burning process.

However, fly ash contains hazardous substance including heavy metals.[38] Zhang[39] prepared coal fly ash/$CoFe_2O_4$ magnetic composite via hydrothermal method. The adsorption capacity of this material for the removal of malachite green was calculated to be 89.3 mg g^{-1} and the adsorbents could be regenerated by thermal and microwave treatment. Red mud is another industrial by-product that used for dye removal, which is a bauxite processing residue discarded in Alumina production. The dye removal of red mud is achieved through ion exchange. Gupta[40] reported the removal of RB, fast green and MB from water by red mud, and the removal percentage were 92.5, 94.0 and 75.0, respectively. And the removal percentage will up to 95-97% in column experiments at 0.5 ml min^{-1} flow rate. Besides, the adsorption process was found to be exothermic in nature.

1.1.2.5 Clays/Zeolites

Clays and zeolites are hydrous aluminosilicates with layered structure.[41,42] The surface chemistry on the surface of clays including the structure, ion exchange capacity, specific surface area and reactivity of the surface contribute to the adsorption process. The main mechanism of clays and zeolites removal for dyes is dependent on the exchangeable ions on their surface,[43] and could then adsorb cations or anions via ion exchange and adsorption.[18]Though clays and zeolites have been proved to exhibit excellent adsorption capacity for dye removal, there still some drawbacks of these materials. As the clays show negative charge, they usually show low adsorption capacity for acid dye.[44]Moreover, since clays have hydrophilic surface which could well dispersed in aqueous solution, it is time and energy consuming for the regeneration of adsorbed clays adsorbents. Besides, the hydrophilic surface and low organic carbon content of clays lead to their low adsorption efficiency for nonionic dyes in aqueous solution.[45] Many modification methods have been reported to introduce alien material into clay substrate in order to improving the adsorption capacity for dye removal.

Chen[46] prepared anion-cationic, anionic, and cationic surfactants modified montmorillonite by introducing cationic surfactant cetyl trimethyl ammonium bromide (CTMAB), anionic surfactants sodium stearate (SSTA) and their complex to MMT. The

results show that CTMAB/10SSTA-MMT has higher adsorption capacity compared to CTMAB-MMT and 10SSTA-MMT, which is contribute to the formation of a highly effective partition medium by anion-cationic surfactant micelle.

Makarchuk[47] reported the synthesis of magnetic content incorporated saponite clays with different amount of magnetite (2-7 wt %) through a simple impregnation method. They find that the specific surface area increased two times compared with pure saponite, which is due to the formation of Fe_3O_4 layer in nano scale on the surface of the saponite clay pores results in the microporous and mesoporous structure. Moreover, the removal efficiency and adsorption capacity are both increased by several times comparting with pure saponite.

Zeolites have highly porous structure and negatively charges, and the adsorption mechanism of dyes is due to the ion exchange properties and the high specific surface area also contribute to its dye removal capacity. Armagan[48] investigated the modification of zeolites to enhance its removal capacity for reactive dyes. After surface modified with quaternary amines, the adsorption capacity of Reactive red, yellow, and black are 111, 89 and 61 mg g^{-1}, respectively, which is comparable to activated carbon.

1.1.2.6 Nanomaterials

Nanotechnology has been rapidly developed over the past few decades, and nanomaterials been applied in various field including water treatment.[49] Here, carbon nanotubes (CNTs) and halloysite nanotubes (HNTs) are mainly introduced due to their tube-like structure with large surface area and adjustable functional groups.

There are two types of CNTs, single walled carbon nanotubes (SWCNTs) and multiwalled carbon nanotubes (MWCNTS). Though pure CNTs have shown good adsorption capacity for dye removal,[50] the separation of CNTs from the aqueous solution is quite complicated. In this case, some alien materials could be introduced to address this issue, such as magnetic particles, GO and chitosan etc.[51]

Wang[52] firstly developed magnetically separable graphene-CNTs via a solvothermal method using graphene, MWCNTs and Fe_3O_4 nanoparticles. They found

that the maximum adsorption capacity of MB was up to 65.79 mg g^{-1}. Moreover, the regeneration of the adsorbents could be easily achieved by washing with acidic ethanol, and well separated by external magnetic field. Hossein[53] prepared MWCNT functionalized with chitosan and poly-2-hydroxyethyl methacrylate (pHEMA) and the adsorption behavior of methyl orange (MO) on the synthesized composites was investigated. The composites exhibited excellent adsorption capacity of 306 mg g^{-1}. And the adsorption thermodynamic result indicated the adsorption process was endothermic.

HNTs also has a tubular structure with negatively charged external surface and positively charged internal surface in the pH range of 2-8.[54] Also, it is abundant exist in nature, which is more economical comparing with CNTs. These specific properties make HNTs a good candidate in adsorption for dye removal. Same with CNTs, some functional groups need to be incorporated to enhance the adsorption capacity and facilitate the regeneration of adsorbents.

Liu[55] reported the HNT@ reduced graphene oxide (rGO) (HGC) composite prepared via an electrostatic assemble process. The outer surface of γ-aminopropyl triethoxysilane (APTES) treated HNTs (APHNTs) was converted into positive charge under acid conditions. So that positively charged APHNTs could be combined with negatively charged rGO sheets through electrostatic force. The adsorption capacity is significantly improved comparing with rGO and HNTs. Due to the abundant exist of rGO, HGC also proved to be an excellent electrode material in supercapacitors. Zou[56] prepared HNTs supported Ag nanoparticles using tea polyphenols (TPs) as reductant. The HNTs were pretreated by N-β-aminoethy-γ-aminopropyl trimethoxysilane (AEAPTMS) to introduce amino groups and binding AgNPs on their surface. The synthesized AgNPs@ N-HNTs catalyst showed excellent photocatalytic activity for the degradation of MB.

Wan[57] developed a core@double-shell structured magnetic HNTs, which was synthesized by a combination of mussel-inspired method, co-precipitate method and modified mussel-inspired co-modification. The well-defined core/double-shell

structured HNTs/Fe_3O_4/poly (DA+KH550) nanohybrids were proved to be of high surface area, and the abundant active adsorption sites on its surface could improve the adsorption capacity of MB, which is 689.66 mg g^{-1} at 25°C. And the removal efficiency retained around 89% after five cycles. Moreover, the adsorbents could be easily separated after MB removal by applying an external magnetic field.

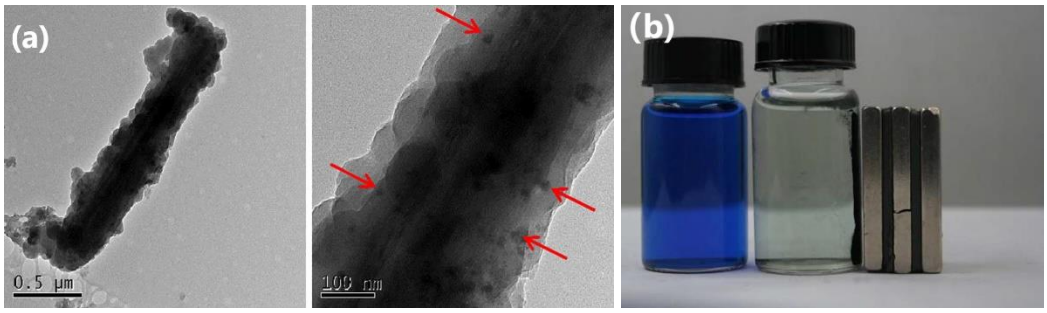

Figure 1.3 (a)TEM images of HNTs/Fe_3O_4/poly(DA+KH550) nanohybrids; (b) separation of core@double-shell structured HNTs/Fe_3O_4/poly(DA+KH550) nanohybrids from MB solution by a magnet.[57]

1.1.2.7 MOFs

Metal organic frameworks (MOFs) are a new class of crystalline organic-inorganic hybrid solids. The porous structure and high surface area will facilitate adsorption of dye.[58] And the adsorption is achieved via the electrostatic interaction between charged sites of MOFs and ionic dye.

Haque[59] investigated the adsorption capacity of MOF-235 for Methyl Orange (MO) and MB from simulated wastewater. The maximum adsorption capacity was 477 and 187 mg g^{-1}, which were significantly improved comparing with activated carbon. However, the synthesis process of MOFs is quite complicated, and the cost of MOFs is high. Thus, developing less cost and facile methods for the preparation of MOFs is highly considered for its application in large scales.

1.2 Polydopamine as a dye removal material

As organic dyes take up a large proportion of the industrial hazardous emissions that that directly discharged to environment, and these dyes are harmful to both human body and biological organism since they are highly toxic and hard to degrade. Hence, it is necessary to develop advanced materials to meet the requirement for dye removal. To improve the performance of dye removal capacity, various polymers have been explored, such as polyacrylamide, polyaniline, polypyrrole, polyethylene glycol.

Dopamine, which is inspired by the adhesion of the foot protein secreted by mussel, could be used to synthesis polydopamine (PDA), and this is firstly reported by Messersmith et al in 2007. Due to the abundant functional groups in polydopamine such as catechol and amino, PDA thin film can be adhered to the surface of virtually any substrate, such as metals oxides, ceramics and synthetic polymers.[60] This evenly distributed PDA thin film could be facile prepared via a dip-coating process, by simply immersing the substances into an alkaline aquatic solution. Furthermore, the functional groups also contribute to PDA serving as a platform for modification and functionalization. Thus, PDA is a promising material for dye removal, for which introducing plenty of functional groups would be easy to implement.

1.2.1 Preparation, structure and adhesion properties of PDA

1.2.1.1 Preparation of PDA

Typically, PDA thin film could be obtained through a spontaneously self-polymerization process under alkaline (pH>7.5) involving oxygen as the oxidant, besides for coating PDA on substrates, the concentration of dopamine should be higher than 2 mg mL^{-1}.[61] Despite the above-mentioned PDA film pristine method has many advantages such as it is facile as a one-step dip-coating process, suitable for virtually all substrates and provides a versatile platform for secondary reactions, it still has some limitations. For example, since the polymerization of dopamine needs alkaline condition, it could not be applied to the materials that may not alkali resistance. Besides, the coating process is time-consuming, usually takes several hours or even tens of hours to form an even thin film on the surface of most materials. Some efforts have been made

to enhance the dopamine oxidation kinetics, such as increasing oxygen concentration [62,63] or dopamine concentration,[64] but the aforementioned problems could not be completely settled.

In order to solve the problems, introducing additional reagents is a good option. Generally, the reagents are oxidants[65,66] including ammonium persulfate, sodium periodate and potassium chlorate and catalyst such as biocatalyst laccase. The addition of oxidants and catalyst will promote the deposition kinetics of PDA and then polymerization of dopamine conduct under neutral and acidic environment. Other than these strategies, PDA film could be formed through electrochemical copolymerization.[67] This electro-polymerization process is conducted in deoxygenated solution, and PDA could be deposited on the gold electrode directly, which provide a simply and feasible method for PDA coating on electrically conductive materials. UV irradiation [68,69] is an alternative method to promote the dopamine polymerization. As the UV irradiation could enable the generation of reactive oxygen species (ROS), such as hydroxyl radicals could accelerate the dopamine polymerization even under acidic conditions. And the decrease of oxygen concentration in solution inhibits both UV- and base -triggered dopamine polymerization at different pH. Lee[70] has reported a simple strategy to prepare multifunctional polydopamine coating, the microwave irradiation of the coating solution results in the formation of about 18 nm PDA coating within 15min, which is approximately 18 times faster than the conventional coating. This is mainly because the radical generation and temperature increase, which could facilitate thermally accelerate radical polymerization of dopamine, and the predominant mechanism was proved to be the radical generation of dopamine by radiation that enhance the PDA-coating kinetics significantly.

1.2.1.2 Structure of PDA

Through PDA and PDA -derived materials have been widely applied in material science [71,72], the mechanism of dopamine polymerization is still elusive. Lee[60] indicated that the formation of PDA involved of oxidation of catechol to a quinone and covalent polymerization process. Dreyer [73] proposed that PDA is a superamolecular

aggregate of monomers involved of 5,6-dihydroxuindole (DHI) and dione derivatives held by interactions of charge transfer, π-stacking and hydrogen bonding(Fig 1.4 B). Hong [74] suggested that the polydopamine is formed via two pathway including non-covalent self-assembly and covalent polymerization, since they found that there is a significant amount of dopamine remains unpolymerized and exist in the form of $(dopamine)_2$/(DHI) (Fig 1.4 C). Liebscher [75] provided evidence that the dopamine unites are not held together by hydrogen bonding, DHI and indoledione units are covalently linked by C-C bonds between their benzene rings (Fig 1.4 D). Moreover, the PDA structure could also be affected by the initial dopamine concentration and buffer solution. Though many further studies are still needed to have a better understanding of PDA structure, it is widely accepted that both covalent and non-covalent interactions are involved in the formation of PDA.

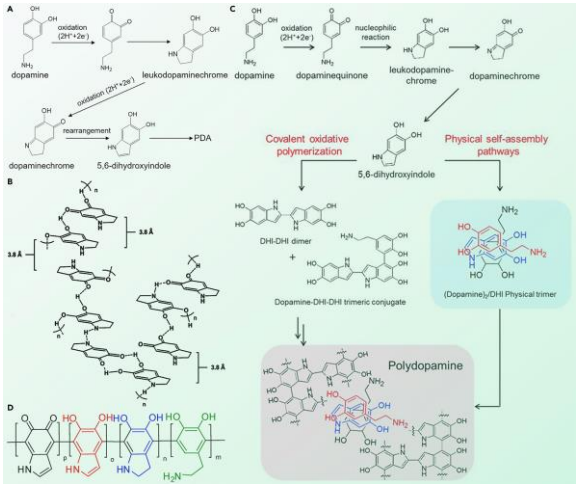

Figure 1.4 Proposed formation pathways and structures of PDA, possible pathways for the formation of PDA and the corresponding structures of PDA proposed by (A) Messersmith's (B) Freeman's (C) Lee's and (D) Liebscher's groups.[76]

1.2.1.3 Properties of PDA

Attribute to its chemical structure and composition, PDA exhibits many properties, including adhesion capability, high reactivity, photothermal conversion capability and biocompatibility which allows its application in many fields. Here, we discuss the two properties which most relevant to dye removal.

One of the most extraordinary properties of PDA is that it exhibits strong adhesion to the surface virtually all kinds of substance. This allows PDA could act as both the adlayer with abundant functional groups and the platform for further functionalization. It is widely accepted that the catechol groups in PDA plays the central role in the adhesion process,[77-79] the exact adhesion mechanism is still elusive. While, according to the pervious study, the interaction between PDA and substrate could be summarized as covalent binding and noncovalent binding.

Covalent binding usually refers to the substrate that contain amine and/or thiol groups and binding via Michael addition and/or Schiff base reactions under basic conditions. While, when under ambient conditions, PDA is likely to diffusion on substrates via noncovalent binding interaction such as metal chelating, π-π stacking and hydrogen bonding. As the surface of metal or metal oxide are usually hydrated under ambient conditions, the free metal ions can chelate with catechol groups in PDA. So, both coordination boding and chelating bonding interactions dominate in the adhesion of PDA on metal or metal oxide surfaces. While several interactions may be involved between PDA and substrate. For instance, Yu [80] studied the binding mechanism of Dopa to TiO_2 surface and found it is strongly related to the environment pH, as increasing the pH will results in overoxidation of catechol and decrease the adhesion. At low pH, hydrogen bonding dominates, when increased to high pH, it mainly depends on the coordination bonds. Lee [79] indicated that the adhesion of PDA to organic surfaces is mainly due to the oxidation of catechol to quinones under alkaline conditions, and thus covalent coupling to organic surfaces. Moreover, PDA coating can serve as a "bridge", which allows it to further react with other compounds. This allows PDA coating could act as a template for the further functionalization targeting different contaminants.

1.2.2 PDA for wastewater treatment

Owing to its above-mentioned properties, PDA could be developed in different nanostructured and modified to meet the demands for dye removal. Till now, diverse types of PDA-derived nanocomposites have been produced. In this section, we will

discuss PDA and PDA-derived nanomaterials that applied for dye removal categorized by nano/microstructure.

As mentioned, there are abundant functional groups in PDA, including catechol, amine groups and aromatic rings, which could be served as adsorption sites to bind organic dyes molecular via electrostatic interaction and π-π interaction. Thus, pristine PDA with different nanostructure could be directly used on dye adsorption.

1.2.2.1 Pure PDA nanoparticles

PDA nanospheres could be simply prepared by the self-polymerization of dopamine reported by Liu.[81]The size-controllable synthesis of PDA nanospheres has been studied to meet the requirement and specific applications. Recently, the factors including DA concentration, DA: NaOH ratio, temperature, reaction time, oxidant type have been discussed.[82] To achieve adjustable synthesis of polydopamine nanospheres, the DA: NaOH molar ratio is of the highest priority since it affects the reaction at the beginning stage. While, the temperature is inadequate to control he diameter and size distribution because of its complexity. Fu[83] prepared PDA microspheres by a modified facile polymerization process, the mixture solution of tris-buffer and ethanol were used as medium and the reaction last for 3 days under dark environment. The narrow diameter with a mean size of 590 nm was proved by both DLS and TEM. The adsorption capacity of the PDA microspheres on methylene blue (MB) could reach up to 90.7 mg g^{-1} at 25^{o} C. The adsorption mechanism was ascribed to be two main reasons, one is due to the abundant existing negatively charged phenolic groups on the surface of PDA microspheres which allows electrostatic interaction with the cationic dye MB. Moreover, π-π stacking interactions take place between the numerous aromatic rings in PDA microspheres and the aromatic backbone in MB molecular, which is confirmed by FTIR results, as the aromatic rings peak shift from 1630 cm^{-1} to 1603 cm^{-1} after adsorption (Fig 2.5). Fu [84] has also further discussed the adsorption selectivity of PDA microspheres based on the a forementioned work. By testing a series of dyes, PDA microspheres shows difference adsorption capacity for different dyes, which is due to the synergistic effect of electrostatic interaction, π-π stacking interaction and chemical

structure of dyes, this work inspires that developing functional PDA based material could enhance the selectivity and separation ability for different dyes in water treatment.

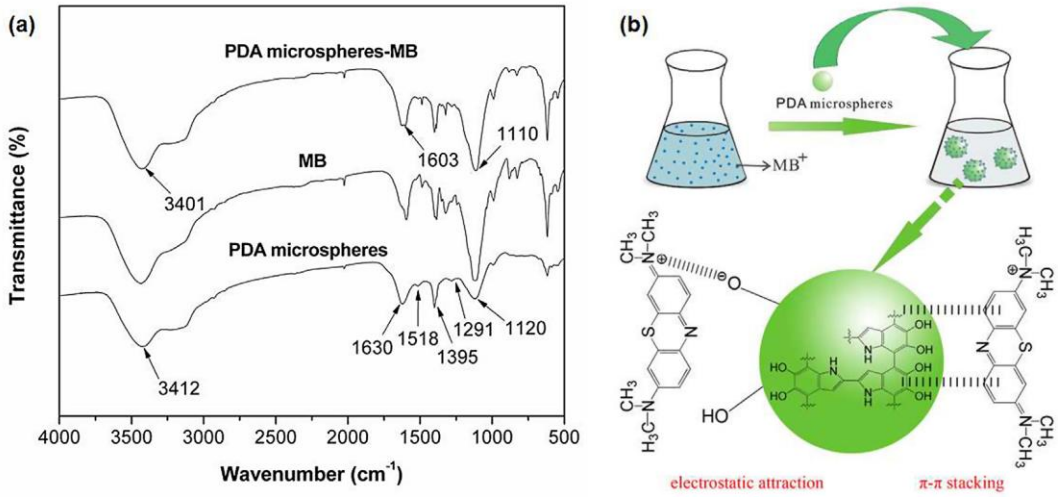

Figure 1.5 (a) FTIR spectra of MB, PDA microspheres, and PDA microspheres-MB. (b) Schematic illustration of the adsorption process and interactions between the PDA microspheres and MB.[83]

Tao [85] reported the adsorption of MB with hollow mesoporous polydopamine (HMPDA) microcapsules. The mesoporous structure of HMPDA is investigated by TEM and nitrogen adsorption-desorption method. The adsorption capacity of HMPDA microcapsules is up to 1172.8 mg g^{-1}, and it is much larger than that of SiO_2@MPDA composites, which is 567.8 mg g^{-1}. The surface mesoporous structure and large central cavity are attributed to the unique adsorption capacity.

Recently, stomatocyte-like hollow polydopamine nanoparticles (SHPNs) were developed for removal water-soluble dyes from water.[86] The maximum adsorption capacity of SHPNs for MB is investigated via adsorption isotherm experiment. And it was calculated to be 2896 mg g^{-1}, which is 30 times larger than the above-mentioned pure PDA microspheres.[83] The adsorption rate was calculated by the kinetics studies, and the result got from the kinetic data shows that more than 98% of MB could be removed after only 20 seconds, which also be demonstrated by a flow-through water treatment for MB solution. Moreover, this material could be regenerated easily by washing with acidic ethanol solution and the adsorption capacity will retained up to be 98% even after 13 adsorption/regeneration cycles. There are three interactions that involved as synergistic effect for the excellent adsorption capacity of SHPNs for MB.

Firstly, PDA exhibits alternation of zeta potential as pH change, and could provide abundant negative charged sites allow the electrostatic interaction with cationic MB, since when pH up to 10 the zeta potential of SHNPs is measured to be -34.7 mv, and when pH reach 1, the zeta potential is large than 20 mv, adsorbed MB is released, resulting in the adsorption process of SHPN is reversible and pH dependent. Besides, large number of aromatic rings in SHPNs could accelerate MB adsorption via π-π interaction. Moreover, there occurs a Michael addition reaction between the catechol phenolic hydroxyl group in PDA and the Eschenmoser structure of MB.[87]

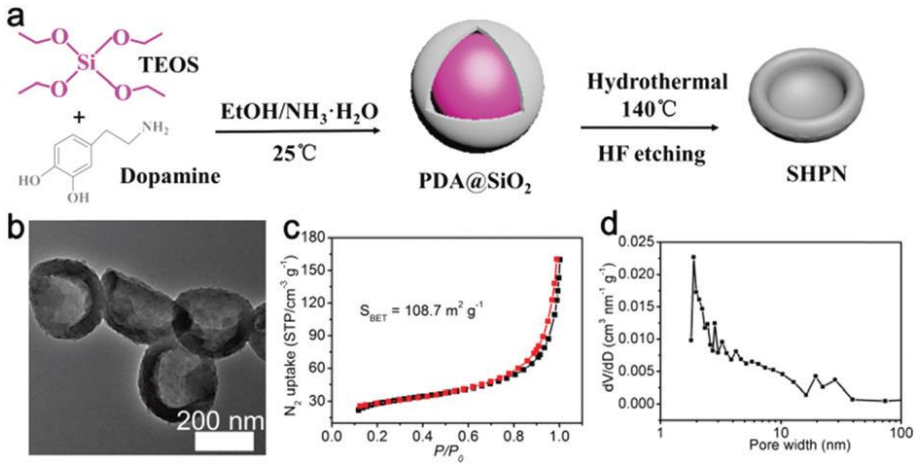

Figure 1.6 Synthesis and characterization of a SHPN: (a) schematic of synthesis route for SHPN; (b) TEM image of SHPN material with a bowl-shaped morphology; (c) N_2 sorption isotherms of SHPNs collected at 77K; (d) pore size distribution of SHPNs based on the nonlocal density functional theory.[86]

1.2.2.2 PDA-derived nanoparticles

Magnetic PDA particles

Various PDA-based multifunctional responsive nanoparticles have been designed aiming at improving the removal efficiency and simplify the regeneration process of the adsorbents. Among the responsive alien material introduced into PDA, magnetic particles are highly preferred as it could be easily conducted by applying an external magnetic field.

Wang [88] fabricated PDA/CS/Fe_3O_4 nano-biosorbent via assembling PDA and CS complex onto magnetic nanoparticles, due to the high surface area and abundant active sites provided by PDA and CS content of obtained magnetic adsorbents, it show high adsorption capacity reached 204 mg $g^{-1}$and 61 mg g^{-1}, and removal percentage up to 96.9% and 92.5% for MB and malachite green, respectively. Besides, the adsorbent retained high adsorption efficiency after four cycles, regenerated by eluent treatment and magnetically separated.

Shao [89] developed highly regenerable magnetic nanoparticles by co-deposition PDA and poly(ethylenimine) (PEI) on Fe_3O_4 nanoparticles presented in Fig 1.7. The highly cationic charge density of PEI lead to selective adsorption performance. Compared with Fe_3O_4@PDA, Fe_3O_4@PDA/PEI adsorbents exhibit significantly opposite effect toward anionic and cationic dyes, which is proved with the adsorption test conducted on mixture of opposite charged dyes. Moreover, the ultrathin (about 3 nm) PDA/PEI coating layer not only increase the surface area but also exhibit excellent alkali resistance compared to Fe_3O_4@PDA. On the other hand, this magnetic adsorbent retained the removal percentage over 90% even after 10 cycles and regenerated in several minutes.

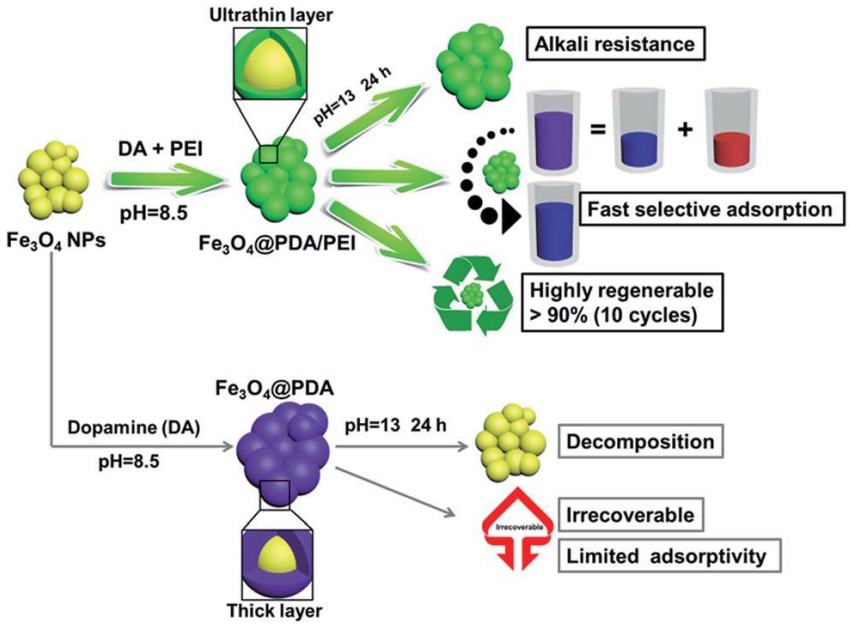

Figure 1.7 Schematic of the fabrication and comparison of novel Fe_3O_4@PDA/PEI and Fe_3O_4@PDA magnetic adsorbents.[89]

Core/Shell magnetic multi-walled carbon nanotubes (MWCNTs) nano-hybrid (MWCNTs/Fe_3O_4@PDA/PEI) [90] was constructed via co-precipitation of Fe_3O_4 particles and copolymerization of PDA and PEI. The adsorbents exhibit excellent adsorption capacity and selectivity for anionic dyes, which attribute to large specific surface area (126m^2 g^{-1}) and the abundant exist active sites in PDA/PEI. It exhibits highly selective adsorption performance for several anionic dyes MB, CR and MO with the maximum adsorption capacity of 1449,1006 and 935 mg g^{-1} at 298.15 K respectively.

Magnetic PDA decorated with Mg-Al layered double hydroxides (LDH) nanoflakes were prepared by a combination of self-polymerization of DA and hydrothermal treatment. [91] This adsorbent could be used for simultaneous removal of toxic metals and anionic dyes, both PDA and LDHs are contribute to the adsorption property. The removal capacities of Methyl Orange (MO) and Congo Red (CR) were 624.89 and 584.56 mg g^{-1}. They found that MO and CR will significantly improve the removal efficiency of Cu (II) in Cu (II)-dye binary system, which is ascribed to the presence of adsorbates enhanced the driving force for ion diffusion and then facilitate

the removal of metal ions. Besides, the regeneration efficiency retained about 80% after five cycles.

PDA with GO composites

Graphene oxide is a well-known carbon-based nanomaterial with lamellar structure. Due to its specific extraordinary surface area, GO is a promising material to improve the adsorption capacity. Thus, the combination of GO and PDA is aiming to utilize the synergistic effect of PDA with large amounts of active sites and GO with high surface area, many PDA-GO nanocomposites were developed for dye removal.

He [92] synthesized a novel adsorbent involved of PDA, kaolin, and reduced GO. With the introduction of rGO, the surface area of PDA-rGO-kaolin was increase by 3.1 times, and the adsorption capacity for MB rase up from 28.4 to 39.6 mg g^{-1} compared to PDA-kaolin. Also, PDA-rGO-kaolin exhibited good regeneration behavior, as the removal efficiency retain 84% after five cycles.

Dong [87] prepared PDA coated GO (PD/GO) via a self-polymerization of DA and applied in the dye removal. It is worth noting that the PD/GO exhibited extremely high capacity and selectively adsorption for dye with Eschenmoser structure which up to 2.1 g g^{-1}. This is supposed to be the Eschenmoser salt assisted 1,4-Michael addition reaction between catechol phenolic hydroxyl moieties of PDA and Eschenmoser groups in the dyes.

PDA-based catalyst

Metal nano-catalysts are more likely to aggregate due to their high surface energy, which lead to the decrease in catalytic activity, then PDA-coated nanomaterials could be served as carriers for the immobilization of metal nano-catalysts.

Lu [93] fabricated PDA nanotubes (NTs) decorated with silver (Ag) nanoparticles (NPs) through template induced self-polymerization of DA, followed by Ag NPs assembled onto PDA-NTs by in situ reduction from nitrate solution (Fig 1.8). The nano-catalyst shows excellent catalytic activity for the reduction of MB with an apparent rate

constant of 3.19 min^{-1} in first-order kinetic model, which is higher than the other reported value. The catalyst efficiency retains at about 94% after 10 cycles. Besides, the Ag@ PDA Nts catalyst could be easily separated from water by sedimentation or filtration.

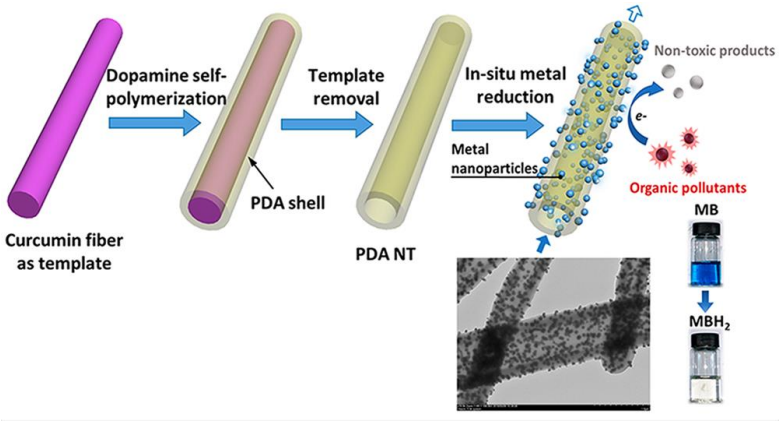

Figure 1.8 Scheme of synthetic procedure for metal@PDA NTs; TEM image of Ag@PDA NTs; scheme of the proposed mechanism for the reduction of organic pollutants by $NaBH_4$ with PDA NTs as nanocatalysts; changes in color of MB after catalytic reduction by Ag@PDA NTs.[93]

Pan [94] reported a novel Fenton-like catalyst (Fe_3O_4@PDA-MnO_2) that fabricated by self-polymerization of DA and deposition of MnO_2 onto magnetic nanoparticles in $KMnO_4$ solution. The MnO_2 loading avoid the aggregation of nanoparticles and facilitate the separation of catalyst from solution. The combination of Fe_3O_4@PDA-MnO_2 and H_2O_2 served as Fenton-like reagent for the removal of MB with a high degradation efficiency of 97.36 % within 4 hr. And the high catalytic activity retained after five cycles.

1.3 Research objectives

As discussed above, PDA-based adsorbents exhibit good adsorption capacity for dyes, especially cationic dyes. However, in practical dye removal process, the dye effluent contains not only cationic but also anionic dyes, which limits the application of PDA-based adsorbents due to their poor adsorption performance for anionic dyes, in other words, their inability to remove cationic and anionic dyes simultaneously.

Moreover, during the adsorption process, both the adsorption capacity and adsorption mechanism are governed by the surface area and surface properties.

Adsorbent with different micro/nano structures are shown to be of different adsorption capacity. And adsorbents with different morphology are constructed though different strategy with different chemicals, which also bring about the imparity of surface chemistry and leading to different adsorption performance and mechanism. So, it is worthy to study not only the morphology effect, but also the effect of different synthesis method on PDA-based adsorbents for dye removal.

To achieve these goals, the first objective of this work is to develop PDA-based adsorbents, PDA nanotube (PDA NT) and hollow PDA sphere (HPDA) were firstly constructed through coating PDA on the surface of SiO_2 and halloysite nanotube and subsequently remove the template, mesoporous PDA (MPDA) was conducted through an emulsion-induced assemble process. Then, due to the abundant exist amino and hydroxyl groups in the chemical structure of PDA, iron ions including Fe^{2+} and Fe^{3+} were chelated and co-precipitate into Fe_3O_4 on the surface, formed magnetic PDA nanoparticles (PDA MNPs). Finally, the simultaneous incorporation of PDA and poly(ethylenimine) (PEI) on PDA MPs to realize the further functionalization of adsorbents. The embedded Fe_3O_4 on the surface of PDA template is conductive to rapid magnetic separation, the employed PEI will be beneficial for the improvement of adsorption for anionic dyes. Combining the merits of magnetic particles and functionalized PDA/PEI layer to fabricate PDA-based adsorbents with different micro/nanostructure makes these adsorbents to be promising candidates for dye remediation. Therefore, the second objective of this work is to evaluate the performance of PDA-based adsorbent for dye removal and study the morphology effect on the adsorption behavior and adsorption mechanism, which is helpful for not only the development of PDA-based adsorbents, but also for other kinds of adsorbents that aiming to be applied for water remediation. Thus, this work will focus on mainly two parts.

1. Develop PDA-based adsorbents with different morphology

Polydopamine was first fabricated as hollow spherical particles, tubular particles, and mesoporous particles. All particles were further modified by the deposition of magnetic nanoparticles on the surface to aid in separation. The abundant catechol and amine groups in polydopamine serve as absorption sites. The particles were further modified by polyethyleneimine to enhance selectivity between cationic and anionic dyes. The morphology, chemical composition and surface properties were investigated by TEM, FTIR, N_2 adsorption-desorption and DLS.

2. Evaluate the adsorption performance for dyes

Here we report adsorption equilibrium and kinetics as a function of particle morphology and chemistry for two model dyes MB and MO. Five adsorption isotherm models and three kinetic models were applied to study the adsorption process. Adsorption thermodynamics, competitive absorption from mixtures of these dyes, ionic strength effect and regeneration of the absorbent was also evaluated. By systematically study the adsorption performance of PDA-based adsorbents, the rate-limiting step and the adsorption mechanism were further investigated.

2. Chapter 2 Synthesis PDA-based adsorbents with different morphology

In chapter 1, we reviewed the PDA-based adsorbents that has been developed for dye removal. The different micro/nanostructure results in the difference of adsorption performance for dyes, which indicates the morphology effect. Designing and synthesis nanomaterials with tailored structure and size is one basic goal and long-term interest for material science. Typically, nanomaterials with various shapes and sizes were synthesized by employing different synthetic approaches.

In this chapter, we synthesized adsorbents based on PDA template with three different structures, PDA nanotube (PDA-NT), hollow PDA sphere (HPDA), and mesoporous PDA (MPDA), which contributing to the immobilization of magnetic Fe_3O_4 particles via co-precipitation. Polyethyleneimine (PEI) is a polymer with plenty amine groups, which has been employed to improve the adsorption performance through surface modification, as the dense positive charges on the PEI branch could promote adsorption for anionic dyes. The formation of co-deposition PDA/PEI coating with improved morphology uniformity, surface hydrophilicity and chemical stability is due to the low-molecular-weight PEI accelerates the co-deposition process and improve the coating stability by acting as crosslinker.[95]

Materials Dopamine hydrochloride (DA), 1,3,5-Trimethylbenzene (TMB), iron (III) chloride ($FeCl_3$, 98%) and iron (II)sulfate heptahydrate ($FeSO_4 \cdot 7H_2O$, 98%) were from Beantown Chemicals. Pluronic F127 was purchased from Bio Vision, Tetraethyl orthosilicate (TEOS,98%) was purchased form Acros. Tris(hydroxymethyl) aminomethane (Tris), polyethyleneimine (PEI) (MW=600, 99% branched) were obtained from VWR life science, ethanol (EtOH), hydrochloric acid (HCl, 10 % v/v), hydrofluoric acid (HF, 50 % v/v) and ammonia solution ($NH_3 \cdot H_2O$, 28-30 % w/v) were purchased from BDH chemicals, halloysite nanotube (HNT) was obtained from Bonding Chemical. All chemicals were used without further purification. Deionized (DI) water was used in all experiments.

Characterization Morphology was obtained using transmission electron microscopy (TEM, Zeiss EM10). Samples were prepared on a 300-meshed formvar/carbon film from Electron Microscopy Sciences. Chemical compositions were investigated via Fourier transform infrared spectra (FTIR) (ThermoScientific iS-50). Hydrodynamic particle size and surface charging properties of particles was obtained from Malvern ZetaSizer Nano ZS90. Magnetic property was studied by Quantum Design Dynacool Physical Property Measurement System (PPMS) equipped with a Vibrating Sample Magnetometer (VSM). Samples were measured at 300K and the external magnetic field ramped between -1T and +1T using the PPMS superconducting cryo-magnet. N_2 adsorption-desorption isotherm was measured by the Micromeritics Tri-Star II 3020 with Micrometrics FlowPrep 060.

2.1 Synthesis of adsorbents

2.1.1 Synthesis of PDA-NT/Mag/PDA/PEI

Synthesis of PDA nanotubes 0.2 g HNT was dispersed in 200 ml 10 mM tris buffer (pH=8.46) through sonication for 2 mins. Then 0.8 g DA was added into the above solution and stirred at R.T. for 24h. The product PDA coated HNT (PDA-HNT) was collected by filtration, centrifugation and washed with DI water until the supernatant was transparent and colorless. The obtained product was then ultrasonically redispersed in DI water. For PDA-HNT fragmentation, it is conducted follow the reported procedure.[96] 10 ml as-prepared PDA-HNT suspension was sonicated for 4h at 350w (QSonica LLC, Q500, 70% amplitude), then the suspension was centrifuged and rinsed by DI water till the supernatant was colorless. For template removal, 1 ml HCl and 0.5 ml HF was added into 10 ml PDA-HNT dispersion and stirred at R.T. for 8h. Then PDA-NT was recovered via centrifugation and washed with DI water until pH of supernatant was over 5. The obtained product (PDA-NT) was ultrasonically redispersed in DI water and preserved for characterization and next step.

Synthesis of PDA-NT/Mag Firstly, prepared 10 mg mL^{-1} $FeCl_3$ solution and $FeSO_4 \cdot 7H_2O$ DI solution. 1.5 mg HPDA was dispersed in 5ml DI water via sonication for 1 min and then 0.192 ml $FeCl_3$ and 0.168 ml $FeSO_4 \cdot 7H_2O$ solution were added.

After reaction at 55 ℃ for 30 min, the temperature was risen to 65 ℃, then 0.5 ml $NH_3 \cdot H_2O$ was dropwise added into the mixture and reaction for 30 min. The product was separated with a magnet, then recovered via centrifugation and washed with DI water repeatedly until the supernatant was transparent and colorless. The obtained product (PDA-NT/Mag) was then ultrasonically redispersed in 10 ml pH=11 NaOH solution for characterization and next step.

Synthesis of PDA-NT/Mag/PDA/PEI 10 mg PDA-NT/Mag was dispersed in 10 ml 10 mM tris buffer (pH=8.46) under ultrasonic conditions for 1 min. Then, 20 mg DA and 60 mg PEI were simultaneously added and allowed to proceed for 24 h under stirring at R.T. The product was separated with a magnet, then recovered via centrifugation and washed with DI water repeatedly until the supernatant was transparent and colorless. The obtained product (PDA-NT/Mag/PDA/PEI) was then ultrasonically redispersed in DI water for characterization.

2.1.2 Synthesis of HPDA/Mag/PDA/PEI

Synthesis of SiO_2 nanoparticles Firstly, 27.5 ml EtOH, 22.5 ml DI water and 7.5 ml $NH_3 \cdot H_2O$ were mixed by stirring for 30 mins, results in a solution with pH=12.2. Then 2.5 ml TEOS was added rapidly into the solution and stirred at R.T. for 24h, the product was obtained via centrifugation and washing by DI water repeatedly until the supernatant was transparent and colorless. The obtained product was dried in the oven at 40°C overnight and collected for characterization and next step.

Synthesis of SiO_2/PDA The as-prepared 200 mg SiO_2 was dispersed in 200 ml 10 mM tris buffer (pH=8.46) via sonication for 2 mins, then (200, 400, 800 mg) DA was added into the SiO_2 suspension and stirred at R.T. for 24 h. The product was obtained via centrifugation and washing by DI water repeatedly until the supernatant was transparent and colorless. The obtained product was then ultrasonically redispersed in DI water for characterization and next step.

Synthesis of Hollow PDA 5 ml as prepared SiO_2/PDA solution was dispersed in 14 ml DI water via sonication for 1 min, then 1 ml HF was added dropwise and stirred at R.T.

for 2h. Then hollow PDA nano-capsule was recovered via centrifugation and washed with DI water until pH of supernatant was over 5. The obtained product was ultrasonically redispersed in DI water and preserved for characterization and next step.

Synthesis of HPDA/Mag Firstly, prepared 10 mg mL^{-1} $FeCl_3$ solution and $FeSO_4 \cdot 7H_2O$ DI solution. 1.5 mg HPDA was dispersed in 5ml DI water via sonication for 1 min and then 0.192 ml $FeCl_3$ and 0.168 ml $FeSO_4 \cdot 7H_2O$ solution were added. After reaction at 55 ℃ for 30 min, the temperature was risen to 65 ℃, then 0.5 ml $NH_3 \cdot H_2O$ was dropwise added into the mixture and reaction for 30 min. The product was separated with a magnet, then recovered via centrifugation and washed with DI water repeatedly until the supernatant was transparent and colorless. The obtained product (HPDA/Mag) was then ultrasonically redispersed in 10 ml pH=11 NaOH solution for characterization and next step.

Synthesis of HPDA/Mag/PDA/PEI 10 mg HPDA/Mag was dispersed in 10 ml 10 mM tris buffer (pH=8.46) under ultrasonic conditions for 1 min. Then, 20 mg DA and 60 mg PEI were simultaneously added and allowed to proceed for 24 h under stirring at R.T. The product was separated with a magnet, then recovered via centrifugation and washed with DI water repeatedly until the supernatant was transparent and colorless. The obtained product (HPDA/Mag/PDA/PEI) was then ultrasonically redispersed in DI water for characterization.

2.1.3 Synthesis of MPDA/Mag/PDA/PEI

Synthesis of MPDA 1 g of F127 and 0.5 g of DA were dissolved in the mixture of 50 mL of water and 50 mL of ethanol. Followed by the addition of 1.5 ml TMB and stirred at R.T. for 30 min. After adding 5 ml $NH_3 \cdot H_2O$ dropwise to the mixture. The reaction was conducted at 70 ℃ for 3h. The MPDA particles were collected via centrifugation and washed 3 times with ethanol and DI water respectively, and then ultrasonically redispersed in DI water for characterization.

Synthesis of MPDA/Mag Firstly, prepared 10 mg mL^{-1} $FeCl_3$ and $FeSO_4 \cdot 7H_2O$ DI water solution. 1.5 mg MPDA was dispersed in 5 ml DI water and then 0.192 ml $FeCl_3$

and 0.168 ml $FeSO_4 \cdot 7H_2O$ solution were added. The mixture was stirred for 30 min at 55 ℃, the temperature was then risen to 65℃, followed by the addition of 0.5 ml $NH_3 \cdot H_2O$ and reaction for another 30 min. The product was separated with a magnet, then recovered via centrifugation and washed with DI water repeatedly until the supernatant was transparent and colorless. The obtained product (MPDA/Mag) was then ultrasonically redispersed in 10 ml pH=11 NaOH solution for characterization.

Synthesis of MPDA/Mag/PDA/PEI particles 10 mg MPDA/Mag was dispersed in 10 ml 10 mM tris buffer (pH=8.46) under ultrasonic conditions for 1 min. Then, 20 mg DA and 60 mg PEI were simultaneously added and allowed to proceed for 24 h under stirring at R.T. The product was separated with a magnet, then recovered via centrifugation and washed with DI water repeatedly until the supernatant was transparent and colorless. The obtained product (MPDA/Mag/PDA/PEI) was then ultrasonically redispersed in DI water for characterization.

2.2 Characterization of the prepared nanoparticles

2.2.1 TEM

The morphology of as-prepared samples is revealed by TEM. The pristine HNT and modified HNT were shown in Fig 2.1, where HNTs shown to be of a cylindrical tubular structure with the diameter of 50-60 nm. After PDA coating, the diameter of PDA-HNT increased to 102-128nm. The deposition of PDA occurred on the surface of HNTs through aggregation of dopamine. As a result, PDA deposited at the ends and internal surface of the HNT sealing the ends of HNTs that shown in Fig 2.1b. Utilizing the interspace of tubular structure could increase the number of binding sites for dye adsorption, so nanotubes with open end are highly preferred. Therefore, sonication-broken method [96] was employed to fracture the close ends PDA-HNT into PDA-HNT with open ends. After HF etching, a clear tubular structure with open ends could be recognized in Fig 2.1c. Then attached with Fe_3O_4 nanoparticles via co-precipitation, it could be clearly seen from Fig 2.1d, magnetic particles dispersed on the outer surface of the PDA-NT and the configuration of the tubular structure maintained well. The

diameter of nanotube increased to 210-224 nm, indicating PDA-NT/Mag was encapsulated by a PDA/PEI coating.

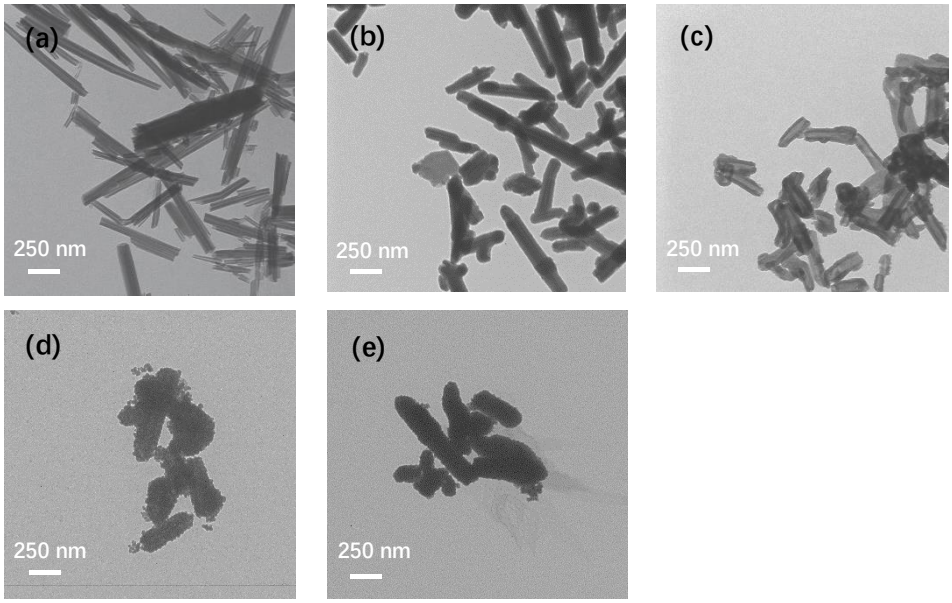

Figure 2.1 TEM images of (a) Pristine HNT,(b) PDA-HNT, (c) PDA-NT, (d) PDA-NT/Mag, (e) PDA-NT/Mag/PDA/PEI.

To attain controllable structure of hollow PDA, the effect of mass ratios of DA:SiO_2 was investigated. As shown in Fig 2.2(a-d). The pristine SiO_2 had smooth surface and sphere shape with a diameter of 185-223 nm. After PDA coating, the surface of nanospheres became rough and their diameters increased. As the weight ratio of DA:SiO_2 raised from 1 to 4, the diameter changed as 202-245nm, 201-240nm, 240-276nm. It is illustrated in Fig 2.2 (b-d) that the PDA coating was much more uniform and thicker when the DA/SiO_2 ratio increased to 4. The SiO_2/PDA that synthesized with the weight ratio of DA to SiO_2 as 4:1 was used for next step. After HF etching, the SiO_2 template was removed, the hollow structure is shown in Fig 2.2 (e). The functionalization of hollow PDA was conducted in two steps, MNPs were firstly introduced followed by the co-deposition of PDA/PEI coatings. As shown in Fig 2.2d, the outer surface of hollow PDA was very smooth. After the attachment of Fe_3O_4 nanoparticles via co-precipitation, it could be clearly seen from Fig 2.2e, the outer surface of the hollow PDA became rough. With the introduction of PDA/PEI, the thickness of shell increased from 32-45 nm to 56-75nm.

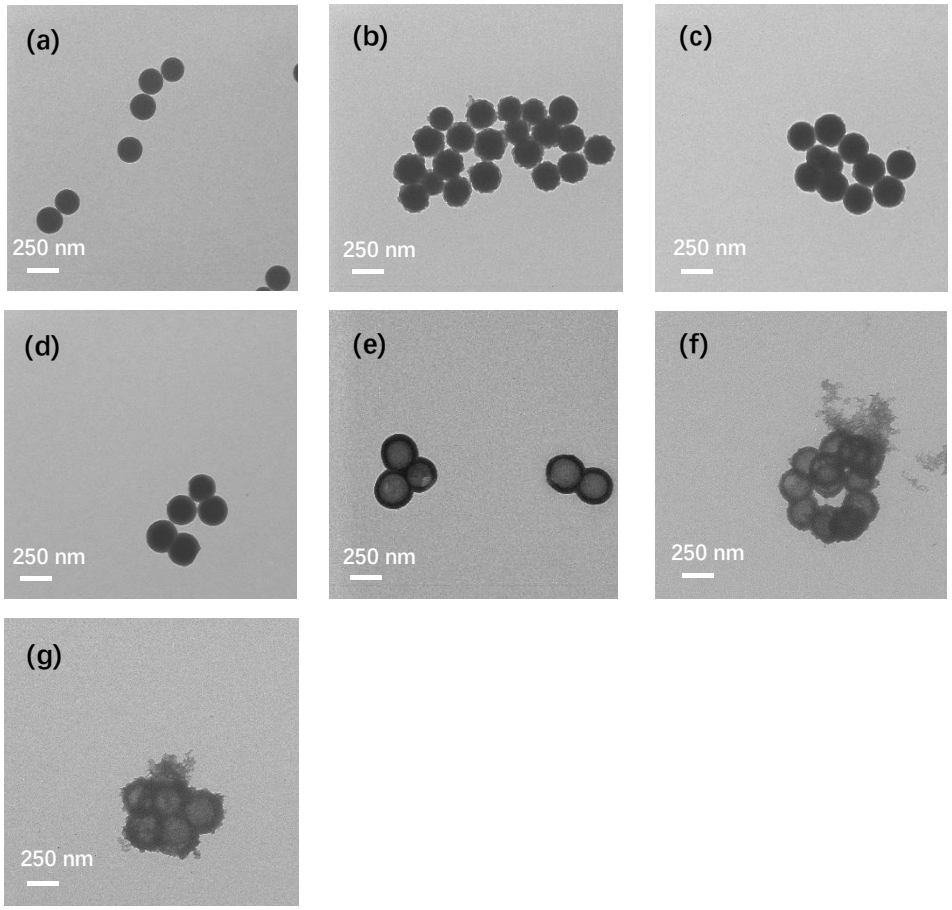

Figure 2.2 TEM images of (a) SiO_2 nanospheres and after PDA coating with different DA to SiO_2 ratios (b)1:1, (c) 2:1, (d) 4:1. (e) hollow PDA, (f) PDA/Mag, (g) HPDA/Mag/PDA/PEI.

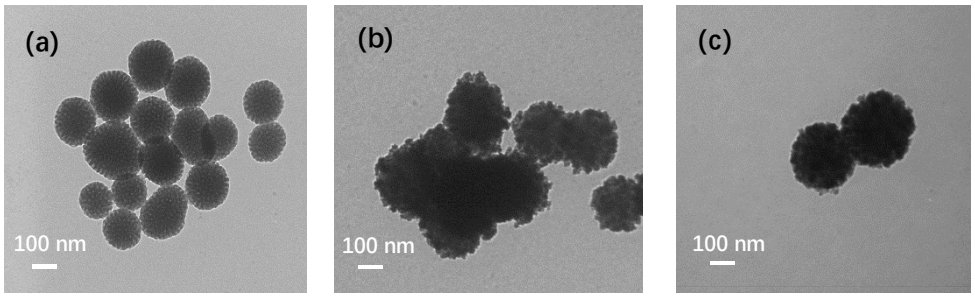

Figure 2.3 TEM images of (a) MPDA (b) MPDA/Mag, (c) MPDA/Mag/PDA/PEI.

The TEM images of MPDA and functionalized MPDA were present in Fig 2.3. In Fig 2.3 (a), ordered mesopores could be seen on the surface MPDA, the average diameter of MPDA is ~186 nm. Then the magnetic particles were attached onto the surface of MPDA via co-precipitation, the smooth surface of MPDA becomes rough (Fig 2.3 (b)) and the diameter of the particles increased to ~202 nm. With introducing PDA/PEI, and the diameter of the particles grow to ~230 nm, indicating the formation of PDA/PEI layer. While the mesoporous structure is almost invisible in Figure 2.3 (b)

and (c), the pore structure in MPDA/Mag/PDA/PEI will be further confirmed by the N_2 adsorption result.

2.2.2 FTIR

The chemical composition of the as-prepared particles was characterized by FT-IR. The FTIR spectra were present in Figure 2.4, in Fig 2.4(a), the peaks at 3694 and 3621 cm^{-1} were assigned to be the O-H stretching of hydroxyl groups, and the peaks at 1000, 907, 521 and 458 cm^{-1} were assigned to be the deformation and stretching of Si-O, Al-O-Si and OH. [97] All these above-mentioned peaks disappeared after the removal of HNT, which indicates that the template is completely removed after HF etching. In Fig 2.4 (b), the peaks at 1069, 951, 798, 458 cm^{-1} were assigned to be stretching vibration of Si-O-Si. [98] All these peaks disappeared after template etching by HF, which indicated the complete removal of SiO_2. After the coating of PDA, broad peak between 2000 and 3650 were ascribed to the stretching of aromatic -NH and phenolic -OH, peak at 1608 cm^{-1} was attributed to the stretching of aromatic ring and bending of N-H, peaks located at 1507 and 1293 cm^{-1} were specified as stretching and shearing vibrations of phenolic C-O, which indicate the existence of PDA. The stretching vibration of Fe-O appeared at the adsorption band of 560 cm^{-1}, indicating the formation of Fe_3O_4 nanoparticles.[99] The peak broadened around 1608 cm^{-1} and the peak at 1446 cm^{-1} appeared in PDA/Mag/PDA/PEI were ascribed to the stretching vibration of C=N and bending vibration of N-H, which was attributed to the introduction of PEI that react with PDA through the Michael addition/Schiff base reaction. [100] In Figure 2.4(c), the curve of MPDA, MPDA/Mag and MPDA/Mag/PDA/PEI shown to be of similar characteristic peak with that of PDA-NT and HPDA, which confirm the chemical composition of MPDA/Mag/PDA/PEI. Moreover, all the peaks around 560 cm^{-1} are weakened after the introduction of PDA/PEI comparing with that of magnetic particles, which is attribute to the increase of non-magnetic component, also confirm the add-layer of PDA/PEI.

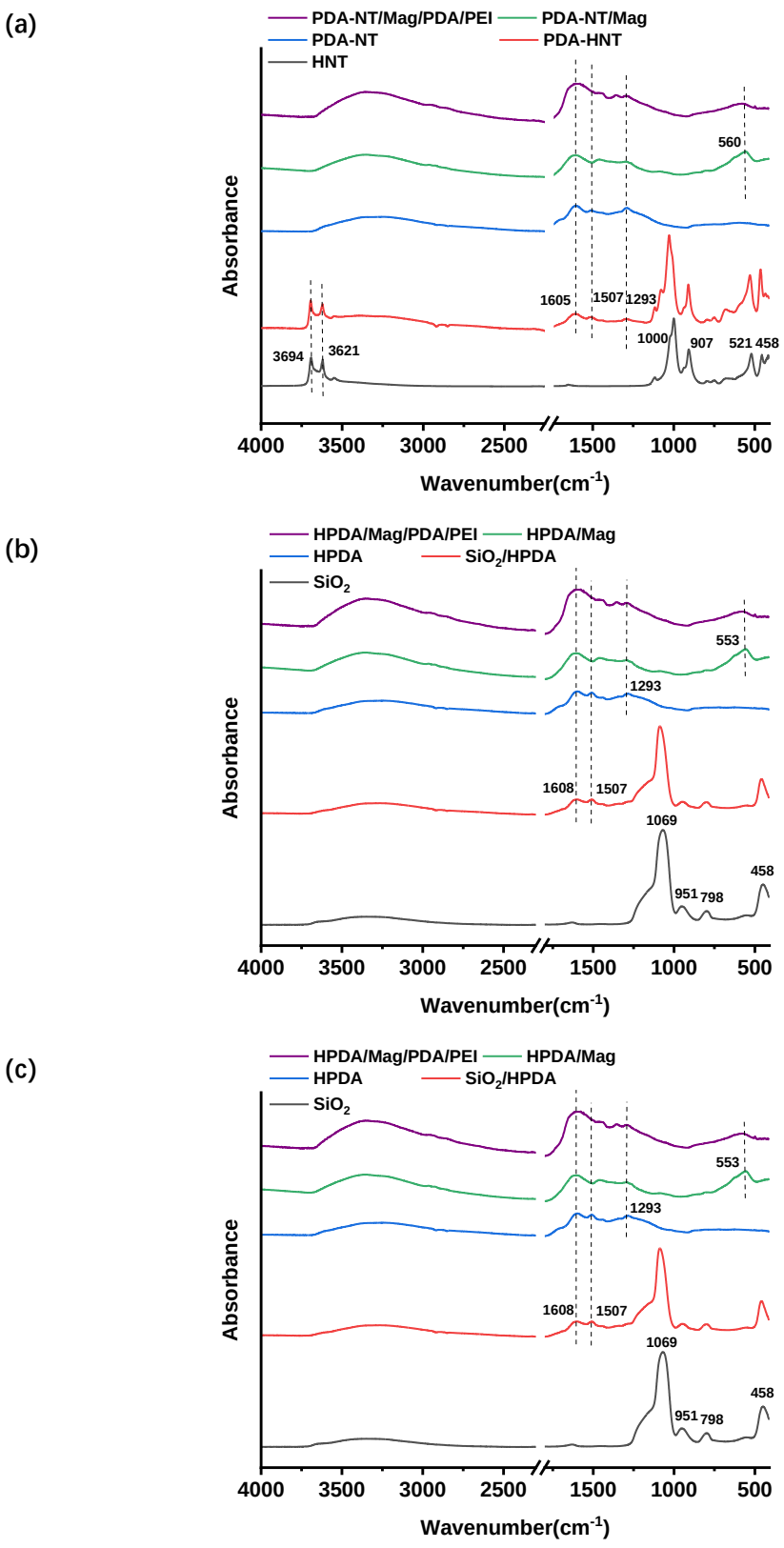

Figure 2.4 FTIR spectra of (a) PDA-NT/Mag/PDA/PEI; (b) HPDA/Mag/PDA/PEI; (c) MPDA/Mag/PDA/PEI.

2.2.3 Magnetic property

The magnetic property of adsorbents was investigated by the VSM. The magnetization curves (Fig 2.5) show no hysteresis or coercivity at 300 K, indicates the superparamagnetic behavior of all the three adsorbents. [101,102] The saturation magnetization (Ms) value of PDA-NT, HPDA and MPDA MNPs are 23.1, 22.3 and 32.4 emu g^{-1}, and the saturation magnetization (M) values of adsorbents are reduced to 20.9, 20.1 and 28.9 emu g^{-1}, respectively. This is mainly due to the introducing of non-magnetic PDA/PEI complex. Nonetheless, these adsorbents were still of strong enough magnetism that could be eligible for magnetic separation as shown in the inset of Fig 2.5. Besides, comparing with those MNPs, it took about 2 min for the quick separation from the DI solution with the aid of magnet, and the DI water remained transparent and colorless after the separation. While for MNPs, the DI water turned to brownish even with the help of magnet for 5 min. This is ascribed to the chelation between catechol and iron ions is weaken in DI water, which may result in the falling of magnetic particles from the surface of PDA template and cause some non-magnetic PDA NPs dispersed in DI that could not be magnetic separation. This implies that the introducing of PDA/PEI could act as a protection layer for the adsorbents, which could immobilize MNPs on the surface and facilitate separation and regeneration. Therefore, these adsorbents have advantages in separation and recovery for practical applications.

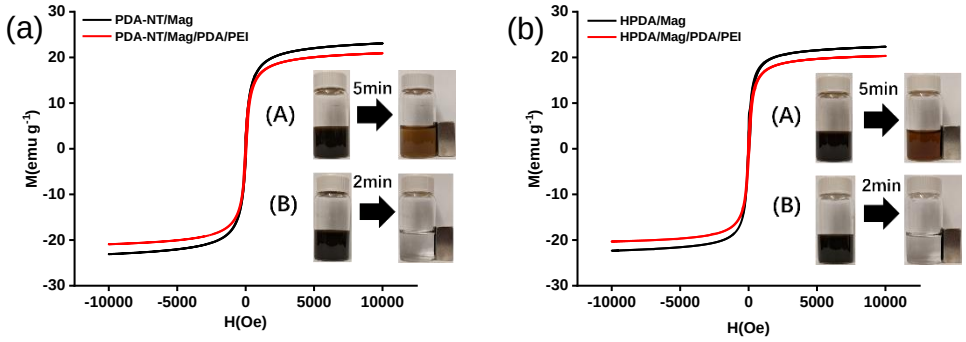

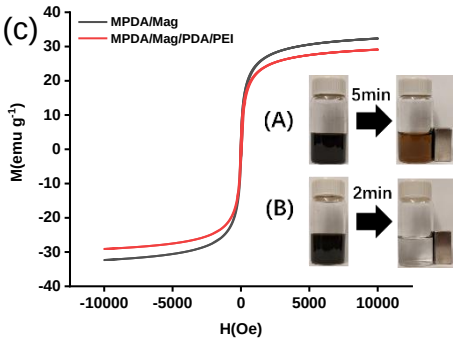

Figure 2.5 Magnetic hysteresis curves of (a) PDA-NT/Mag and PDA-NT/Mag/PDA/PEI; (b) HPDA/Mag and HPDA/Mag/PDA/PEI; (c) MPDA/Mag/PDA/PEI at 300K. The inset photos show vials with the (A) MNPs; (B) corresponding adsorbents well-dispersed in water and attracted to the side wall by a hand-hold magnet, respectively.

2.2.4 N_2 adsorption-desorption

The N_2 adsorption-desorption isotherm and pore size distribution curves of three adsorbents are shown in Fig 2.6 And the BET-specific surface, total pore volume and average pore diameter of three adsorbents were summarized in Table 1. From the N_2 adsorption-desorption curves of three adsorbents, we could see there is an obvious hysteresis loop in curve of MPDA/Mag/PDA/PEI, which suggests the exist of mesopores. [103] Besides, the average pore size of MPDA/Mag/PDA/PEI is in the range of 2-50 nm, [104] which also confirmed the mesoporous structure, and the pore width distribution indicates that the pores in MPDA/Mag/PDA/PEI are more uniform than that of PDA-NT/Mag/PDA/PEI and HPDA/Mag/PDA/PEI. Moreover, the mesopores could act as diffusion channels and enhance the adsorption capacity and adsorption rate. The large surface area of three adsorbents furnishes plenty of active sites for binding dye molecules, which will also benefit for the adsorption of dyes.

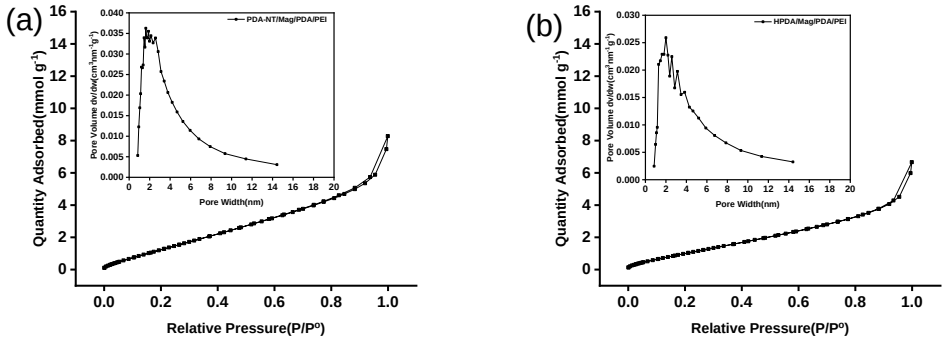

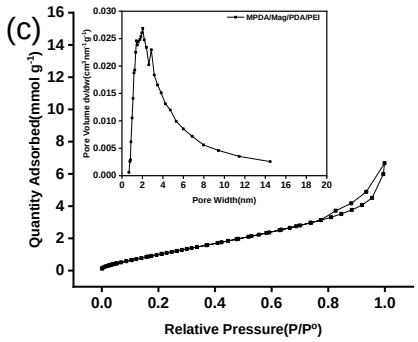

Figure 2.6 N_2 adsorption-desorption isotherm and pore size distribution curves of (a) PDA-NT/Mag/PDA/PEI; (b) HPDA/Mag/PDA/PEI; (c) MPDA/Mag/PDA/PEI.

Table 1 BET-surface area, total pore volume and average pore diameter of three adsorbents

Adsorbents	BET-Surface Area ($m^2 g^{-1}$)	Total pore volume ($cm^3 g^{-1}$)	Average pore diameter (nm)
PDA-NT/Mag/PDA/PEI	158.10	0.173	1.90
HPDA/Mag/PDA/PEI	118.78	0.136	1.91
MPDA/Mag/PDA/PEI	112.11	0.130	2.85

2.2.5 Zeta Potential

The surface charge of the adsorbent is very important since it has a significantly effect on the electrostatic interactions between adsorbent and dye molecules. The Z ave of three PDA template and adsorbents at different pH were determined by DLS. The result show that the hydrodynamic radius of these particles varies with pH. The particles in suspension will tend to repel each other and there will be no tendency for them to come together when they have a large negative or positive zeta potential. On the contrary, if the particles have relatively low absolute value of zeta potential, then there will be no force to prevent them from coming together and flocculating. [105] Combing the result of zeta potential, it could be found that, when pH reaches 3 and 9, the zeta potential is either more positive than + 30 mV or more negative than -30 mV, which are normally considered to be stable suspension. So that the Z ave value of particles is smaller than that of pH 5 and 7 as the zeta potential are in the range of -20 mV to 30 mV, which may lead to the particles coming together and measured with larger Z ave. Moreover, the Z ave increased after functionalization compared to the pristine PDA template for all the adsorbents, confirmed the formation of PDA/PEI coating, which is consistent with the TEM result.

The zeta potential of three PDA template and adsorbents at different pH were measured. The result in Fig 2.7 shows that the pH $_{pzc}$ of PDA-NT, HPDA, MPDA were about 4.3,4.6 and 4.2, whereas that of three adsorbents were about 6.0, 6.1 and 5.8. This is ascribed to the introduction of PEI that increase the amount of positive charge for the adsorbents, which could improve the adsorption performance for anionic dyes. The increase of zeta potential at pH 3 and 5 could be attributed to the -NH_2 groups on the surface of adsorbents could combine the large amount of H^+ that exist in acid medium and convert into -NH_2^+. In consequence, the surface of adsorbents will show to be of higher zeta potential due to the increased positive charge density, which will enhance the adsorption performance for anionic dyes.

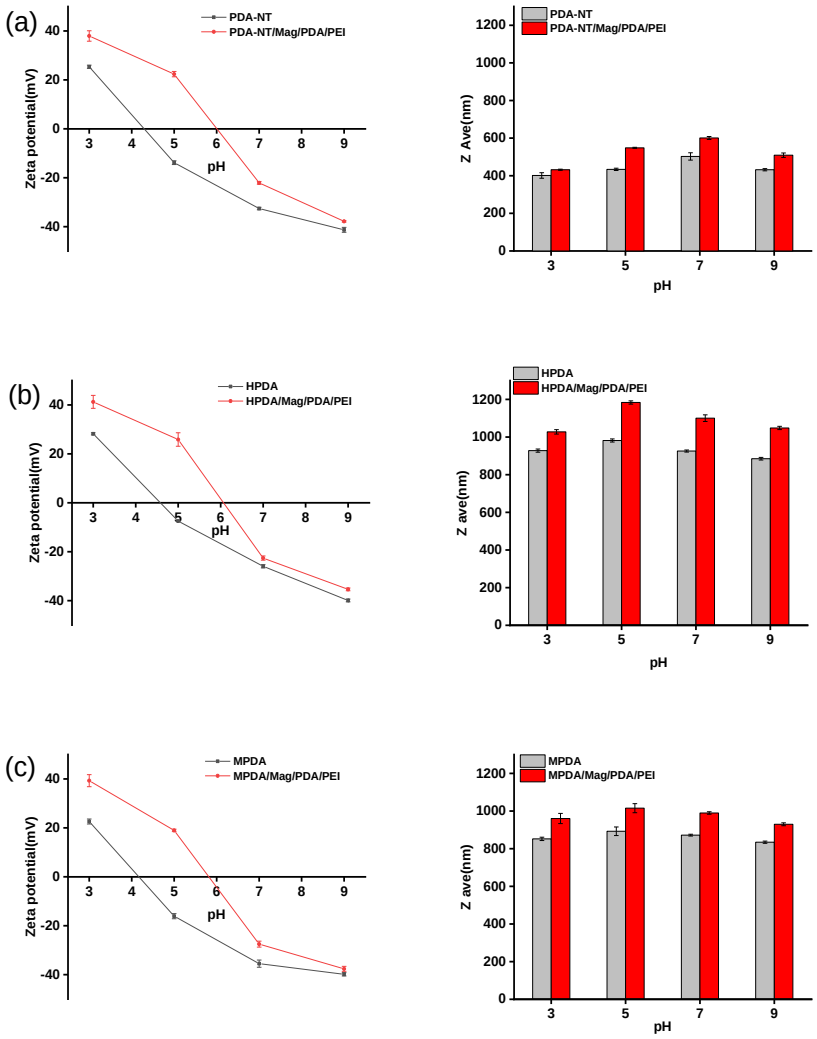

Figure 2.7 Zeta potential and Z ave of (a) PDA-NT and PDA-NT/Mag/PDA/PEI;(b) HPDA and HPDA/Mag/PDA/PEI;(c) MPDA and MPDA/Mag/PDA/PEI.

2.3 Summary

1. The PDA-based adsorbents with different morphology were successfully synthesized based on the self-polymerization of DA through template-based method and emulsion-induced assemble strategy, followed by the immobilization of magnetic particles on the surface via co-precipitation, finally the as-prepared particles were further functionalized by the co-deposition of PDA and PEI to realize the formation of functionalized coating.
2. The as-prepared adsorbents were characterized by FT-IR, TEM, the chemical composition and the microstructure were confirmed. The surface charging behavior and the hydrodynamic dimension of the particles that measure by DLS indicates that with the introduction of PEI, the adsorbents show increased amount of surface positive charge at pH 3-9, and the hydrodynamic dimension increased by the functionalization, which is consistent with the TEM result. Moreover, the adsorbents exhibited good magnetic properties and large surface area.

3. Chapter 3 Adsorption performance study

In Chapter 2, all the three as-prepared adsorbents were synthesized successfully and characterized by different technique to confirm their chemical composition and micro/nano structure. In this chapter, all the three above-prepared adsorbents will be evaluated through the adsorption test to investigate the morphology effect. After introducing of PEI with dense positive charges, the adsorbents are expected to show improved adsorption capacity for anionic dyes. Methylene blue (MB) and methyl orange (MO) were selected as cationic and anionic model dyes to study the adsorption behavior of these adsorbents. At first, the primary study of adsorption is conducted to study the key factors for the adsorption, and then determine optimal condition for the adsorption experiment, including contact time for adsorption, pH and mass of adsorbents. Then adsorption kinetic, isotherm and thermodynamic were studied to investigate the rate-control step and adsorption mechanism. The possible adsorption mechanism was confirmed according to the above-mentioned adsorption experiment. Followed by the study of ionic strength effect and regeneration property to evaluate the feasibility of adsorbents in practical applications. Moreover, the adsorption behavior for binary dye system was also evaluated from two aspects including removal simultaneously and step-by-step removal.

Materials Methylene Blue chloride (MB) was purchased from Harleco, Methyl Orange (MO) and sodium chloride (NaCl) were obtained from were obtained from VWR life science.

Characterization The absorbance of dye solution was ascertained by UV-vis spectroscopy, the concentration of the dye solution can be calculated then.

3.1 Adsorption experiments

Firstly, stock solutions of two dyes with the concentration of 500 mg L^{-1} were prepared by dissolving 0.5 g dye in 1000 ml DI water. Then accurate volumes of the two dyes stock solution were transferred into 10 mL volumetric flasks and diluted to prepare standard dye solution with different concentration.

To study the effect of pH on the adsorption performance. the pH values of dye solution were adjusted to 3,5,7,9 by 0.1 M HCl and 0.1 M NaOH aqueous solutions. The standard MB and MO solutions with different pH values were scanned by UV-vis spectrophotometer in the range of 400-700 nm and the wavelength of maximum adsorption (λ_{max}) for the two dyes were determined at first. Calibration curve for two model dyes were obtained by plotting absorbance at λ_{max} against concentration of dyes with different pH values and summarized in Table 2.

Table 2 Spectrophotometric method for the determination of prepared standards of model dyes

Model Dye	pH	λ_{max} (nm)	Regression equation	Regression coefficient (R^2)
MB	3	663	A=0.20223C+0.10661	0.9961
	5	662	A=0.21288C+0.04886	0.9979
	7	664	A=0.17907C+0.15021	0.9966
	9	664	A=0.20301C+0.04550	0.9993
MO	3	506	A=0.11732C+0.11010	0.9999
	5	466	A=0.08051C+0.11569	0.9990
	7	466	A=0.07938C+0.11866	0.9999
	9	467	A=0.07983C+0.11859	0.9997

A stands for Absorbance; C stands for concentration

3.1.1 Study of key factors

The effect of contact time was studied at first to determine the contact time required to reach equilibrium. Typically, aliquot of 0.1 g L^{-1} three adsorbents were added into 1 ml of dye solutions with the initial concentration (10 mg L^{-1}) at neutral pH (pH=7) and shaken in a water-bath oscillator at 20 ℃ with a speed of 150 rpm. After defined time intervals, adsorbents were separated with a hand-hold magnet and the absorbance of residual dyes in the supernatant were determined by UV-vis based on the obtained calibration curve.

The effect of pH was studied by adding 0.1 g L^{-1} of three adsorbents to 1 ml 10 mg L^{-1} dye solutions with pH of 3,5,7,9, then shaken in a water-bath oscillator for 3 h at 20 ℃ with a speed of 150 rpm.

To study the effect of adsorbents mass, three adsorbents with dosage of 0.05, 0.1 0.2 and 0.3 g L^{-1} were added to 1 mL 10 mg L^{-1} dye solution. The pH was adjusted to pH=9 for MB and pH =3 for MO, shaken in a water-bath oscillator for 3h at 20 ℃ with

a speed of 150 rpm. Adsorption capacity (q_e) and removal efficiency (E) were then calculated to determine the optimal adsorbents mass.

$$q_e = \frac{(C_0 - C_e) \times V}{m} \quad (1)$$

$$E = \frac{C_0 - C_e}{C_0} \times 100\% \quad (2)$$

where C_0 and C_e (mg L^{-1}) are the initial and equilibrium concentration of MB and MO. V (ml) is the volume of the MB and MO aqueous solution, m (mg) is the dosage of the adsorbents, q_e (mg g^{-1}) is adsorption capacity at equilibrium state.

3.1.2 Adsorption isotherm

For adsorption isotherm, the experiment was conducted by adding 0.1g L^{-1} of all the three adsorbents into two model dyes with the concentrations in the range of 5-50 mg L^{-1} and pH of 3,5,7 and 9, then shaken for in a water-bath oscillator for 3h at 20°C with a speed of 150 rpm. After equilibrium, the adsorption capacity (q_e, mg g^{-1}) was determined according to equation (1), and plotted against the initial concentration (C_0, mg L^{-1}) of dyes.

3.1.3 Adsorption kinetics

The kinetic study was performed by shaking dyes solution MB (pH=9) and MO (pH=3) and at 10 mg L^{-1} with 0.1 g L^{-1} of all the three adsorbents for different time intervals (20-180 min). After each time interval, the concentration of dye was measured by UV-vis. The adsorption capacity at each time interval was determined by the following equation,

$$q_t = \frac{(C_0 - C_t) \times V}{m} \quad (3)$$

where C_0 and C_t (mg L^{-1}) are the initial and residual concentration of MB and MO at time t. V (ml) is the volume of the MB and MO solution, m (mg) is the weight of the adsorbents, q_t (mg g^{-1}) is the adsorption capacity at time t.

3.1.4 Adsorption thermodynamics

For the adsorption thermodynamic studies, the experiment was conducted by shaking 1 ml 10 mg L^{-1} MB (pH=9) and MO (pH=3) aqueous solutions with 0.1 g L^{-1} of all the three adsorbents in a water-bath oscillator at 20, 30 and 40℃ for 3h with a speed of 150 rpm.

3.1.5 Simultaneous adsorption of cationic and ionic dyes

The adsorption experiments were carried out by adding 0.1g L^{-1} of three adsorbents into 1ml binary solutions of MB and MO (C_{MB}=C_{MO}=10 mg L^{-1}) with the volume ratio of 1:1 at pH 3, 7 and 9. Then the above mixtures were shaken in a water-bath oscillator for 3h at 20℃ with a speed of 150 rpm.

3.1.6 Step-by-step adsorption of cationic and ionic dyes

The adsorption experiment was conducted by firstly adding 10 mg of each adsorbent into 10 ml MB solution (pH=9) with concentration of 10 mg L^{-1}, the mixture was shaken for 3h 20℃ with a speed of 150 rpm. The dye-loaded adsorbents were then shaken with 10 ml of 50% (v/v) ethanol and 50% (v/v) 0.1 M HCl for 3h at 20℃ with a speed of 150 rpm separately. Followed by collected with magnet and rinsed with DI water for 3 times. After this, the adsorbents were added into 10 ml MO solution (pH=3) with concentration of 10 mg L^{-1}, the mixture was shaken for 3h 20℃ with a speed of 150 rpm. The dye-loaded adsorbents were then shaken separately with 10 ml of 50% (v/v) ethanol and 50% (v/v) 0.1 M NaOH for 3h 20℃ with a speed of 150 rpm.

3.1.7 Regeneration study

The regeneration behavior of adsorbents was studied by five successive step-by-step adsorption/desorption cycles for MB and MO in turns. In each cycle, the procedure was conducted following the above-mentioned method in step-by-step adsorption. After each cycle, the adsorbents were washed with DI water for 3 times followed by collected with a magnet and used for next adsorption-desorption cycle.

3.2 Results and Discussion

3.2.1 Effect of contact time

The effect of contact time on the adsorption for model dyes was studied to determine the time that reach adsorption equilibrium. This was carried out by using 0.1g L^{-1} adsorbents to remove 10 mg L^{-1} dye solutions at neutral pH, the adsorption capacity of three prepared adsorbents at each time interval was shown in Fig 3.1 respectively. For adsorption of MB and MO, within the first 20 min, the fast adsorption could be seen for all the three adsorbents, which was due to the enough available adsorption sites on the surface of adsorbents and the fast diffusion from adsorbate dye molecules for the adsorbents driven by the high concentration at the early stage of adsorption process. Further increase in the contact time, the slow increase in adsorption capacity of adsorbents could be observed, this is mainly because the available adsorption sites were occupied by dye molecules gradually and the concentration of dye decrease results in the driving force of diffusion decrease. And the adsorption capacity of MPDA/Mag/PDA/PEI was higher than those of PDA-NT/Mag/PDA/PEI and HPDA/Mag/PDA/PEI. The experiment time was extended to 220 min, and it shown that the adsorption capacity reach equilibrium after 180 min. While the adsorption capacity of MO was much lower than that of MB, which is due to the pH effect, as when the pH reaches 7, the surface charge of all the three adsorbents turn to negative (Fig 2.7), there occurs the electrostatic repulsion between negatively charged adsorbent and anionic dye MO. This indicates that 180 min (3hr) is an optimal contact time and was applied in this work.

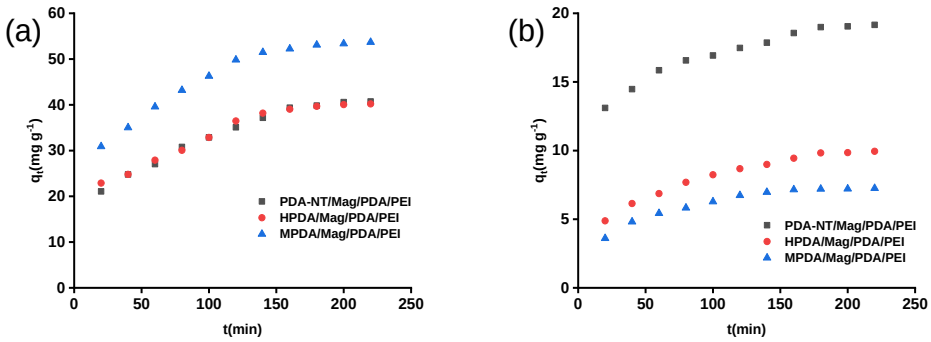

Figure 3.1 Effect of contact time on the adsorption capacity q_t (mg g^{-1}) of (a) MB; (b) MO. Adsorbents: 0.1 g L^{-1}, dyes: 10 mg L^{-1}; pH=7; temperature: 20^{o}C.

3.2.2 Effect of pH

The pH is a very important factor for dye adsorption process. As it will control the magnitude of electrostatic charges provided by the ionized dye molecules, on the other hand the surface charge of adsorbents also vary with the pH of an aqueous medium which was discussed in charpter 2. As Fig 3.2(a) show, for cationic dye MB, the adsorption capacity increase with pH and reaching its maxmium at pH 9, low adsorption capacity was observed at low pH values 3 and 5. This was ascribed to the presence of H^+ ions in low pH dye solution will compete with cationic MB molecule and consume available adosoprtion sites , on the other hand the surface of adsorbents were in the state of positively charged at low pH, which occurs the electrostatic repulsion between cationic dyes molecules and positive charged adsorbents surface. The increase of adsorption capacity with the increasing of pH may attribute to the presence of O^- in PDA molecules could interact with N^+ in MB dye molecules through electrostatic interactions, [106,107] which contribute to the adsorption for MB. Besides, in alkaline conditions the cation MB and OH^- in medium could co-adsorb, resulting in the amount of adsorbed MB increase. Therefore, neutral and alkaline conditions are conducive to the adsorption of MB.

For MO, shown in Fig 3.2(b) the adsorption capacity was high in acidic dye solution and significantly decrease with the increase of pH. This can be attribute to the groups of NH_2^+ in PEI segement were deprotonated and the surfaces of adsorbents will become negative as the pH increase, which weaken the electrostatic interactions with

SO_3^- in MO molecules. These results indicate that acidic environment favors the adsorption for anionic dye and alkaline condition is conducive to the adsorption of cationic dyes.

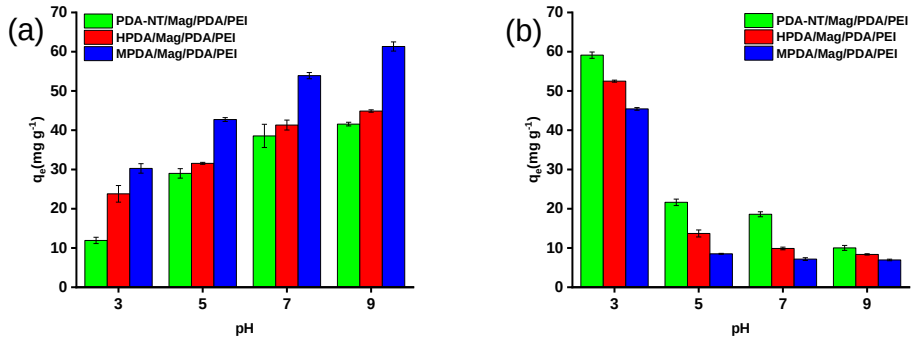

Figure 3.2 Effect of pH on the adsorption capacity q_e (mg g^{-1}) of (a) MB and (b) MO. Adsorbents: 0.1 g L^{-1}, dyes: 10 mg L^{-1}; temperature: 20°C; time: 3 hr.

3.2.3 Effect of adsorbent dosage

Mass of dsorbent effect was studied to determine the adsorption capacity for dye solutions with certain initial concentration. Both the removal efficiency and adsorption capacity of three adsorbents of MB and MO was studied. The removal efficiency increased with the adsorbent dosage could be observed from Fig 3.3(b) and (d), this is mainly due to the increase in available sites on adsorbents that contribute to the adsorption for dyes.While, Fig 3.3(a) and (c) show that adsorption capcity decrease as adsorbent dosage increase may ascribe to the aggregation of adsorbents, which in turn reduced available binding sites per mass of adsorbents. For the removal efficiency, when 0.1g L^{-1} of the three adsorbents were employed, it could reach 57.3%-65.6% for MO and 30.2% -85% for MB, and the adsorption capacity is 57-63 mg g^{-1} for MO and 39-80 mg g^{-1} for MB. 0.1g L^{-1} adsorbents is selected as the adsorbent dosage for the further study since it present high adsorption capacity and desired removal efficiency.

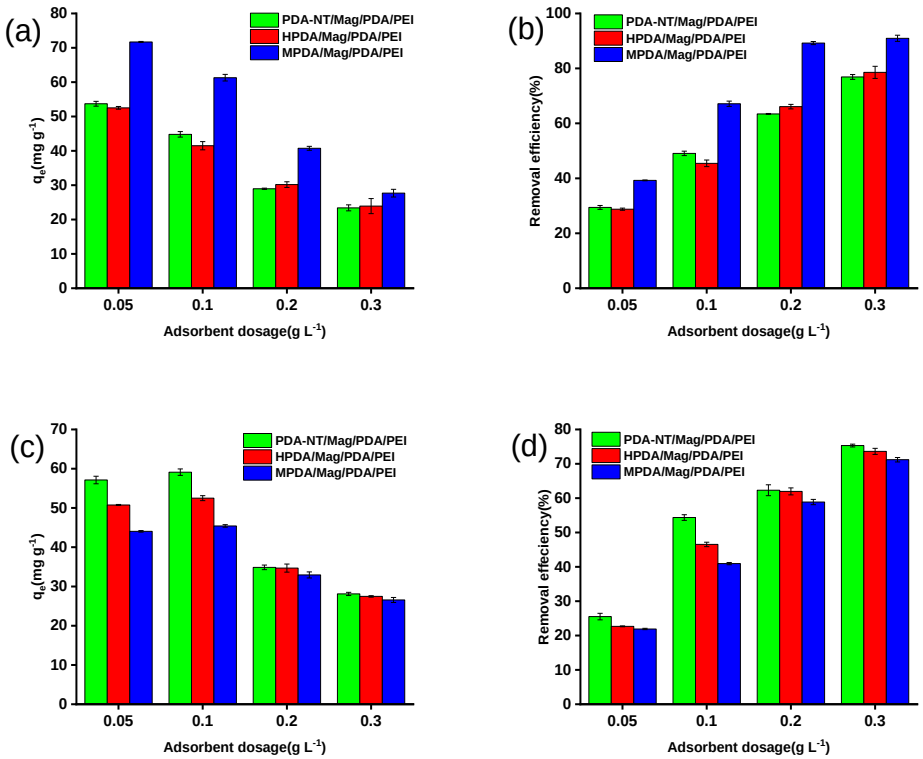

Figure 3.3 Effect of adsorbent mass on adsorption capacity q_e and the removal efficiency of dyes (a) and (b) MB (pH=9) ; (c) and (d) MO (pH=3). Dyes:10 mg L^{-1}; temperature : 20°C; time: 3hr.

3.2.4 Adsorption kinetics

Adsorption kinetic performance of the adsorbents is of great importance to be studied for a better understanding of the adsorption mass transfer mechanism, evaluate the adsorption performance and the pilot application of the adsorbents. Therefore, adsorption kinetics modeling is used to find the appropriate adsorption rate expression for the adsorption system and calculate the adsorption rate during the adsorption process. Typically, these mathematical models could be classified as adsorption diffusion models and adsorption reaction models.[108] The adsorption diffusion models are generally dependent on the steps occurring during adsorption as follows: [109]

(a) Bulk diffusion: adsorbate diffusion from the bulk solution to the liquid film surrounding the adsorbent particles.

(b) External or film diffusion: the diffusion take place across the liquid film surrounding adsorbent.

(c) Internal or intraparticle diffusion: the diffusion in the liquid contained within pores and along the pore walls.

(d) Mass action: the adsorption and desorption take place between the active sites of the adsorbents and the adsorbate.

The adsorption reaction models are based on chemical reaction kinetic models and take the entire adsorption process as a whole and do not consider the different steps involved. For the adsorption reaction models, the Pseudo first-order model and Pseudo second-order model were used to study adsorption kinetics. Lagergren [110] presented a first-order rate equation to describe the kinetic process of oxalic acid and malonic acid onto charcoal, this rate equation has been called pseudo-first-order (PFO) model. [111] It assumes that the rate of change of solute uptake with time is directly proportional to difference in saturation concentration and the amount of solid uptake with time, which is generally applicable over the initial stage of an adsorption process. It is commonly observed that kinetics follows this pseudo-first-order rate equation when adsorption occurs through diffusion through the interface. The pseudo-second-order (PSO) kinetic model [111] is based on the assumption that the rate of adsorption of solute is proportional to the available sites on the adsorbent. [112] The driving force (q_e-q_t) is proportional to the number of active sites on the surface of adsorbent. In this condition, the adsorption rate is dependent on adsorption capacity not on concentration of adsorbate. PSO model assumes that the process is controlled by the adsorption reactions at the liquid/solid interface in the adsorbent. Besides, Zhang [113] suggested that the conditions for the PFO models are: the first one is the value of initial dye concentration is high; second, the adsorption process is in the initial stage; third one is that the adsorbent has a few actives sites. And for PSO model, Guo [114] concluded that the PSO model could represent three conditions: the first one is that the initial dye concentration is low; second is at the final stage of the adsorption process; third one is that the adsorbent is abundant with active sites. To calculate the model parameters, the linearized form of two models were given by,

$$\ln(q_e - q_t) = \ln q_e - k_1 t \qquad (4)$$

$$\frac{t}{q_t} = \frac{1}{k_2 q_e^2} + \frac{t}{q_e} \quad (5)$$

where k_1 (min^{-1}) is the adsorption rate constant of the pseudo-first-order model and k_2 ($g \cdot mg^{-1} \cdot min^{-1}$) is adsorption rate constant of the pseudo-second order, they could be calculated by the slope and intercept of In (q_e-q_t) vs t and t/q_t vs t, respectively.

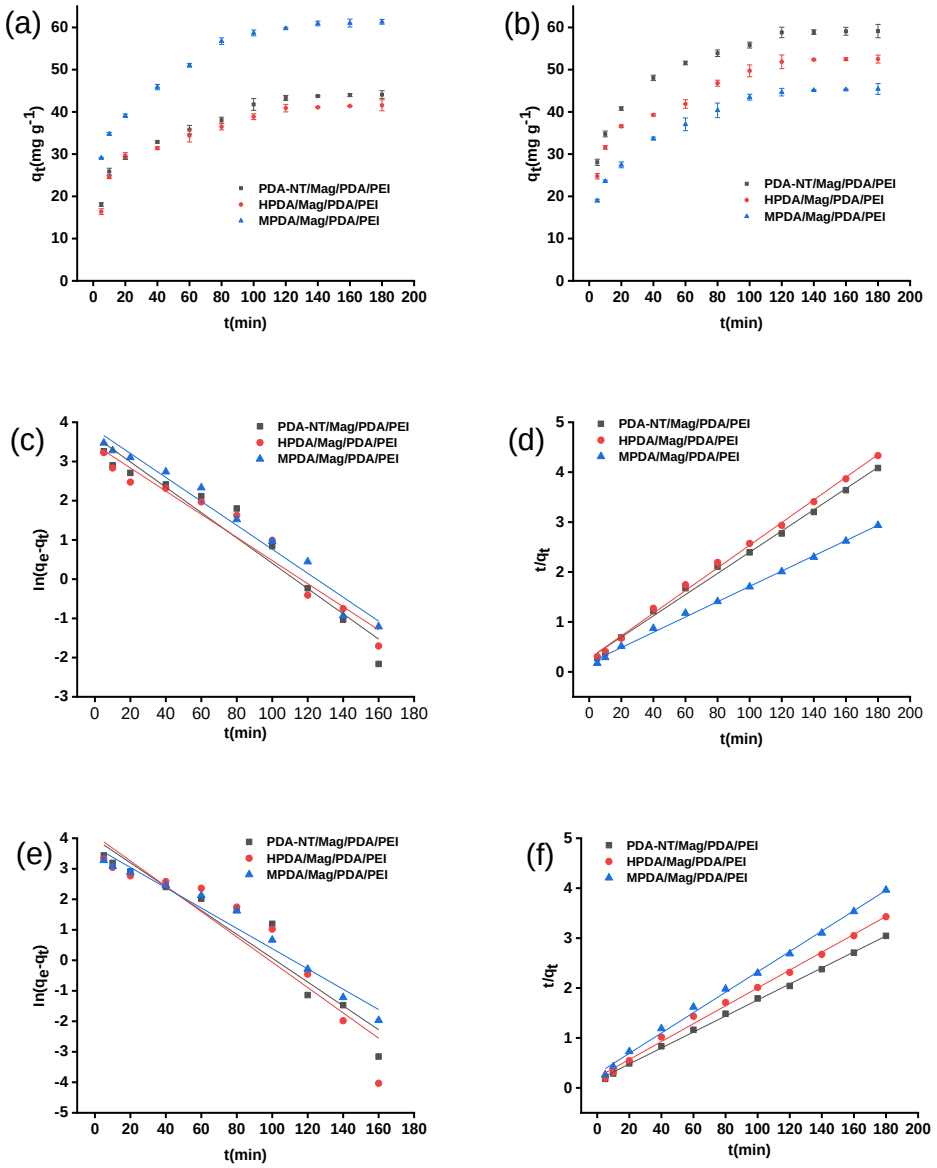

Figure 3.4 The effect of time on adsorption capacity of (a) MB and (b) MO; (c) PFO for adsorption of MB; (d) PSO for adsorption of MB; (e) PFO for adsorption of MO; (f) PSO model for adsorption of MO.

Table 3 Parameter of PSO and PFO models for the adsorption of dyes

Dye	Adsorbents	q_e(exp)	Pseudo 1st order	Pseudo 2nd order

		($mg\,g^{-1}$)	q_e(cal) ($mg\,g^{-1}$)	K_1 (min^{-1})	R^2	q_e(cal) ($mg\,g^{-1}$)	K_2 ($g\,mg^{-1}\,min^{-1}$)	R^2
MB	PDA-NT/Mag/PDA/PEI	44.08	37.88	0.03228	0.9461	47.06	$1.66*10^{-3}$	0.9960
	HPDA/Mag/PDA/PEI	41.55	30.71	0.02949	0.9542	44.05	$1.92*10^{-4}$	0.9970
	MPDA/Mag/PDA/PEI	61.32	45.41	0.03054	0.9759	65.27	$1.31*10^{-3}$	0.9971
MO	PDA-NT/Mag/PDA/PEI	59.12	53.39	0.04272	0.9260	62.38	$1.64*10^{-3}$	0.9987
	HPDA/Mag/PDA/PEI	52.50	59.73	0.04153	0.8862	55.83	$1.52*10^{-3}$	0.9977
	MPDA/Mag/PDA/PEI	45.42	40.91	0.03322	0.9695	48.97	$1.47*10^{-3}$	0.9969

Fig 3.4 (a) and (b) show the effect of contact time on the adsorption capacity of three adsorbents for MB and MO with the initial concentration of 10 mg L^{-1} at 20°C under the pH that has the highest adsorption capacity for MB and MO. It shows that the adsorption capacity increased significantly within the first 20 min. Further increase in contact time was accompanied by slow increase in the adsorption capacity of adsorbents and the curve reach plateau around 120 min. The experiment data was then fitted by PFO and PSO model respectively, and the kinetics model parameters were calculated and listed. The result presented in Table 3 shows that the linear correlation coefficient (R^2) of all the PSO model is larger than that of the PFO model. Besides, the calculated adsorption capacity at equilibrium $q_{e,cal}$ obtained from PSO model is closer to the q_e obtained from experiment comparing to that of PFO model. This result shows the PSO model is applicable to describe the adsorption process of all the three adsorbents for MB and MO, indicating that there are abundant active sites contribute to the adsorption of MB and MO, and the adsorption process is controlled by the interaction between active sites and adsorbate.

To confirm the interactions between dye molecules and adsorbents and explore the adsorption mechanism. The UV-Vis adsorption spectra of MB, MO, pristine PDA-NT/Mag/PDA/PEI, HPDA/Mag/PDA/PEI, MPDA/Mag/PDA/PEI, and after adsorption for MB and MO, which were named as PDA-NT/Mag/PDA/PEI-MB and PDA-NT/Mag/PDA/PEI-MO respectively were measured and presented in Fig 3.5. As the adsorbents were rinsed by DI water for at least three times to reduce the interference effect of dye residues, the characteristic absorbance peak (293 nm, 665 nm for MB, 509 nm for MO) of both MB and MO occurs on the spectra of three adsorbents after

adsorption compared with that of pristine adsorbents, confirmed the interactions between dye molecules and adsorbents.

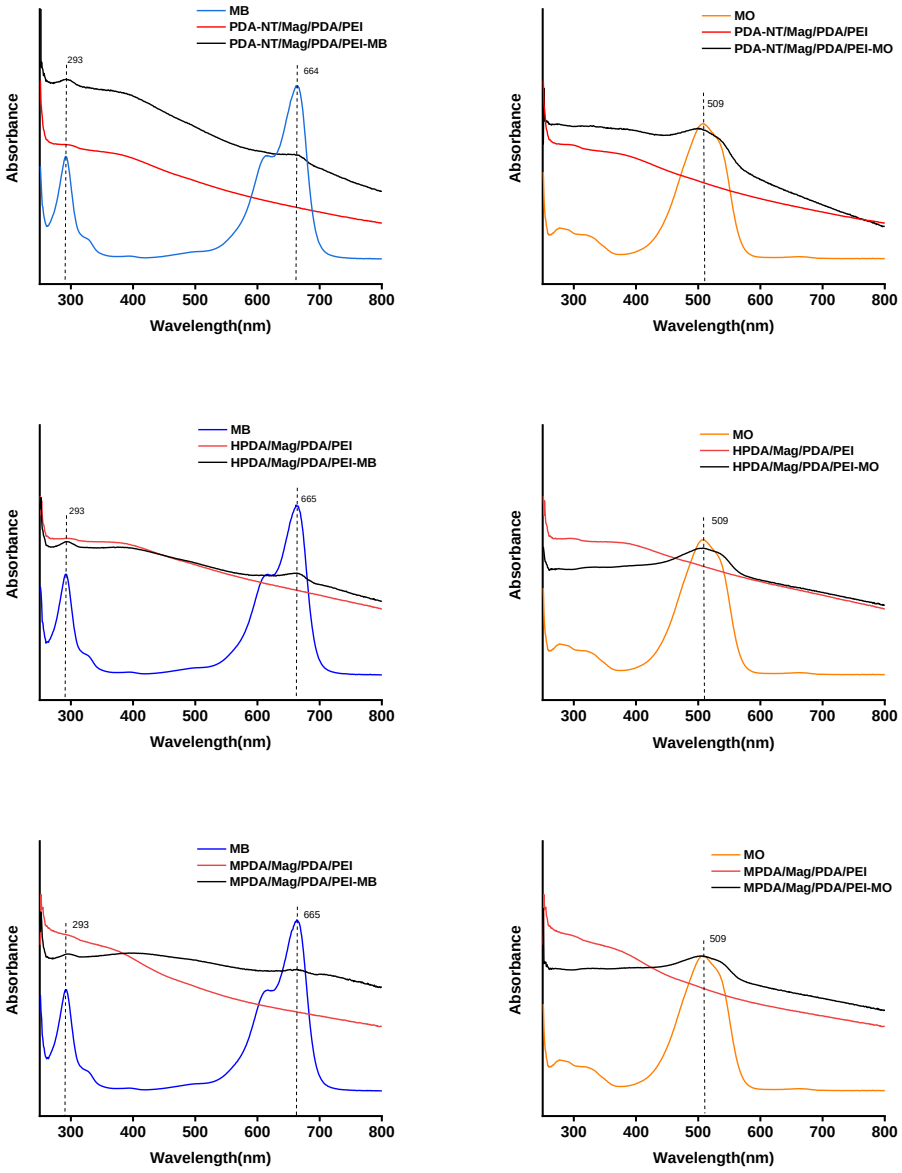

Figure 3.5 UV-Vis adsorption spectra of dyes, adsorbents before and after adsorption.

It is essential to investigate the adsorption mechanism of adsorbents for understanding the properties and the adsorption. The hypothesis of the adsorption for MB and MO by as-prepared PDA-based absorbents is a process with multiple synergistic interactions including hydrogen bonding, π-π interactions and electrostatic interactions. [115] The external surface is PDA/PEI layer that contribute to the adsorption for MO, and the PDA internal surface provides active sites for MB (Fig 3.6). The FT-IR spectra shows massive hydroxyl and amino groups on the surface of adsorbents (Fig

2.4), which will form hydrogen bonds to promote the adsorption of MB and MO. Moreover, π-π interactions between the aromatic rings of PDA-based adsorbents and the aromatic rings of MB and MO molecules also contribute to the adsorption of MB and MO from water. The kinetic analysis study by PFO and PSO models indicates that the adsorption process is controlled by the interaction between active sites and adsorbate. It implies that the electrostatic interactions between the NH_2^+ groups on the surface of adsorbents and the SO^{3-} within the MO molecules attribute to the adsorption of MO on absorbents, and the electrostatic interactions between O^- in adsorbent and N^+ within the MB molecules. [90]

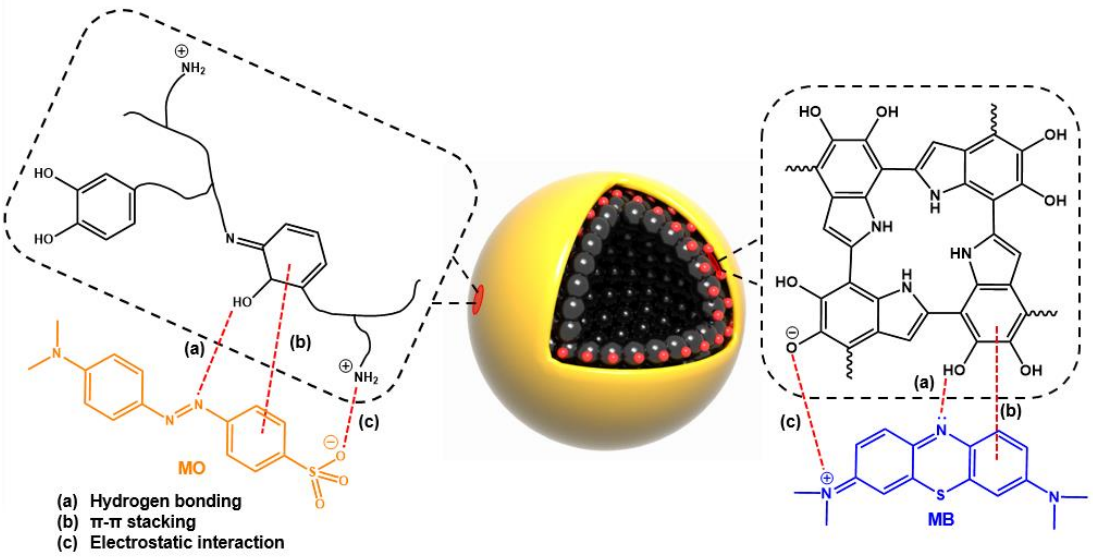

Figure 3.6 Schematic illustration of the possible adsorption mechanism between MPDA/Mag/PDA/PEI with MB and MO.

Though the PSO model could describe the adsorption experiment data appropriately, it is inadequate to reveal the adsorption mechanism. Herein, Weber-Morris intraparticle diffusion model [116] was employed to investigate the rate-limiting step in the adsorption process. The intraparticle diffusion model is presented as follows:

$$q_t = K_i t^{\frac{1}{2}} \tag{6}$$

where K_i (mg g $^{-1}$ min ^{½}) is the rate constant.

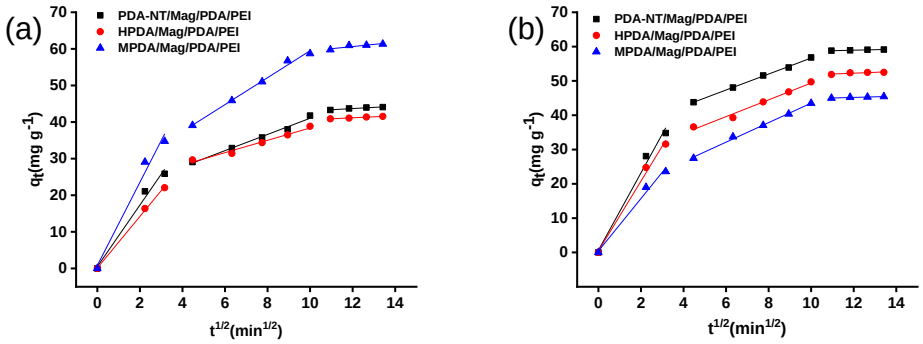

Figure 3.7 Fitting plot of adsorption for (a) MB; (b) MO by intraparticle diffusion model.

As seen from the fitting curve in Fig 3.7, the plot was not linear over the whole-time range and could be fitted into three discrete linear regions corresponding to the three steps in the adsorption process respectively. The parameters calculated according to the intraparticle diffusion model were listed in Table 4, of which K_{i1} corresponds to the diffusion occurs from the bulk solution to the external surface of adsorbents including the bulk diffusion of solute adsorbate to the liquid film surrounding the adsorbent and across the liquid film surrounding adsorbents, and the driving force is the concentration difference between the bulk solution and the surface of the adsorbents. K_{i2} refers to the intraparticle diffusion of dye molecules along liquid filled in the pores of adsorbents and/or the surface of adsorbent. K_{i3} is attribute to the final tedious adsorption equilibrium stage as the intraparticle diffusion started to slow down due to lower concentration of adsorbate left in the solution. The values of K_i indicate the first portion of the curve, which is the diffusion in bulk phase to the external surface of adsorbents is the fastest. And the second portion is the rate-limiting step as the lower value of K_{i2}, except for the third portion, which is a dynamic equilibrium between adsorption and desorption. While the intraparticle diffusion is not the only rate-limiting step, as the plot of q_t vs $t^{1/2}$ does not pass through the origin, the boundary layer diffusion also contributes to the adsorption to some degree and could be express by the C value listed in Table 4. The larger value of C means the greater boundary layer effect contribute to the adsorption. It worth noting that the K_{i2} value of MPDA/Mag/PDA/PEI is significantly larger than that of the other two adsorbents, which indicates the mesoporous structure will enhance the intraparticle diffusion of adsorbate along the

porous structure. This also prove the hypothesis that inner PDA surface contribute to the adsorption of MB and PDA/PEI surface contribute to the adsorption of MO.

Table 4 Parameters of intraparticle diffusion kinetics model for adsorption of dyes

Dye	Adsorbents	K_{i1} (mg g^{-1} min$^{1/2}$)	C_1 (mg g^{-1})	R^2	K_{i2} (mg g^{-1} min$^{1/2}$)	C_1 (mg g^{-1})	R^2	K_{i3} (mg g^{-1} min$^{1/2}$)	C3 (mg g^{-1})	R^2
MB	PDANT/Mag/PDA/PEI	7.6869	0.18	0.9980	2.2122	18.92	0.9881	0.3218	39.83	0.9439
	HPDA/Mag/PDA/PEI	7.0424	0.14	0.9985	1.6889	21.50	0.9775	0.2780	37.83	0.9913
	MPDA/Mag/PDA/PEI	11.3653	0.83	0.9817	3.6761	22.72	0.9923	0.5895	53.56	0.9183
MO	PDANT/Mag/PDA/PEI	11.2858	0.64	0.9888	2.3316	33.34	0.9985	0.1399	57.27	0.9536
	HPDA/Mag/PDA/PEI	10.1828	0.45	0.9932	2.4425	24.93	0.9836	0.2505	49.24	0.9143
	MPDA/Mag/PDA/PEI	7.6483	0.42	0.9893	2.8423	15.10	0.9965	0.1726	43.12	0.9413

3.2.5 Adsorption isotherm

Studying the adsorption mechanisms is of great importance to developing adsorbents and adsorption systems. Adsorption isotherm models are designed to describe the interaction mechanisms between adsorbent and adsorbate at constant temperature for sufficient time, and the interface concentration. Furthermore, modeling of adsorption equilibrium data is a very important way for predicting and investigating the adsorption mechanisms of different adsorption systems. Adsorption isotherm refers to the relationship between the equilibrium adsorbate concentrations in the liquid-phase and the equilibrium adsorption amount on the solid-phase at a certain temperature. The initial dye concentration for adsorption isotherm study was in the range of 5 mg L^{-1} to 50 mg L^{-1}. [117] Recently, linear regression analysis has been a generally acknowledge method for determining the best fitting model since it analyzes the adsorption system and verifies the consistency of theoretical assumptions of adsorption isotherm model [118]. In this work, five models including Langmuir, [119] Freundlich, [120] Temkin, [121] Dubinin-Radushkevich, [122] and Harkin-Jura [123] model were used to understanding and interpretation of adsorption isotherms. Additionally, the effect of pH has also been considered in the isotherm study according to the pH effect result since the adsorption performance is highly depended on pH. Based on the study by different isotherm model, the parameters in each model could provide information about the surface properties

and the degree of affinity between adsorbate and adsorbent, which are conducive to the study of adsorption mechanisms.

The relationship between adsorption capacity and initial dye concentration at different pH was presented in Fig 3.8. It shows that the adsorption capacity varies under different pH, for MB, the adsorption capacity increase with pH, while for MO, the adsorption capacity decreases with pH, which is consistent with the pH effect result. And the highest adsorption capacity that obtained by the adsorption equilibrium data among three adsorbents are 140.6 and 198.7 mg g^{-1} for MB and MO, respectively. The adsorption capacity increased with initial concentration under all pH value is mainly because that the adsorbed dye molecules did not occupy all the active sites on adsorbents, resulting in the lower adsorption capacity. While for the higher concentrations, the concentration difference between dye solution and adsorbents will be higher and produce greater driving force that enhance the interaction between dye molecules and active sites on adsorbents. Therefore, the adsorption capacity would reach equilibrium and maximum value at higher concentration.

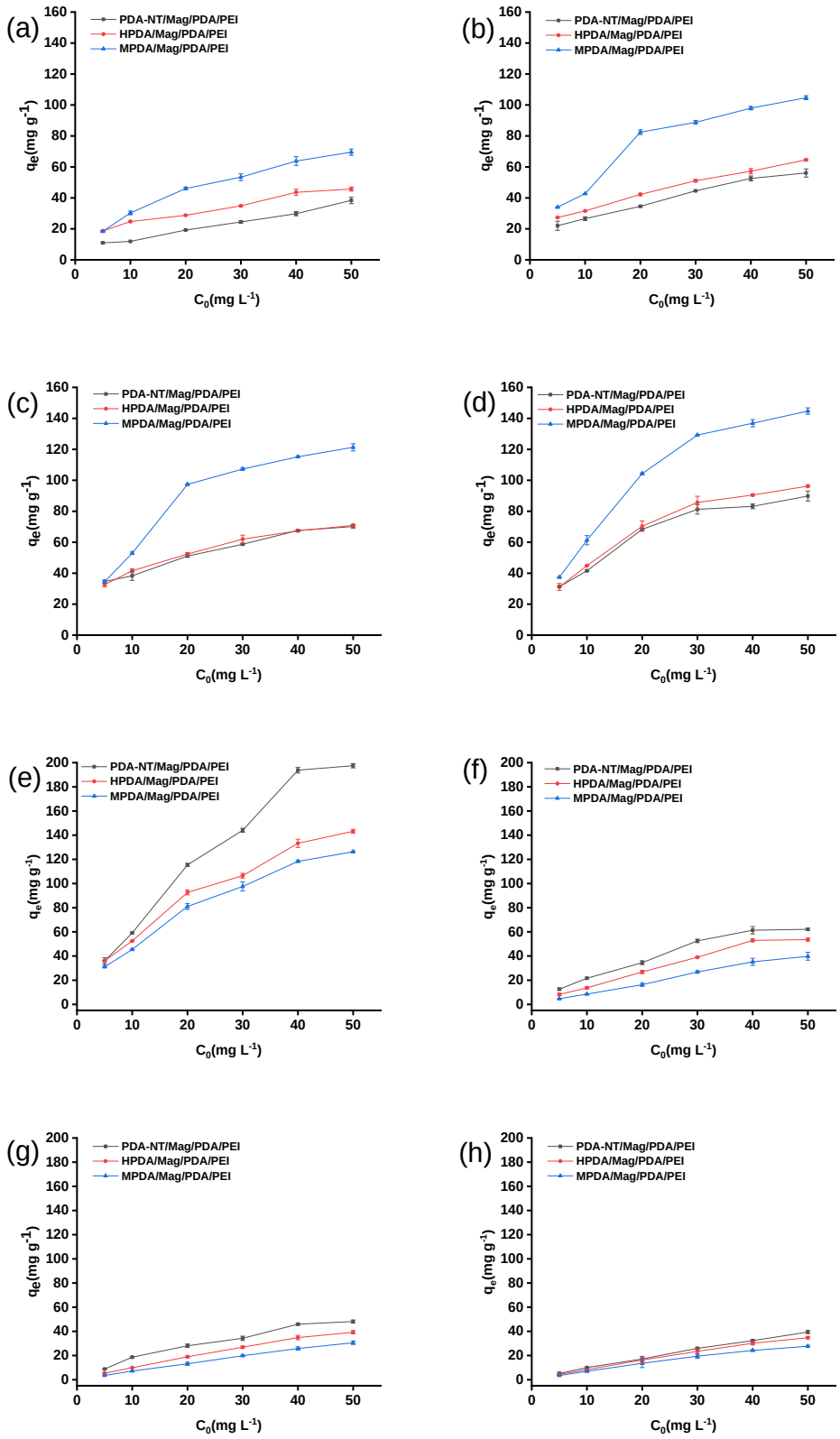

Figure 3.8 Adsorption isotherms for the adsorption of MB and MO on three adsorbents at different pH. (a) MB, pH=3 ;(b) MB, pH=5; (c) MB, pH=7; (d) MB, pH=9; (e) MO, pH=3; (f) MO, pH=5; (g)MO, pH=7; (d) MO, pH=9.

Langmuir isotherm model based on the assumption that the surface is homogeneous, and the process is monolayer adsorption. All sites are energetically equivalent, and the energy of adsorption is equal for all sites. Besides each site can hold at most one molecule, and no interactions between adsorbate molecules on adjacent sites. [124] The general form of the Langmuir mode eqn (7) and linearized form eqn (8) were shown as follows,

$$q_e = \frac{Q_0 K_L C_e}{1 + K_L C_e} \tag{7}$$

$$\frac{C_e}{q_e} = \frac{C_e}{Q_0} + \frac{1}{K_L Q_0} \tag{8}$$

where C_e (mg L^{-1}) is the equilibrium concentration of MB and MO, q_e (mg g^{-1}) is adsorption amount at equilibrium state, K_L (L mg^{-1}) refers to the Langmuir adsorption constant. Q_0 (mg g^{-1}) refers to the theoretical maximum adsorption capacity. The values of K_L and Q_0 were obtained from the slope and intercept of the plot of C_e/q_e vs C_e for the three adsorbents respectively.

Furthermore, the separation factor (R_L) [125] is defined as a dimensionless constant that present as following:

$$R_L = \frac{1}{1 + K_L C_0} \tag{9}$$

Where, C_0 (mg L^{-1}) is the initial concentration of the adsorbate. And nature of the adsorption process could be determined by the separation factor. R_L=1, linear; R_L=0, irreversible; R_L>1, unfavorable and 0<R_L<1, favorable.

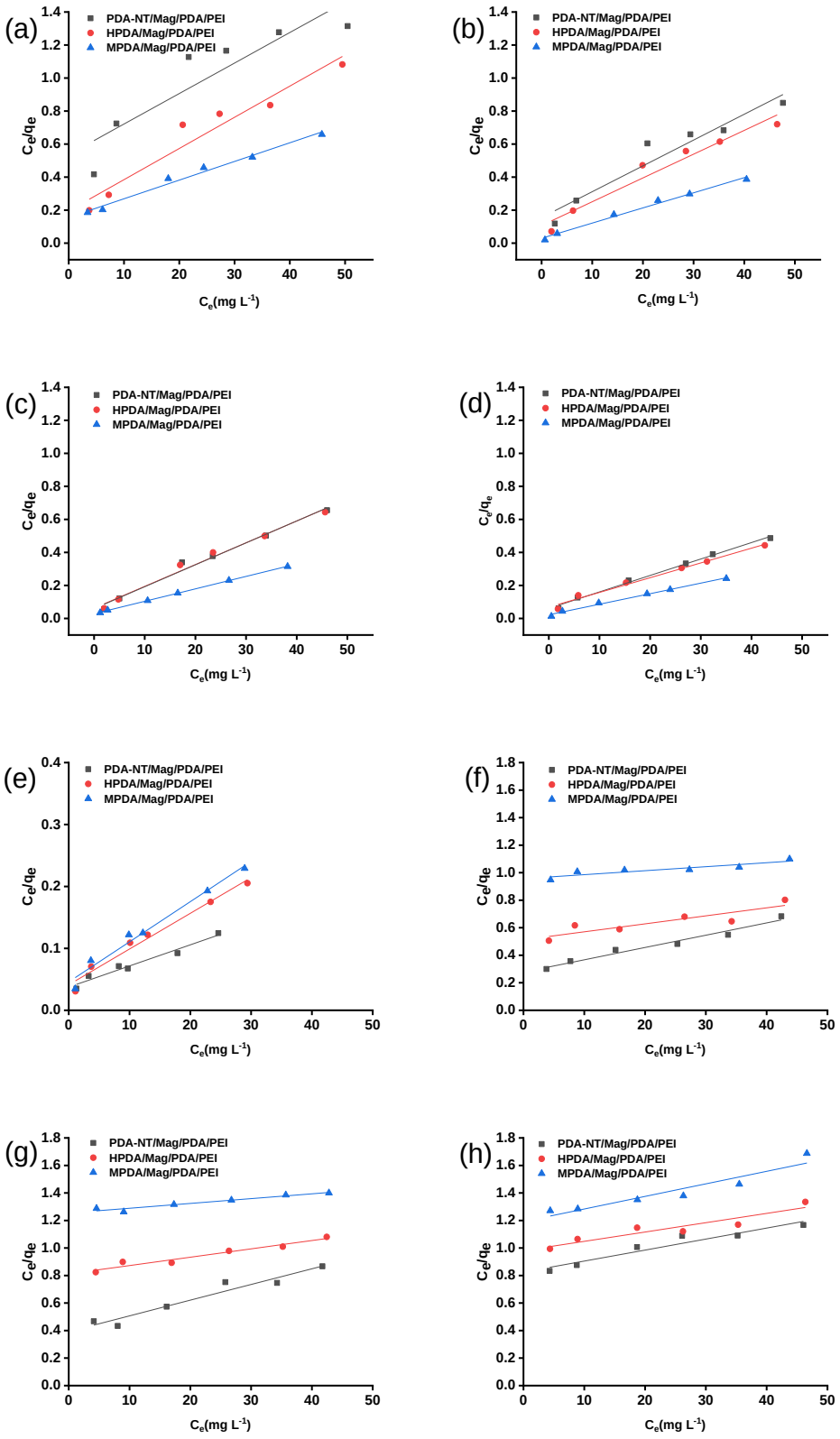

Figure 3.9 Langmuir isotherm fitting for the adsorption of MB and MO on three adsorbents at different pH. (a) MB, pH=3 ;(b) MB, pH=5; (c) MB, pH=7; (d) MB, pH=9. (e) MO, pH=3; (f) MO, pH=5; (g)MO, pH=7; (d) MO, pH=9.

Table 5 Parameters of adsorption isotherms using Langmuir model for three adsorbents at different pH

Dye	pH	Adsorbent	Q_0 (mg g^{-1})	K_L (L mg^{-1})	R^2	R_L
MB	3	PDA-NT/Mag/PDA/PEI	54.14	0.0344	0.8023	0.3263
		HPDA/Mag/PDA/PEI	52.96	0.0963	0.9420	0.1475
		MPDA/Mag/PDA/PEI	88.49	0.0724	0.9847	0.1871
	5	PDA-NT/Mag/PDA/PEI	63.94	0.1006	0.9318	0.1421
		HPDA/Mag/PDA/PEI	69.44	0.1347	0.9532	0.1101
		MPDA/Mag/PDA/PEI	108.93	0.3073	0.9905	0.0514
	7	PDA-NT/Mag/PDA/PEI	75.30	0.2224	0.9856	0.0697
		HPDA/Mag/PDA/PEI	75.75	0.2113	0.9859	0.0731
		MPDA/Mag/PDA/PEI	132.62	0.2623	0.9997	0.0597
	9	PDA-NT/Mag/PDA/PEI	100.40	0.1627	0.9945	0.0929
		HPDA/Mag/PDA/PEI	111.98	0.1303	0.9869	0.1133
		MPDA/Mag/PDA/PEI	156.25	0.2861	0.9944	0.0550
MO	3	PDA-NT/Mag/PDA/PEI	255.75	0.1045	0.9619	0.1375
		HPDA/Mag/PDA/PEI	173.31	0.1400	0.9757	0.1064
		MPDA/Mag/PDA/PEI	154.08	0.1419	0.9759	0.1051
	5	PDA-NT/Mag/PDA/PEI	111.85	0.0127	0.8245	0.5662
		HPDA/Mag/PDA/PEI	172.11	0.0113	0.7915	0.5950
		MPDA/Mag/PDA/PEI	344.82	0.0030	0.8227	0.8461
	7	PDA-NT/Mag/PDA/PEI	87.64	0.0290	0.9406	0.3646
		HPDA/Mag/PDA/PEI	165.01	0.0074	0.9484	0.6907
		MPDA/Mag/PDA/PEI	285.71	0.0028	0.9398	0.8565
	9	PDA-NT/Mag/PDA/PEI	125.15	0.1627	0.9300	0.6325
		HPDA/Mag/PDA/PEI	147.71	0.1303	0.8790	0.7071
		MPDA/Mag/PDA/PEI	109.64	0.2861	0.8977	0.7854

From the adsorption isotherm parameters that listed in Table 5, it could be found that the Q_0 value for MB that calculated by applying Langmuir isotherm model is much closer to the experimental data that obtained by the adsorption isotherm than the Q_0 value for MO. This may be due to -C=N in MB molecules may only bind to -OH in the catechol groups of PDA through hydrogen bonding and electrostatic interaction, so the surface for the adsorption for MB could be considered as homogeneous surface. While, for MO, -N= may bind to the -OH in PDA and SO_3^- may interact with $-NH_2^+$ in PEI segment through hydrogen bonding and electrostatic interaction, which is considered as heterogeneous surface. [90] Moreover, for the separation factor that listed in Table 5 are all in the range of 0 to 1, it reveals that adsorption for MB and MO are favorable.

Unlike the Langmuir model that restricted to the monolayer of adsorbate on adsorbent forms. The equation of Freundlich isotherm model presumes that the multilayer of the adsorption process occurs on a heterogeneous surface, and interactions

between adsorbed molecules results in the available sites with a heterogeneous energetic distribution, which contribute to the adsorption simultaneously. The general form of Freundlich model and linearized form were presented as follows,

$$q_e = K_F C_e^{1/n} \tag{9}$$

$$\ln q_e = \ln K_F + \frac{1}{n} \ln C_e \tag{10}$$

Where K_F (L mg^{-1}) is the Freundlich adsorption constant. n is the heterogeneity factor which indicates the intensity of adsorption. The values of K_F and n were obtained from the slope and intercept of the plot of $\ln q_e$ vs $\ln C_e$ for the three adsorbents respectively.

Comparing the R^2 of Freundlich model with that of Langmuir model, the higher value of R^2 is obtained, which indicates the adsorption for MB and MO are more likely to occur on heterogeneous surface with the multilayer formation of adsorbate on adsorbent. Moreover, the value of 1/n that indicating the energy relative distribution and the adsorbate sites' heterogeneity lies between 0 and 1 demonstrated the adsorption process is favorable. [126]

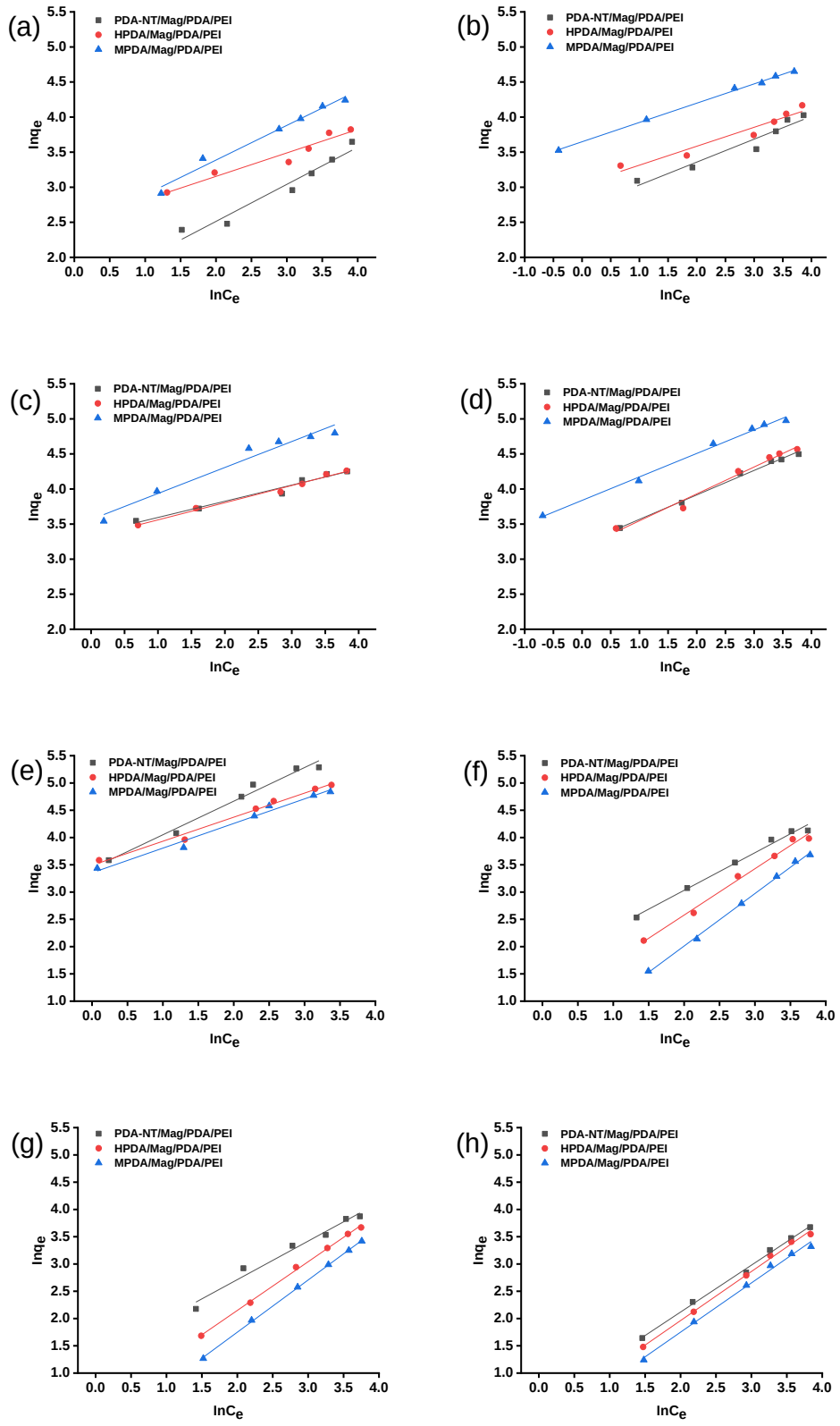

Figure 3.10 Freundlich isotherm fitting for the adsorption of MB and MO on three adsorbents at different pH. (a) MB, pH=3 ;(b) MB, pH=5; (c) MB, pH=7; (d) MB, pH=9. (e) MO, pH=3; (f) MO, pH=5; (g)MO, pH=7; (d) MO, pH=9.

Table 6 Parameters of adsorption isotherms using Freundlich model for three adsorbents at different pH

Dye	pH	Adsorbent	1/n	K_F (L g^{-1})	R^2
MB	3	PDA-NT/Mag/PDA/PEI	0.5284	4.2874	0.9502
		HPDA/Mag/PDA/PEI	0.3344	12.0141	0.9443
		MPDA/Mag/PDA/PEI	0.4945	11.0050	0.9808
	5	PDA-NT/Mag/PDA/PEI	0.3266	14.9510	0.9393
		HPDA/Mag/PDA/PEI	0.2699	21.0008	0.9385
		MPDA/Mag/PDA/PEI	0.2749	38.4085	0.9978
	7	PDA-NT/Mag/PDA/PEI	0.2306	28.9002	0.9720
		HPDA/Mag/PDA/PEI	0.2449	27.5309	0.9893
		MPDA/Mag/PDA/PEI	0.3708	35.3387	0.9621
	9	PDA-NT/Mag/PDA/PEI	0.3491	24.9646	0.9944
		HPDA/Mag/PDA/PEI	0.3840	23.6291	0.9815
		MPDA/Mag/PDA/PEI	0.3348	46.4023	0.9939
MO	3	PDA-NT/Mag/PDA/PEI	0.6165	30.9886	0.9814
		HPDA/Mag/PDA/PEI	0.4413	32.7954	0.9887
		MPDA/Mag/PDA/PEI	0.4518	28.6161	0.9828
	5	PDA-NT/Mag/PDA/PEI	0.6903	5.2108	0.9897
		HPDA/Mag/PDA/PEI	0.8493	2.4112	0.9908
		MPDA/Mag/PDA/PEI	0.9620	1.0911	0.9983
	7	PDA-NT/Mag/PDA/PEI	0.7065	3.6712	0.9752
		HPDA/Mag/PDA/PEI	0.8934	1.4352	0.9983
		MPDA/Mag/PDA/PEI	0.9574	1.1792	0.9995
	9	PDA-NT/Mag/PDA/PEI	0.8598	1.4906	0.9966
		HPDA/Mag/PDA/PEI	0.8993	1.1781	0.9973
		MPDA/Mag/PDA/PEI	0.9022	0.9470	0.9948

The Temkin model presumes that the adsorption is a multilayer process, the adsorption heat as a function of temperature, which is linear decreased with increasing coverage that attribute to the interactions between adsorbate and adsorbent. The Temkin model is presented as follows,

$$q_e = BlnK_T + BlnC_e \quad (11)$$

where B is constant related to the heat of adsorption and is defined as $B=RT/b_T$, b_T (J mol^{-1}) is Temkin constant, K_T (L g^{-1}) is Temkin isotherm constant. [127] Suggesting that the Temkin isotherm is applied when ignoring the extremely high and low concentrations. Thus, in present work, the initial concentration of 5 mg L^{-1} is ignored.

From the data listed in Table 7, it shows that the value of R^2 is depended on pH. As the value of R^2 is much higher when pH=9 for MB and pH=3 for MO than those at other pH. This result indicates that at the favorable pH for MB and MO, the adsorption is a multilayer physisorption process.

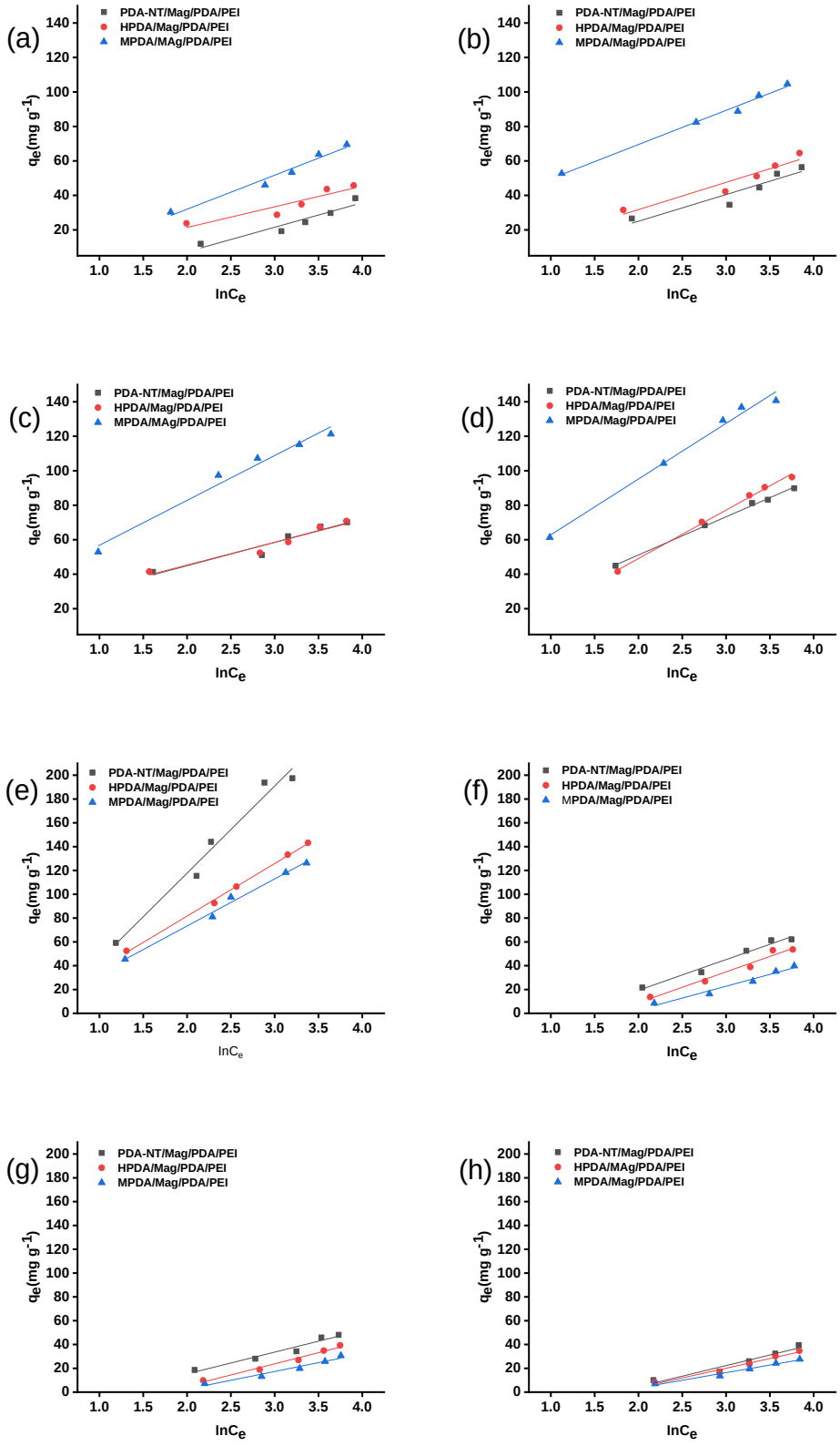

Figure 3.11 Temkin isotherm fitting for the adsorption of MB and MO on three adsorbents at different pH. (a) MB, pH=3 ;(b) MB, pH=5; (c) MB, pH=7; (d) MB, pH=9. (e) MO, pH=3; (f) MO, pH=5; (g) MO, pH=7; (h) MO, pH=9.

Table 7 Parameters of adsorption isotherms using Temkin model for three adsorbents at different pH

Dye	pH	Adsorbent	b_T (J mol^{-1})	K_T (L g^{-1})	R^2
MB	3	PDA-NT/Mag/PDA/PEI	171.6401	0.2265	0.9110
		HPDA/Mag/PDA/PEI	203.8394	0.8255	0.8661
		MPDA/Mag/PDA/PEI	123.5412	0.6843	0.9704
	5	PDA-NT/Mag/PDA/PEI	157.2426	0.6782	0.8869
		HPDA/Mag/PDA/PEI	154.3743	1.0110	0.9215
		MPDA/Mag/PDA/PEI	122.9768	4.5097	0.9912
	7	PDA-NT/Mag/PDA/PEI	179.2516	3.6785	0.9340
		HPDA/Mag/PDA/PEI	185.2331	4.2284	0.9477
		MPDA/Mag/PDA/PEI	93.6766	3.2623	0.9760
	9	PDA-NT/Mag/PDA/PEI	109.9979	1.3599	0.9974
		HPDA/Mag/PDA/PEI	86.8216	0.7777	0.9959
		MPDA/Mag/PDA/PEI	75.4131	2.5715	0.9883
MO	3	PDA-NT/Mag/PDA/PEI	33.3016	0.6757	0.9743
		HPDA/Mag/PDA/PEI	55.2092	0.8600	0.9979
		MPDA/Mag/PDA/PEI	61.5808	0.8628	0.9915
	5	PDA-NT/Mag/PDA/PEI	95.0943	0.2847	0.9775
		HPDA/Mag/PDA/PEI	93.9499	0.1903	0.9715
		MPDA/Mag/PDA/PEI	122.3052	0.1559	0.9708
	7	PDA-NT/Mag/PDA/PEI	133.2805	0.3127	0.9541
		HPDA/Mag/PDA/PEI	129.8842	0.1765	0.9808
		MPDA/Mag/PDA/PEI	164.6441	0.1603	0.9611
	9	PDA-NT/Mag/PDA/PEI	137.1191	0.1745	0.9497
		HPDA/Mag/PDA/PEI	149.2383	0.1698	0.9729
		MPDA/Mag/PDA/PEI	190.0908	0.1778	0.9811

The Dubinin-Radushkevich (D-R) isotherm assumes a multilayer adsorption with Gaussian energy distribution onto heterogeneous surfaces and can be applied to physisorption process. Unlike Langmuir and Freundlich models, D-R model is a semiempirical equation in which follows pore filling mechanism. Generally, it is used to distinguish the type of adsorption is physical or chemical adsorption.[126] It worth noting that, this isotherm only applicable for intermediate range of adsorbate concentration since it exhibits unrealistic asymptotic behavior and does not predict Henry's laws at low pressure. It was originally developed to describe the adsorption of gases and vapors on microporous sorbents, and recently used for the description of solid/ solution adsorption system. The model is shown as follows,

$$lnq_e = (lnq_0 - K_{D-R}\varepsilon^2) \quad (12)$$

$$\varepsilon = RTln\left(1 + \frac{1}{C_e}\right) \quad (13)$$

$$E = \frac{1}{\sqrt{2K_{D-R}}} \quad (14)$$

where q_0 (mg g^{-1}) is the maximum adsorbed amount, K_{D-R} (mol^2 kJ^{-2}) is the D-R model constant. Ɛ (kJ mol^{-1}) is the adsorption potential based on the Polanyi's potential theory, [128] E (kJ mol^{-1}) is mean free energy.

Generally, D-R isotherm model is only suitable for intermediate range of adsorbate concentration, so only the initial concentration in the range of 10-50 mg L^{-1} was studied. Besides, the mean free energy (E) is used to determine the adsorption process is controlled by physical process or chemical process. As the values of E that listed in Table 8 are less than 8 kJ mol^{-1} for both MB and MO at different pH, it indicates that the adsorption is controlled by physical process. [129] Moreover, the value of q_0 obtained from D-R model that listed in Table 8 approach to the experimental data than that calculated by using Langmuir model, which indicates the theoretical adsorption capacity could be better predicted by D-R isotherm model and the process may occur on heterogeneous surfaces through a physisorption process.

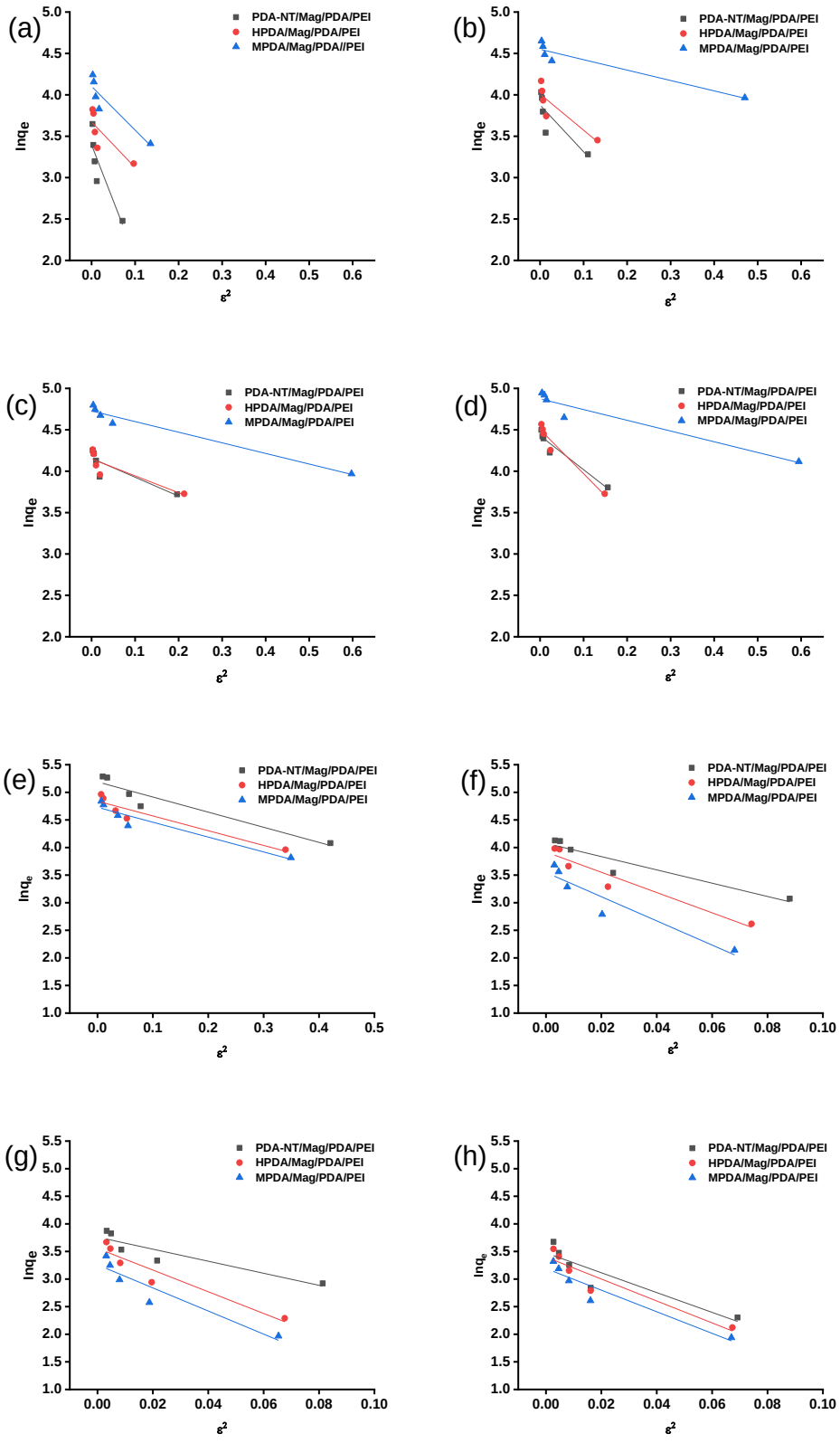

Figure 3.12 D-R isotherm fitting for the adsorption of MB and MO on three adsorbents at different pH. (a) MB, pH=3 ;(b) MB, pH=5; (c) MB, pH=7; (d) MB, pH=9. (e) MO, pH=3; (f) MO, pH=5; (g)MO, pH=7; (d) MO, pH=9.

Table 8 Parameters of adsorption isotherms using D-R model for three adsorbents at different pH

Dye	pH	Adsorbent	q_0(mg g^{-1})	K_{D-R} (mol^2 KJ^{-2})	E (KJ mol^{-1})	R^2
MB	3	PDA-NT/Mag/PDA/PEI	29.84	13.5069	0.1924	0.7849
		HPDA/Mag/PDA/PEI	39.35	5.5007	0.3015	0.6475
		MPDA/Mag/PDA/PEI	60.50	5.2746	0.3079	0.8390
	5	PDA-NT/Mag/PDA/PEI	48.28	5.6416	0.2977	0.7115
		HPDA/Mag/PDA/PEI	55.07	4.3540	0.3388	0.7579
		MPDA/Mag/PDA/PEI	94.63	1.2553	0.6311	0.9099
	7	PDA-NT/Mag/PDA/PEI	63.79	2.2809	0.4682	0.7556
		HPDA/Mag/PDA/PEI	63.29	2.0389	0.4952	0.7554
		MPDA/Mag/PDA/PEI	112.98	1.2816	0.6246	0.9672
	9	PDA-NT/Mag/PDA/PEI	83.817	4.1012	0.3491	0.9371
		HPDA/Mag/PDA/PEI	90.34	5.3371	0.3060	0.9511
		MPDA/Mag/PDA/PEI	130.88	1.2964	0.6210	0.9295
MO	3	PDA-NT/Mag/PDA/PEI	179.34	2.7399	0.4272	0.9101
		HPDA/Mag/PDA/PEI	126.37	2.6736	0.4324	0.9003
		MPDA/Mag/PDA/PEI	113.09	2.6958	0.4306	0.9117
	5	PDA-NT/Mag/PDA/PEI	58.94	12.0519	0.2037	0.9015
		HPDA/Mag/PDA/PEI	50.34	18.3777	0.1649	0.9252
		MPDA/Mag/PDA/PEI	34.72	21.9291	0.1510	0.8949
	7	PDA-NT/Mag/PDA/PEI	42.94	10.9206	0.2139	0.8474
		HPDA/Mag/PDA/PEI	35.01	19.6543	0.1595	0.9143
		MPDA/Mag/PDA/PEI	26.00	20.9325	0.1545	0.8818
	9	PDA-NT/Mag/PDA/PEI	32.24	17.9377	0.1669	0.8356
		HPDA/Mag/PDA/PEI	29.92	19.8898	0.1585	0.8891
		MPDA/Mag/PDA/PEI	24.30	19.5612	0.1599	0.9032

The Harkin-Jura (H-J) isotherm presumes the adsorption is multilayer adsorption on the surface with heterogeneous pore distribution. The model is presented as follows,

$$\frac{1}{q_e^2} = \frac{B}{A} - \frac{1}{A} log C_e \quad (15)$$

where both B and A are Harkin-Jura constant that determined by plotting curve of $1/q_e^2$ vs $\log C_e$.

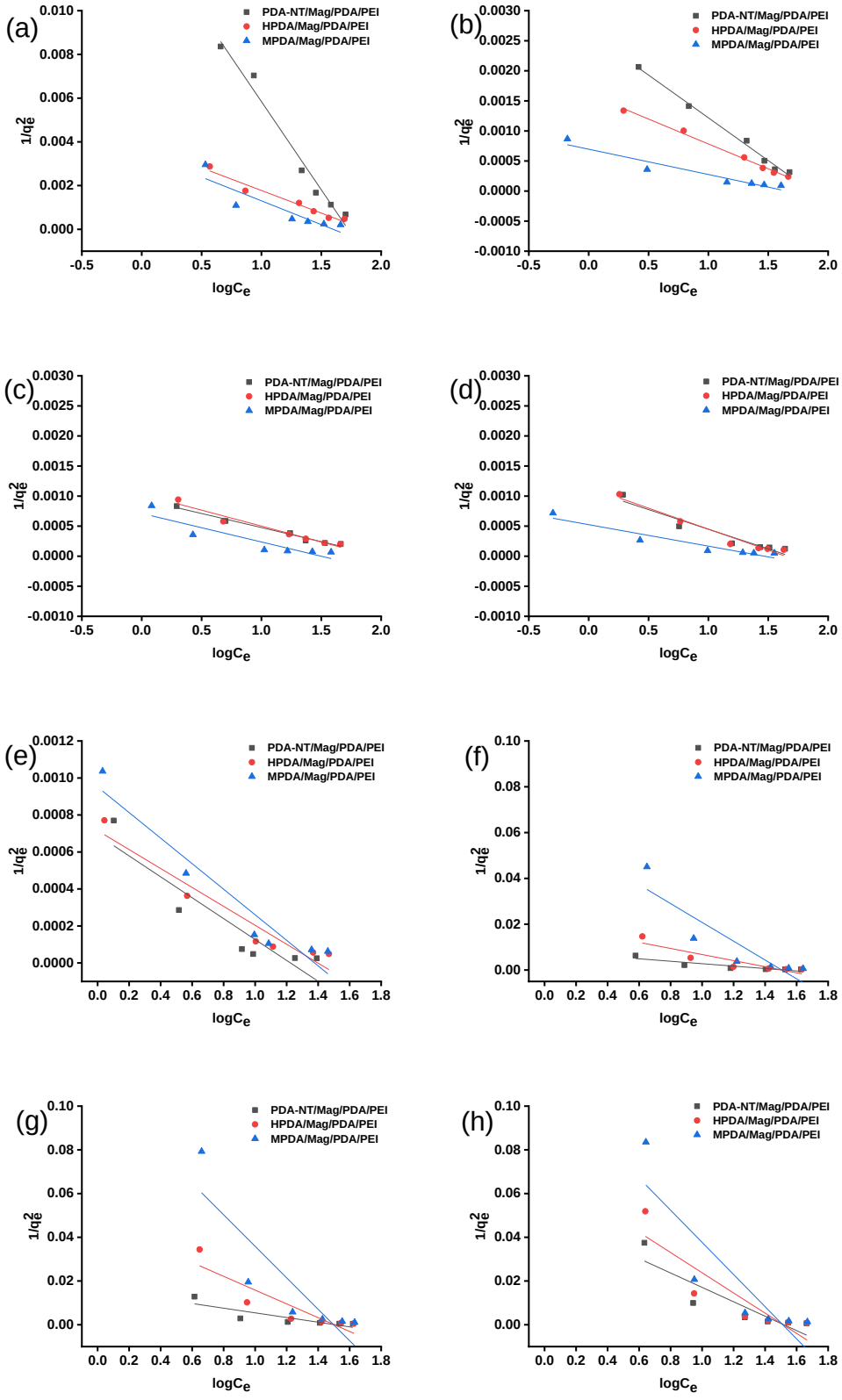

Figure 3.13 H-J isotherm fitting for the adsorption of MB and MO on three adsorbents at different pH (a) MB, pH=3 ;(b) MB, pH=5; (c) MB, pH=7; (d) MB, pH=9. (e) MO, pH=3; (f) MO, pH=5; (g)MO, pH=7; (h) MO, pH=9.

Table 9 Parameters of adsorption isotherms using H-J model for three adsorbents at different pH

Dye	pH	Adsorbent	B	A	R^2
MB	3	PDA-NT/Mag/PDA/PEI	1.7236	123.9157	0.9774
		HPDA/Mag/PDA/PEI	1.8599	483.0918	0.9614
		MPDA/Mag/PDA/PEI	1.6036	460.8295	0.8114
	5	PDA-NT/Mag/PDA/PEI	1.8591	704.2253	0.9926
		HPDA/Mag/PDA/PEI	1.9453	1208.2840	0.9944
		MPDA/Mag/PDA/PEI	1.6553	2377.8781	0.9213
	7	PDA-NT/Mag/PDA/PEI	2.0169	2135.9945	0.9831
		HPDA/Mag/PDA/PEI	1.9448	1888.1890	0.9601
		MPDA/Mag/PDA/PEI	1.4978	2105.2188	0.8287
	9	PDA-NT/Mag/PDA/PEI	1.6820	1529.1291	0.9276
		HPDA/Mag/PDA/PEI	1.6484	1433.404	0.9462
		MPDA/Mag/PDA/PEI	1.4680	2797.1871	0.8867
MO	3	PDA-NT/Mag/PDA/PEI	1.2243	1770.0525	0.8493
		HPDA/Mag/PDA/PEI	1.3515	1954.0219	0.9279
		MPDA/Mag/PDA/PEI	1.0013	1447.7626	0.9228
	5	PDA-NT/Mag/PDA/PEI	1.5188	187.9699	0.8236
		HPDA/Mag/PDA/PEI	1.5083	75.18797	0.8358
		MPDA/Mag/PDA/PEI	1.5066	24.2546	0.8085
	7	PDA-NT/Mag/PDA/PEI	1.5075	93.4579	0.7400
		HPDA/Mag/PDA/PEI	1.5025	31.7057	0.8068
		MPDA/Mag/PDA/PEI	1.4982	13.8850	0.7753
	9	PDA-NT/Mag/PDA/PEI	1.5189	30.3674	0.7978
		HPDA/Mag/PDA/PEI	1.5148	21.6309	0.8004
		MPDA/Mag/PDA/PEI	1.5120	13.5943	0.7783

Table 10 Comparison of the adsorption capacity of other PDA-based adsorbents in the previous studies

Material	Q_e (mg g^{-1})		Ref.
	MB	MO	
PDA microspheres	147.0	Almost zero	[84]
PDA/GO	1890	30.0	[87]
Fe_3O_4 @PDA NPs	10.0	2.1	[130]
PCL/PEO@PDA-45	14.8	60.2	[131]
PDA-Fe_3O_4-Ag	115.0	19.8	[132]
PDA/Mag/PDA/PEI	156.2	255.7	This work

The comparison of adsorption capacity of adsorbent prepared in this work with that of other PDA-based materials is presented in Table 10. It should be noted that the PDA/Mag/PDA/PEI adsorbents that constructed in this work exhibited a relatively high adsorption capacity for both MB and MO, indicating that these adsorbents could be applied as candidates for treating wastewater that contains cationic and anionic dyes.

Furthermore, by comparing the correlation coefficient R^2 that obtained from the adsorption isotherm fits by several isotherm equations, it could be found for adsorption

of MB on PDA-NT/Mag/PDA/PEI, it fits H-J model better, indicating the heterogenous pore distribution of the adsorbent, for adsorption of MB on HPDA/Mag/PDA/PEI, it fits Langmuir, Freundlich, and H-J isotherm model, for adsorption of MB on MPDA/Mag/PDA/PEI, it fits well with Langmuir isotherm model, indicating the adsorption occurs on a homogeneous surface. For the adsorption of MO, it shows for all the three adsorbents, the R^2 of Freundlich isotherm model is higher than the other model. This suggests that the adsorption equilibrium of MO can be better described by Freundlich isotherm.

3.2.6 Temperature effect and thermodynamic studies

Thermodynamic studies are essential in exploring the adsorption mechanisms (i.e., physisorption or chemisorption) and the spontaneous nature of the adsorption process. The experiment data of three adsorbents were collected at three different temperature 293.15, 303.15, 313.15K. The amount of MB and MO that adsorbed on three adsorbents as a function of temperature was depicted in Fig 3.13. These data were used to determine the thermodynamic parameter including the change of free energy (ΔG^o), enthalpy(ΔH^o) and entropy (ΔS^o). These parameters could be calculated according to the following equations,

$$\Delta G^o = -RT \ln K \tag{15}$$

$$K = \frac{q_e}{C_e} \tag{16}$$

$$\ln K = \frac{\Delta S^o}{R} - \frac{\Delta H^o}{RT} \tag{17}$$

$$\Delta G^o = \Delta H^o - T\Delta S^o \tag{18}$$

where K is the equilibrium constant, R is the gas constant (8.314 J mol $^{-1}$ K^{-1}). T(K) is temperature, q_e (mg L^{-1}) is the amount of dye adsorbed per volume of dye solution at equilibrium state, C_e (mg L^{-1}) is the equilibrium concentration of the dye solution.

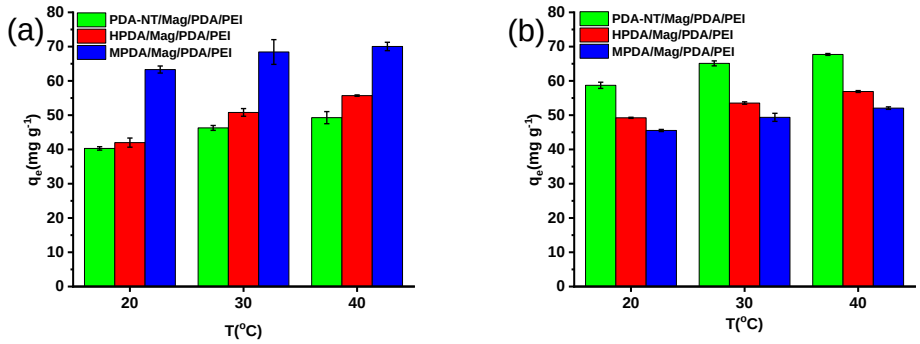

Figure 3.14 Effect of temperature on the adsorption capacity q_e (mg g^{-1}) for (a) MB; (b) MO.

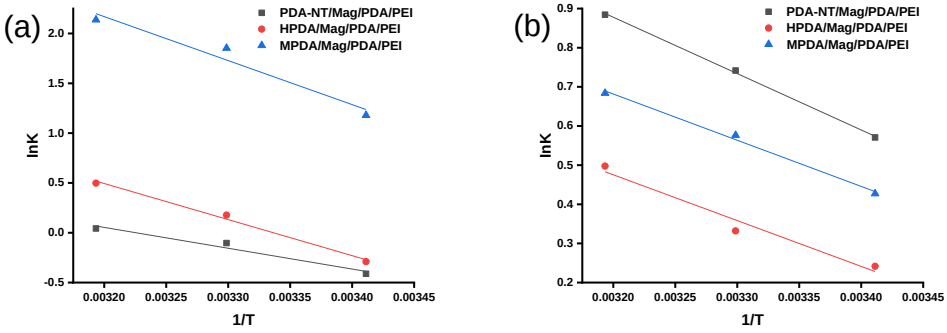

Figure 3.15 Van't Hoff linear plot of adsorption for (a)MB; (b)MO.

Table 11 Thermodynamic parameters of adsorption

Dye	Adsorbent	T (K)	K	ΔG^o (KJ mol^{-1})	ΔH^o (KJ mol^{-1})	ΔS^o (J mol^{-1})	R^2
MB	PDA-NT/Mag/PDA/PEI	293.15	0.6625	1.0033	17.3961	56.1158	0.9666
		303.15	0.9015	0.2613			
		313.15	1.0434	-0.1108			
	HPDA/Mag/PDA/PEI	293.15	0.7484	0.7061	30.1015	100.4352	0.9923
		303.15	1.1938	-0.4465			
		313.15	1.6450	-1.2959			
	MPDA/Mag/PDA/PEI	293.15	3.2521	-2.8742	36.7125	135.5179	0.9560
		303.15	6.3777	-4.6698			
		313.15	8.4774	-5.5648			
MO	PDA-NT/Mag/PDA/PEI	293.15	1.7696	-1.3911	11.9765	45.6240	0.9989
		303.15	2.0994	-1.8693			
		313.15	2.4216	-2.3026			
	HPDA/Mag/PDA/PEI	293.15	1.2733	-0.5890	9.7304	35.0894	0.9652
		303.15	1.3936	-0.8365			
		313.15	1.6447	-1.2954			
	MPDA/Mag/PDA/PEI	293.15	1.5327	-1.0408	9.8096	37.0585	0.9943
		303.15	1.7797	-1.4529			
		313.15	1.9813	-1.7801			

The Van't Hoff linear plot of adsorption for MB and MO are depicted in Fig 3.15, from which the value of ΔH^o and ΔS^o could be determined from the slope and intercept of the plot of In K vs 1/T, respectively. The thermodynamic parameters are presented in Table 11. The values of ΔG^o shown to be negative except that for PDA-NT/Mag/PDA/PEI at 293.15, 303.15K and HPDA/Mag/PDA/PEI at 293.15K for MB, indicates that the adsorption process is spontaneous in nature under all conditions except the above-mentioned. The positive ΔG^o at those certain temperature for these two adsorbents suggesting the adsorption process require some external energy, i.e., agitation. Moreover, the value of ΔG^o decrease with increasing temperature, indicates higher operating temperature is favorable for the adsorption of both MB and MO, this is consistent with the results show in Fig 3.14, which may be due to the mobility of dye molecules increase with temperature and thus enhance the interactions with active sites on the surface of adsorbents. The positive value of ΔH^o further confirmed the endothermic nature of adsorption. The positive values of ΔS^o show the increased randomness at the solid/liquid interface during the adsorption process. Besides, the magnitude of ΔH^o is lower than 40 KJ mol^{-1} and ΔG^o values between -20 and 0 kJ mol^{-1} indicate that the adsorption is physisorption process. [133]

3.2.7 Effect of ionic strength

Since salts commonly exist in dying effluent, the effect of ionic strength was also studied for the dye adsorption onto adsorbents. Sodium chloride was selected as a model salt and added into dye solutions MB (pH=9) and MO (pH=3) and with different concentrations of 0.02, 0.04, 0.06, 0.08 and 0.1 mol L^{-1} ahead adsorption process. As shown in Fig 3.16, the removal efficiency of both anionic and cationic dyes decreased with the increase of salt concentration. Such findings can be attribute to the following reasons. On the one hand is the presence of Na^+ and Cl^{-1} could interfere with the electrostatic interactions between the charged ions in dye molecules and positive charged PDA/PEI external surface and negatively charged internal PDA surface. On the other hand, these salt ions could consume some of the adsorption sites, which will

also hinder the adsorption for dyes. Nonetheless, the removal efficiency drops 9-14% for MB and 17-19% for MO even when the ionic strength increased to 1 mol L^{-1}.

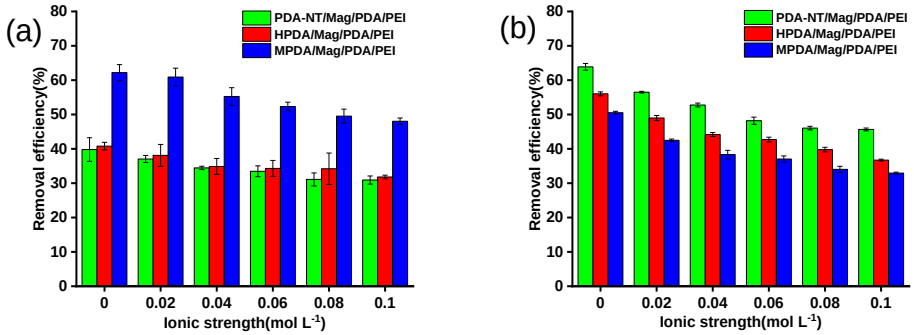

Figure 3.16 Ionic strength effect on the adsorption of three adsorbents for (a) MB; (b) MO.

3.2.8 Adsorption studies in binary dye system

The effect of both MO and MB in simultaneous adsorption on the adsorbents was evaluated by using the ratio of adsorption capacities (R_q), [134]

$$R_q = \frac{q_{b,i}}{q_{m,i}} \tag{19}$$

where $q_{b,i}$ (mg g^{-1}) and $q_{m,i}$ (mg g^{-1}) are the adsorbed dye i in a binary dye system and mono-dye system with the same initial dye concentration, respectively. If $R_q > 1$, the adsorption of dye i is enhanced by the presence of the other dye; if $R_q = 1$, the adsorption of dye i is not affected by the presence of the other dye; if $R_q < 1$, the adsorption of dye i is impeded by the presence of the other dye. The UV-Vis spectra of binary dye system of dyes and that after adsorption at different pH was presented in Fig 3.17. It could be seen that the adsorption is still pH dependent as that of single dye system. The adsorption capacity for both dyes in binary dye system and single dye system were summarized in Table 12. The results show that the value of R_q is in the range of 0.84-1.05, which indicates that all three adsorbents maintain the adsorption capacity in binary dye system, and the effect of interactions between MB and MO could be neglected.

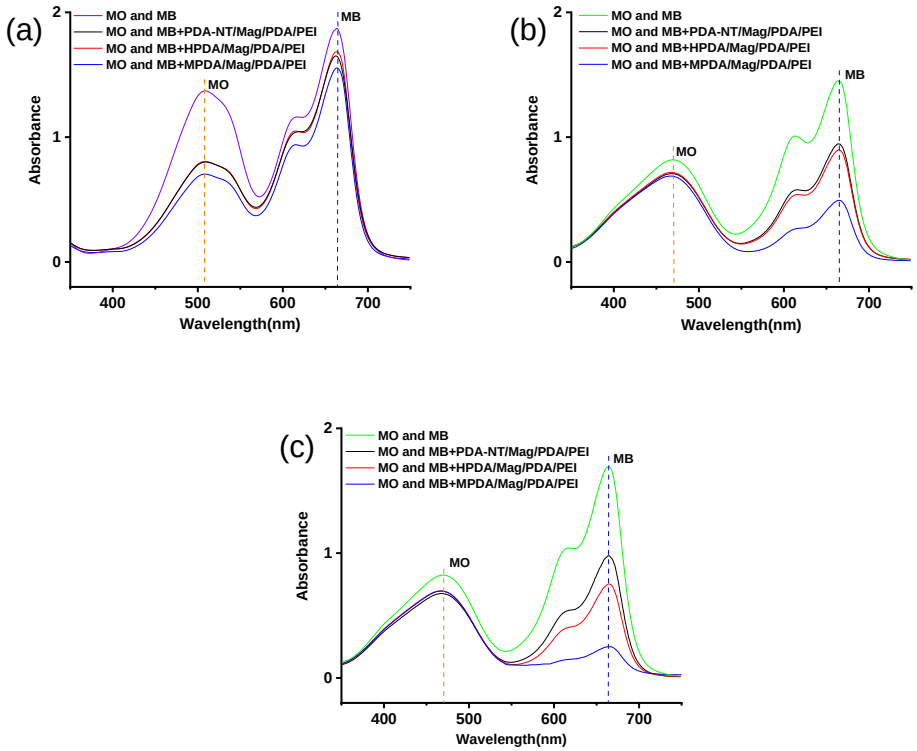

Figure 3.17 UV-vis spectra of binary dyes system before and after adsorption by three adsorbents at different pH (a) pH=3; (a) pH=7; (c) pH=9.

Table 12 Adsorption capacity for binary and single dye system at different pH

Dye	pH	Adsorbent	Q_m (mg g^{-1})	^{Qb} (mg g^{-1})	R_q
MB	3	PDA-NT/Mag/PDA/PEI	11.9	10.1	0.85
		HPDA/Mag/PDA/PEI	23.8	22.3	0.94
		MPDA/Mag/PDA/PEI	30.3	28.2	0.93
	7	PDA-NT/Mag/PDA/PEI	41.3	40.1	0.97
		HPDA/Mag/PDA/PEI	41.5	38.2	0.92
		MPDA/Mag/PDA/PEI	52.9	52.3	0.98
	9	PDA-NT/Mag/PDA/PEI	44.9	45.4	1.01
		HPDA/Mag/PDA/PEI	41.6	42.0	1.01
		MPDA/Mag/PDA/PEI	61.3	63.8	1.04
MO	3	PDA-NT/Mag/PDA/PEI	59.1	56.2	0.95
		HPDA/Mag/PDA/PEI	52.5	49.0	0.93
		MPDA/Mag/PDA/PEI	45.4	41.8	0.92
	7	PDA-NT/Mag/PDA/PEI	18.6	17.1	0.92
		HPDA/Mag/PDA/PEI	9.9	10.2	1.03
		MPDA/Mag/PDA/PEI	7.2	7.6	1.05
	9	PDA-NT/Mag/PDA/PEI	10.0	8.5	0.85
		HPDA/Mag/PDA/PEI	8.3	6.9	0.83
		MPDA/Mag/PDA/PEI	6.9	5.8	0.84

Moreover, the adsorption behavior of both cationic and anionic dyes was further evaluated by step-by-step adsorption. Fig 3.18 shows the color change of the dye solutions during the adsorption/desorption process, after reach the adsorption equilibrium of MB, the solution turned to colorless and transparent, which was also confirmed by the UV-Vis result in Fig 3.19 (a). The absorbance peak at 663 nm disappear after adsorption indicates the completely removal of MB. Besides, the desorption of MB was achieved with the aid of ethanol and acid. From the UV-vis spectra of desorption that presented in Fig 3.19 (b), MPDA/Mag/PDA/PEI shows the lowest absorbance intensity for the absorbance peaks at 663 nm, which may be due to the higher adsorption capacity of MB by MPDA/Mag/PDA/PEI at equilibrium, so it is more difficult for it to desorb completely.

From the color change of dye solution presented in Fig 3.20, it shows after the adsorption of MO, the solution turned to colorless and transparent, which was also confirmed by the UV-Vis result in Fig 3.21 (a). The absorbance peak at 506 nm nearly disappeared and a little hump left after adsorption which indicates that the majority of MO are removed removal. Besides, the hump around 663 nm are assigned to be the MB residues that bind with adsorbents that could not be completely removed during desorption process. Moreover, the desorption of MO was achieved with the aid of ethanol and alkali. From the UV-vis spectra that presented in Fig 3.21 (b), PDA-NT/Mag/PDA/PEI shows the lowest absorbance intensity for the absorbance peaks at 464 nm, which may be due to the higher adsorption capacity of MO by PDA-NT/Mag/PDA/PEI at equilibrium, so it is more difficult for it to desorb completely.

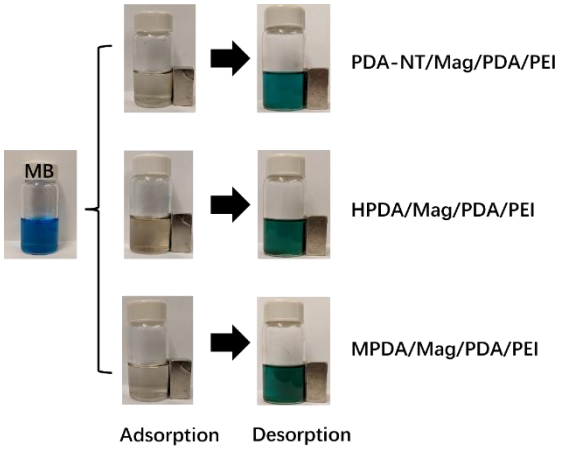

Figure 3.18 Digital images of dye solution of adsorption and desorption for MB

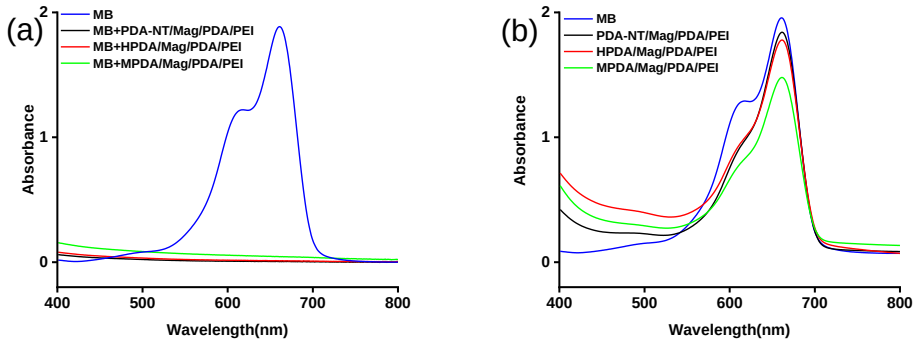

Figure 3.19 UV-vis spectra of adsorption for MB (a)After adsorption; (b) After desorption.

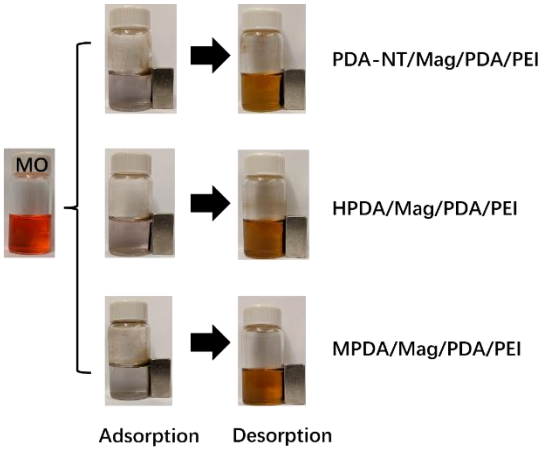

Figure 3.20 Digital images of dye solution of adsorption and desorption for MO.

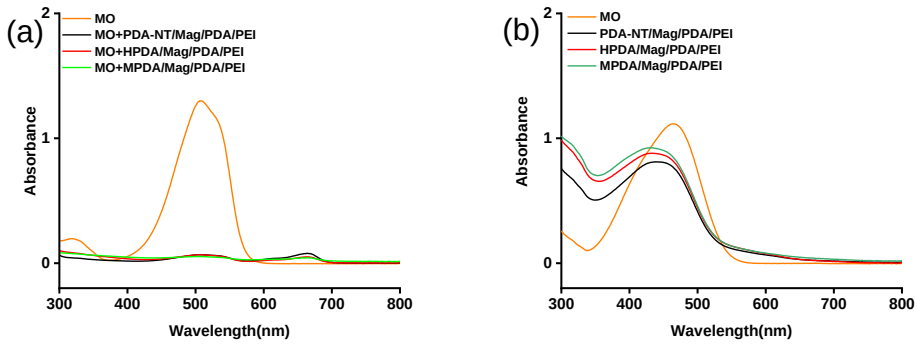

Figure 3.21 UV-vis spectra of adsorption for MO (a) After adsorption; (b) After desorption.

3.2.9 Desorption and regeneration property

The regeneration property of adsorbents is an important aspect when evaluating performance of adsorbents in practical applications. Various regeneration techniques including thermal, electrochemical, ultrasonic, chemical methods have been reported for regeneration. In the above studies, three adsorbents did not significantly adsorb MB (when pH=3) and MO (when pH=9), which suggests that the adsorbed dyes could be desorbed at those pH values.[135] The Fig 3.22 presents the removal efficiency of MB and MO in five successive step-by-step adsorption-desorption cycles. The result shows that after five consecutive cycles, the removal efficiency is around 82-84% for MB and 68-74% for MO. This is mainly due to the incompletion of desorption, and the desorption efficiency is around 73-78% for MB and 63-69% for MO after five cycles, which shows in Fig 3.23. These results indicate the excellent long-term reusability property of adsorbents.

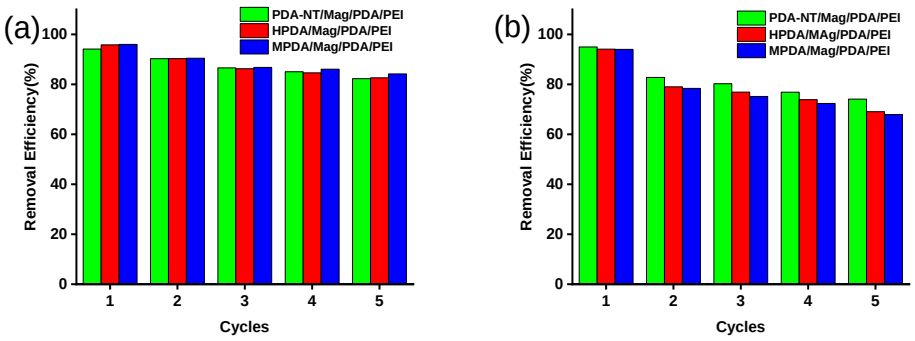

Figure 3.22 Adsorption performance of three adsorbents for (a) MB; (b) MO.

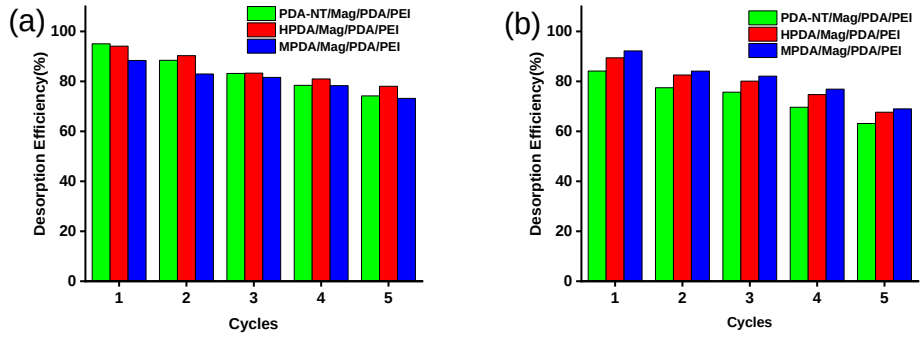

Figure 3.23 Desorption performance of three adsorbents for (a) MB; (b) MO.

3.3 Summary

The maximum adsorption capacity of as-prepared three adsorbents for MB and MO could reach 156.2 and 255.7 mg g^{-1} at 293.15 K. Adsorption kinetic study indicates that the adsorption for both MB and MO conforms to PSO kinetic model. The adsorption process can be divided into three stages and the intraparticle diffusion is not the unique rate-limiting step according to analysis using the Weber-Morris intraparticle diffusion model. Besides, the adsorption isotherm consequences show that the adsorption of MO follows the Freundlich isothermal linear models, and the adsorption of MB conformed to different isothermal models for different adsorbents. Adsorption thermodynamic study implies that the adsorption process for MB and MO were endothermic, and spontaneous. Moreover, the as-prepared adsorbents exhibit excellent long-term reusability and regeneration property.

4. Chapter 4 Conclusions

In this work, PDA-based adsorbents with three different morphologies including, nanotubes, hollow spheres, and mesoporous structure were conducted by template-based method and emulsion-induced assemble processes. The polydopamine templates with different structure were further functionalized by attaching magnetic particles on the surface and coating with PDA/PEI. The introduction of PEI increases the positive charge on the surface, allowing for adsorption of anionic dyes. Moreover, the add-layer served as protective coating to immobilized magnetic particles, which contributes to the good magnetic response of these adsorbents.

The adsorption performance of the as-prepared adsorbents was evaluated. Methylene blue and methyl orange are used as model cationic and anionic dyes, respectively. Three kinetic models and five adsorption isotherm models evaluated. The results indicated that the polydopamine-based adsorbents possessed good adsorption capacity for both cationic and anionic dyes. Adsorption kinetic fits pseudo-second-order model, and the adsorption equilibrium data fitted well by Freundlich isotherm model for the adsorption of MO and conformed to different isotherm model for the adsorption of MB. The thermodynamic evaluation indicated that the adsorption is an endothermic and spontaneous process. Moreover, the adsorbents exhibit excellent regeneration property after five adsorption-desorption cycles. The adsorption mechanism was attributed to the electrostatic interaction, π-π stacking and hydrogen bonding.

5. Chapter 5 Further work

Throughout this research, I have studied the morphology effect on PDA-based adsorbents and adsorption mechanisms for their applications in dye remediation. These studies yield me a better understanding of the advantages and limitation of PDA-based adsorbents. In light of such understanding, I'd like to extend my research to the following three parts:

1. Develop hollow mesoporous PDA adsorbents (HMPDA/Mag/PDA/PEI).

The adsorption capacity of as-prepared adsorbent MPDA/Mag/PDA/PEI for MB does not show to be very high comparing others' work that reported, this may be due to the particle are not hollow that results in less surface area, which could be confirmed by TEM and N_2 adsorption results. Thus, developing the adsorbents with hollow mesoporous structure will be promising for the enhancement of adsorption for MB. The hollow mesoporous PDA could be prepared with the aid of template such as SiO_2 NPs, followed by the method that used in this research. Other than the adsorption isotherm and kinetics, the desorption isotherm and kinetics will also be investigated to have a further understanding of the desorption mechanism and rate-control step in the desorption process.

2. Develop PDA-based hydrogels for dye removal.

Other than nanomaterials, hydrogels are widely studied material for dye removal due to their high porosity and the flexible network of polymer chains that contribute to the penetration of solutes into network. Designing hydrogels with well-defined, three-dimensional structures and high swelling ratio allows the internal active sites within the hydrogel fully exposed to dye molecules, followed by introducing magnetic PDA segment into hydrogel matrix, which is promising for the enhancement of adsorption performance for different dyes and realize magnetic separation of hydrogel. Moreover, the mechanical properties of the hydrogel need to be explored to ensure that the introduction of PDA-segment will not impair the mechanical strength of hydrogel.

3. Develop adsorbents for dye removal with polyphenol.

Polyphenol could be employed as an alternative to PDA due to the high cost of DA, and it can be prepared through mussel-inspired method to realize surface functionalization. Besides, a thorough understanding of the toxicity of polyphenol-based adsorbents need to be studied to ensure that them as safe adsorbents for dye removal. Moreover, the adsorption performance of polyphenol-based adsorbents needs to be investigated and compared to that of PDA-based adsorbents.

References

1. Nguyen, T. A.; Juang, R. S., Treatment of waters and wastewaters containing sulfur dyes: A review. *Chem Eng J* **2013,** *219*, 109-117.

2. Yagub, M. T.; Sen, T. K.; Afroze, S.; Ang, H. M., Dye and its removal from aqueous solution by adsorption: a review. *Adv Colloid Interface Sci* **2014,** *209*, 172-84.

3. Vakili, M.; Rafatullah, M.; Salamatinia, B.; Abdullah, A. Z.; Ibrahim, M. H.; Tan, K. B.; Gholami, Z.; Amouzgar, P., Application of chitosan and its derivatives as adsorbents for dye removal from water and wastewater: A review. *Carbohydrate Polymers* **2014,** *113*, 115-130.

4. Ma, J.; Guo, X. Y.; Ying, Y. P.; Liu, D. H.; Zhong, C. L., Composite ultrafiltration membrane tailored by MOF@GO with highly improved water purification performance. *Chem Eng J* **2017,** *313*, 890-898.

5. Abdi, G.; Alizadeh, A.; Zinadini, S.; Moradi, G., Removal of dye and heavy metal ion using a novel synthetic polyethersulfone nanofiltration membrane modified by magnetic graphene oxide/metformin hybrid. *Journal of Membrane Science* **2018,** *552*, 326-335.

6. Sahinkaya, E.; Sahin, A.; Yurtsever, A.; Kitis, M., Concentrate minimization and water recovery enhancement using pellet precipitator in a reverse osmosis process treating textile wastewater. *Journal of Environmental Management* **2018,** *222*, 420-427.

7. Gupta, V. K.; Suhas, Application of low-cost adsorbents for dye removal - A review. *Journal of Environmental Management* **2009,** *90* (8), 2313-2342.

8. Bassyouni, D. G.; Hamad, H. A.; El-Ashtoukhy, E. S. Z.; Amin, N. K.; Abd El-Latif, M. M., Comparative performance of anodic oxidation and electrocoagulation as clean processes for electrocatalytic degradation of diazo dye Acid Brown 14 in aqueous medium. *J Hazard Mater* **2017,** *335*, 178-187.

9. Malik, P. K.; Saha, S. K., Oxidation of direct dyes with hydrogen peroxide using ferrous ion as catalyst. *Sep Purif Technol* **2003,** *31* (3), 241-250.

10. Punzi, M.; Anbalagan, A.; Borner, R. A.; Svensson, B. M.; Jonstrup, M.; Mattiasson, B., Degradation of a textile azo dye using biological treatment followed by

photo-Fenton oxidation: Evaluation of toxicity and microbial community structure. *Chem Eng J* **2015,** *270*, 290-299.

11. Khuntia, S.; Majumder, S. K.; Ghosh, P., A pilot plant study of the degradation of Brilliant Green dye using ozone microbubbles: mechanism and kinetics of reaction. *Environmental Technology* **2015,** *36* (3), 336-347.

12. Chang, Y. C.; Chen, D. H., Preparation and adsorption properties of monodisperse chitosan-bound Fe3O4 magnetic nanoparticles for removal of Cu(II) ions. *Journal of Colloid and Interface Science* **2005,** *283* (2), 446-451.

13. Bandara, N.; Zeng, H. B.; Wu, J. P., Marine mussel adhesion: biochemistry, mechanisms, and biomimetics. *Journal of Adhesion Science and Technology* **2013,** *27* (18-19), 2139-2162.

14. Zeng, H. B.; Hwang, D. S.; Israelachvili, J. N.; Waite, J. H., Strong reversible Fe3+-mediated bridging between dopa-containing protein films in water. *Proceedings of the National Academy of Sciences of the United States of America* **2010,** *107* (29), 12850-12853.

15. Gao, H. C.; Sun, Y. M.; Zhou, J. J.; Xu, R.; Duan, H. W., Mussel-Inspired Synthesis of Polydopamine-Functionalized Graphene Hydrogel as Reusable Adsorbents for Water Purification. *Acs Applied Materials & Interfaces* **2013,** *5* (2), 425-432.

16. Liu, R.; Guo, Y. L.; Odusote, G.; Qu, F. L.; Priestley, R. D., Core-Shell Fe3O4 Polydopamine Nanoparticles Serve Multipurpose as Drug Carrier, Catalyst Support and Carbon Adsorbent. *Acs Applied Materials & Interfaces* **2013,** *5* (18), 9167-9171.

17. Adegoke, K. A.; Bello, O. S., Dye sequestration using agricultural wastes as adsorbents. *Water Resources and Industry* **2015,** *12*, 8-24.

18. Rafatullah, M.; Sulaiman, O.; Hashim, R.; Ahmad, A., Adsorption of methylene blue on low-cost adsorbents: A review. *J Hazard Mater* **2010,** *177* (1-3), 70-80.

19. Srinivasan, A.; Viraraghavan, T., Decolorization of dye wastewaters by biosorbents: A review. *Journal of Environmental Management* **2010,** *91* (10), 1915-1929.

20. Bouabidi, Z. B.; El-Naas, M. H.; Cortes, D.; Mckay, G., Steel-Making dust as a potential adsorbent for the removal of lead (II) from an aqueous solution. *Chem Eng J* **2018,** *334*, 837-844.

21. Dutta, S.; Gupta, B.; Srivastava, S. K.; Gupta, A. K., Recent advances on the removal of dyes from wastewater using various adsorbents: a critical review. *Materials Advances* **2021,** *2* (14), 4497-4531.

22. Nandi, B. K.; Goswami, A.; Purkait, M. K., Removal of cationic dyes from aqueous solutions by kaolin: Kinetic and equilibrium studies. *Applied Clay Science* **2009,** *42* (3-4), 583-590.

23. Salleh, M. A. M.; Mahmoud, D. K.; Karim, W. A. W. A.; Idris, A., Cationic and anionic dye adsorption by agricultural solid wastes: A comprehensive review. *Desalination* **2011,** *280* (1-3), 1-13.

24. Savova, D.; Petrov, N.; Yardim, M. F.; Ekinci, E.; Budinova, T.; Razvigorova, M.; Minkova, V., The influence of the texture and surface properties of carbon adsorbents obtained from biomass products on the adsorption of manganese ions from aqueous solution. *Carbon* **2003,** *41* (10), 1897-1903.

25. Eren, Z.; Acar, F. N., Adsorption of Reactive Black 5 from an aqueous solution: equilibrium and kinetic studies. *Desalination* **2006,** *194* (1-3), 1-10.

26. Ofomaja, A. E., Sorptive removal of Methylene blue from aqueous solution using palm kernel fibre: Effect of fibre dose. *Biochemical Engineering Journal* **2008,** *40* (1), 8-18.

27. Senthilkumaar, S.; Kalaamani, P.; Subburaam, C. V., Liquid phase adsorption of Crystal violet onto activated carbons derived from male flowers of coconut tree. *J Hazard Mater* **2006,** *136* (3), 800-808.

28. Deniz, F.; Kepekci, R. A., Dye biosorption onto pistachio by-product: A green environmental engineering approach. *J Mol Liq* **2016,** *219*, 194-200.

29. Silva, T. L.; Ronix, A.; Pezoti, O.; Souza, L. S.; Leandro, P. K. T.; Bedin, K. C.; Beltrame, K. K.; Cazetta, A. L.; Almeida, V. C., Mesoporous activated carbon from industrial laundry sewage sludge: Adsorption studies of reactive dye Remazol Brilliant Blue R. *Chem Eng J* **2016,** *303*, 467-476.

30. Crini, G., Non-conventional low-cost adsorbents for dye removal: A review. *Bioresource Technology* **2006,** *97* (9), 1061-1085.

31. Guo, D. M.; An, Q. D.; Xiao, Z. Y.; Zhai, S. R.; Yang, D. J., Efficient removal of Pb(II), Cr(VI) and organic dyes by polydopamine modified chitosan aerogels. *Carbohydrate Polymers* **2018,** *202*, 306-314.

32. Peng, Q.; Liu, M. X.; Zheng, J. W.; Zhou, C. R., Adsorption of dyes in aqueous solutions by chitosan-halloysite nanotubes composite hydrogel beads. *Microporous and Mesoporous Materials* **2015,** *201*, 190-201.

33. Zhou, Y. B.; Cheng, G.; Chen, K.; Lu, J.; Lei, J. Y.; Pu, S. Y., Adsorptive removal of bisphenol A, chloroxylenol, and carbamazepine from water using a novel beta-cyclodextrin polymer. *Ecotoxicology and Environmental Safety* **2019,** *170*, 278-285.

34. Wang, D. X.; Liu, L. L.; Jiang, X. Y.; Yu, J. G.; Chen, X. Q., Adsorption and removal of malachite green from aqueous solution using magnetic beta-cyclodextrin-graphene oxide nanocomposites as adsorbents. *Colloids and Surfaces a-Physicochemical and Engineering Aspects* **2015,** *466*, 166-173.

35. Ozacar, M.; Sengil, I. A., Adsorption of metal complex dyes from aqueous solutions by pine sawdust. *Bioresource Technology* **2005,** *96* (7), 791-795.

36. Demarchi, C. A.; Debrassi, A.; Rodrigues, C. A., The use of Jatoba bark for removal of cationic dyes. *Coloration Technology* **2012,** *128* (3), 208-217.

37. Gunes, E.; Kaygusuz, T., Adsorption of Reactive Blue 222 onto an industrial solid waste included Al(III) hydroxide: pH, ionic strength, isotherms, and kinetics studies. *Desalination and Water Treatment* **2015,** *53* (9), 2510-2517.

38. Janos, P.; Buchtova, H.; Ryznarova, M., Sorption of dyes from aqueous solutions onto fly ash. *Water Research* **2003,** *37* (20), 4938-4944.

39. Zhang, M. M.; Mao, Y. P.; Wang, W. L.; Yang, S. X.; Song, Z. L.; Zhao, X. Q., Coal fly ash/CoFe2O4 composites: a magnetic adsorbent for the removal of malachite green from aqueous solution. *Rsc Advances* **2016,** *6* (96), 93564-93574.

40. Gupta, V. K.; Suhas; Ali, I.; Saini, V. K., Removal of rhodamine B, fast green, and methylene blue from wastewater using red mud, an aluminum industry waste. *Industrial & Engineering Chemistry Research* **2004,** *43* (7), 1740-1747.

41. Pinnavaia, T. J., Intercalated Clay Catalysts. *Science* **1983,** *220* (4595), 365-371.

42. Babel, S.; Kurniawan, T. A., Low-cost adsorbents for heavy metals uptake from contaminated water: a review. *J Hazard Mater* **2003,** *97* (1-3), 219-243.

43. Eren, E., Adsorption Performance and Mechanism in Binding of Azo Dye by Raw Bentonite. *Clean-Soil Air Water* **2010,** *38* (8), 758-763.

44. Errais, E.; Duplay, J.; Elhabiri, M.; Khodja, M.; Ocampo, R.; Baltenweck-Guyot, R.; Darragi, F., Anionic RR120 dye adsorption onto raw clay: Surface properties and adsorption mechanism. *Colloids and Surfaces a-Physicochemical and Engineering Aspects* **2012,** *403*, 69-78.

45. Boyd, S. A.; Mortland, M. M.; Chiou, C. T., Sorption Characteristics of Organic-Compounds on Hexadecyltrimethylammonium-Smectite. *Soil Science Society of America Journal* **1988,** *52* (3), 652-657.

46. Chen, D. M.; Chen, J.; Luan, X. L.; Ji, H. P.; Xia, Z. G., Characterization of anion-cationic surfactants modified montmorillonite and its application for the removal of methyl orange. *Chem Eng J* **2011,** *171* (3), 1150-1158.

47. Makarchuk, O. V.; Dontsova, T. A.; Astrelin, I. M., Magnetic Nanocomposites as Efficient Sorption Materials for Removing Dyes from Aqueous Solutions. *Nanoscale Research Letters* **2016,** *11*.

48. Armagan, B.; Ozdemir, O.; Turan, M.; Celik, M. S., The removal of reactive azo dyes by natural and modified zeolites. *Journal of Chemical Technology and Biotechnology* **2003,** *78* (7), 725-732.

49. Santhosh, C.; Velmurugan, V.; Jacob, G.; Jeong, S. K.; Grace, A. N.; Bhatnagar, A., Role of nanomaterials in water treatment applications: A review. *Chem Eng J* **2016,** *306*, 1116-1137.

50. Yao, Y. J.; He, B.; Xu, F. F.; Chen, X. F., Equilibrium and kinetic studies of methyl orange adsorption on multiwalled carbon nanotubes. *Chem Eng J* **2011,** *170* (1), 82-89.

51. Kyzas, G. Z.; Matis, K. A., Nanoadsorbents for pollutants removal: A review. *J Mol Liq* **2015,** *203*, 159-168.

52. Wang, P. F.; Cao, M. H.; Wang, C.; Ao, Y. H.; Hou, J.; Qian, J., Kinetics and thermodynamics of adsorption of methylene blue by a magnetic graphene-carbon nanotube composite. *Appl Surf Sci* **2014,** *290*, 116-124.

53. Mahmoodian, H.; Moradi, O.; Shariatzadeha, B.; Salehf, T. A.; Tyagi, I.; Maity, A.; Asif, M.; Gupta, V. K., Enhanced removal of methyl orange from aqueous solutions by poly HEMA-chitosan-MWCNT nano-composite. *J Mol Liq* **2015,** *202*, 189-198.

54. Yah, W. O.; Takahara, A.; Lvov, Y. M., Selective Modification of Halloysite Lumen with Octadecylphosphonic Acid: New Inorganic Tubular Micelle. *J Am Chem Soc* **2012,** *134* (3), 1853-1859.

55. Liu, Y. S.; Jiang, X. Q.; Li, B. J.; Zhang, X. D.; Liu, T. Z.; Yan, X. S.; Ding, J.; Cai, Q.; Zhang, J. M., Halloysite nanotubes@reduced graphene oxide composite for removal of dyes from water and as supercapacitors. *Journal of Materials Chemistry A* **2014,** *2* (12), 4264-4269.

56. Zou, M. L.; Du, M. L.; Zhu, H.; Xu, C. S.; Fu, Y. Q., Green synthesis of halloysite nanotubes supported Ag nanoparticles for photocatalytic decomposition of methylene blue. *Journal of Physics D-Applied Physics* **2012,** *45* (32).

57. Wan, X.; Zhan, Y.; Long, Z.; Zeng, G.; He, Y., Core@ double-shell structured magnetic halloysite nanotube nano-hybrid as efficient recyclable adsorbent for methylene blue removal. *Chem Eng J* **2017,** *330*, 491-504.

58. Khan, N. A.; Hasan, Z.; Jhung, S. H., Adsorptive removal of hazardous materials using metal-organic frameworks (MOFs): A review. *J Hazard Mater* **2013,** *244*, 444-456.

59. Haque, E.; Jun, J. W.; Jhung, S. H., Adsorptive removal of methyl orange and methylene blue from aqueous solution with a metal-organic framework material, iron terephthalate (MOF-235). *J Hazard Mater* **2011,** *185* (1), 507-511.

60. Lee, H.; Dellatore, S. M.; Miller, W. M.; Messersmith, P. B., Mussel-inspired surface chemistry for multifunctional coatings. *Science* **2007,** *318* (5849), 426-430.

61. Liu, Y. L.; Ai, K. L.; Lu, L. H., Polydopamine and Its Derivative Materials: Synthesis and Promising Applications in Energy, Environmental, and Biomedical Fields. *Chemical Reviews* **2014,** *114* (9), 5057-5115.

62. Kim, H. W.; McCloskey, B. D.; Choi, T. H.; Lee, C.; Kim, M. J.; Freeman, B. D.; Park, H. B., Oxygen Concentration Control of Dopamine-Induced High Uniformity Surface Coating Chemistry. *Acs Applied Materials & Interfaces* **2013,** *5* (2), 233-238.

63. Yang, H. C.; Wu, Q. Y.; Wan, L. S.; Xu, Z. K., Polydopamine gradients by oxygen diffusion controlled autoxidation. *Chemical Communications* **2013,** *49* (89), 10522-10524.

64. Ball, V.; Del Frari, D.; Toniazzo, V.; Ruch, D., Kinetics of polydopamine film deposition as a function of pH and dopamine concentration: Insights in the polydopamine deposition mechanism. *Journal of Colloid and Interface Science* **2012,** *386*, 366-372.

65. Wei, Q.; Zhang, F. L.; Li, J.; Li, B. J.; Zhao, C. S., Oxidant-induced dopamine polymerization for multifunctional coatings. *Polymer Chemistry* **2010,** *1* (9), 1430-1433.

66. Bernsmann, F.; Ball, V.; Addiego, F.; Ponche, A.; Michel, M.; Gracio, J. J. D.; Toniazzo, V.; Ruch, D., Dopamine-Melanin Film Deposition Depends on the Used Oxidant and Buffer Solution. *Langmuir* **2011,** *27* (6), 2819-2825.

67. Ouyang, R. Z.; Lei, H. P.; Ju, H. X.; Xue, Y. D., A molecularly imprinted copolymer designed for enantioselective recognition of glutamic acid. *Advanced Functional Materials* **2007,** *17* (16), 3223-3230.

68. Sheng, W. B.; Li, B.; Wang, X. L.; Dai, B.; Yu, B.; Jia, X.; Zhou, F., Brushing up from "anywhere" under sunlight: a universal surface-initiated polymerization from polydopamine-coated surfaces. *Chemical Science* **2015,** *6* (3), 2068-2073.

69. Du, X.; Li, L. X.; Li, J. S.; Yang, C. W.; Frenkel, N.; Welle, A.; Heissler, S.; Nefedov, A.; Grunze, M.; Levkin, P. A., UV-Triggered Dopamine Polymerization: Control of Polymerization, Surface Coating, and Photopatterning. *Advanced Materials* **2014,** *26* (47), 8029-+.

70. Lee, M.; Lee, S. H.; Oh, I. K.; Lee, H., Microwave-Accelerated Rapid, Chemical Oxidant-Free, Material-Independent Surface Chemistry of Poly(dopamine). *Small* **2017,** *13* (4).

71. Chen, C. T.; Martin-Martinez, F. J.; Jung, G. S.; Buehler, M. J., Polydopamine and eumelanin molecular structures investigated with ab initio calculations. *Chemical Science* **2017,** *8* (2), 1631-1641.

72. Dreyer, D. R.; Miller, D. J.; Freeman, B. D.; Paul, D. R.; Bielawski, C. W., Perspectives on poly(dopamine). *Chemical Science* **2013,** *4* (10), 3796-3802.

73. Dreyer, D. R.; Miller, D. J.; Freeman, B. D.; Paul, D. R.; Bielawski, C. W., Elucidating the Structure of Poly(dopamine). *Langmuir* **2012,** *28* (15), 6428-6435.

74. Hong, S.; Na, Y. S.; Choi, S.; Song, I. T.; Kim, W. Y.; Lee, H., Non-Covalent Self-Assembly and Covalent Polymerization Co-Contribute to Polydopamine Formation. *Advanced Functional Materials* **2012,** *22* (22), 4711-4717.

75. Liebscher, J.; Mrowczynski, R.; Scheidt, H. A.; Filip, C.; Hadade, N. D.; Turcu, R.; Bende, A.; Beck, S., Structure of Polydopamine: A Never-Ending Story? *Langmuir* **2013,** *29* (33), 10539-10548.

76. Wang, Z. X.; Yang, H. C.; He, F.; Peng, S. Q.; Li, Y. X.; Shao, L.; Darling, S. B., Mussel-Inspired Surface Engineering for Water-Remediation Materials. *Matter* **2019,** *1* (1), 115-155.

77. Tsai, W. B.; Chien, C. Y.; Thissen, H.; Lai, J. Y., Dopamine-assisted immobilization of poly(ethylene imine) based polymers for control of cell-surface interactions. *Acta Biomaterialia* **2011,** *7* (6), 2518-2525.

78. Coyne, K. J.; Qin, X. X.; Waite, J. H., Extensible collagen in mussel byssus: A natural block copolymer. *Science* **1997,** *277* (5333), 1830-1832.

79. Lee, B. P.; Chao, C. Y.; Nunalee, F. N.; Motan, E.; Shull, K. R.; Messersmith, P. B., Rapid gel formation and adhesion in photocurable and biodegradable block copolymers with high DOPA content. *Macromolecules* **2006,** *39* (5), 1740-1748.

80. Yu, J.; Wei, W.; Menyo, M. S.; Masic, A.; Waite, J. H.; Israelachvili, J. N., Adhesion of Mussel Foot Protein-3 to TiO2 Surfaces: the Effect of pH. *Biomacromolecules* **2013,** *14* (4), 1072-1077.

81. Liu, Y. L.; Ai, K. L.; Liu, J. H.; Deng, M.; He, Y. Y.; Lu, L. H., Dopamine-Melanin Colloidal Nanospheres: An Efficient Near-Infrared Photothermal Therapeutic Agent for In Vivo Cancer Therapy. *Advanced Materials* **2013,** *25* (9), 1353-1359.

82. Wu, M.; Wang, T.; Muller, L.; Muller, F. A., Adjustable synthesis of polydopamine nanospheres and their nucleation and growth. *Colloids and Surfaces a-Physicochemical and Engineering Aspects* **2020,** *603*.

83. Fu, J. W.; Chen, Z. H.; Wang, M. H.; Liu, S. J.; Zhang, J. H.; Zhang, J. N.; Han, R. P.; Xu, Q., Adsorption of methylene blue by a high-efficiency adsorbent (polydopamine microspheres): Kinetics, isotherm, thermodynamics and mechanism analysis. *Chem Eng J* **2015,** *259*, 53-61.

84. Fu, J. W.; Xin, Q. Q.; Wu, X. C.; Chen, Z. H.; Yan, Y.; Liu, S. J.; Wang, M. H.; Xu, Q., Selective adsorption and separation of organic dyes from aqueous solution on polydopamine microspheres. *Journal of Colloid and Interface Science* **2016,** *461*, 292-304.

85. Tao, C. H.; Chen, T. D.; Liu, H.; Su, S. S., Preparation and adsorption performance research of large-volume hollow mesoporous polydopamine microcapsules. *Mrs Communications* **2019,** *9* (2), 744-749.

86. Lin, J. Y.; Wang, H. B.; Ren, E. H.; Song, Q. S.; Lan, J. W.; Chen, S.; Yan, B., Stomatocyte-like hollow polydopamine nanoparticles for rapid removal of water-soluble dyes from water. *Chemical Communications* **2019,** *55* (56), 8162-8165.

87. Dong, Z. H.; Wang, D.; Liu, X.; Pei, X. F.; Chen, L. W.; Jin, J., Bio-inspired surface-functionalization of graphene oxide for the adsorption of organic dyes and heavy metal ions with a superhigh capacity. *Journal of Materials Chemistry A* **2014,** *2* (14), 5034-5040.

88. Wang, Y.; Zhang, Y.; Hou, C.; Liu, M. Z., Mussel-inspired synthesis of magnetic polydopamine-chitosan nanoparticles as biosorbent for dyes and metals removal. *Journal of the Taiwan Institute of Chemical Engineers* **2016,** *61*, 292-298.

89. Wang, Z. X.; Guo, J.; Ma, J.; Shao, L., Highly regenerable alkali-resistant magnetic nanoparticles inspired by mussels for rapid selective dye removal offer high-efficiency environmental remediation. *Journal of Materials Chemistry A* **2015,** *3* (39), 19960-19968.

90. Zhao, S. M.; Zhan, Y. Q.; Wan, X. Y.; He, S. J.; Yang, X. L.; Hu, J. X.; Zhang, G. Y., Selective and efficient adsorption of anionic dyes by core/shell magnetic

MWCNTs nano-hybrid constructed through facial polydopamine tailored graft polymerization: Insight of adsorption mechanism, kinetic, isotherm and thermodynamic study. *J Mol Liq* **2020,** *319*.

91. Li, J.; Fan, Q. H.; Wu, Y. J.; Wang, X. X.; Chen, C. L.; Tang, Z. Y.; Wang, X. K., Magnetic polydopamine decorated with Mg-Al LDH nanoflakes as a novel bio-based adsorbent for simultaneous removal of potentially toxic metals and anionic dyes. *Journal of Materials Chemistry A* **2016,** *4* (5), 1737-1746.

92. He, K.; Zeng, G. M.; Chen, A. W.; Huang, Z. Z.; Peng, M.; Huang, T. T.; Chen, G. Q., Graphene hybridized polydopamine-kaolin composite as effective adsorbent for methylene blue removal. *Composites Part B-Engineering* **2019,** *161*, 141-149.

93. Lu, J. Y.; Fang, J. C.; Li, J. Q.; Wang, C. H.; He, Z. J.; Zhu, L. P.; Xu, Z. K.; Zeng, H. B., Polydopamine Nanotubes Decorated with Ag Nanoparticles as Catalyst for the Reduction of Methylene Blue. *Acs Applied Nano Materials* **2020,** *3* (1), 156-164.

94. Pan, X. H.; Cheng, S. Y.; Su, T.; Zuo, G. C.; Zhao, W.; Qi, X. L.; Wei, W.; Dong, W., Fenton-like catalyst Fe3O4@polydopamine-MnO2 for enhancing removal of methylene blue in wastewater. *Colloids and Surfaces B-Biointerfaces* **2019,** *181*, 226-233.

95. Lv, Y.; Yang, S. J.; Du, Y.; Yang, H. C.; Xu, Z. K., Co-deposition Kinetics of Polydopamine/Polyethyleneimine Coatings: Effects of Solution Composition and Substrate Surface. *Langmuir* **2018,** *34* (44), 13123-13131.

96. Sun, Y.; Davis, E. W., Multi-Stimuli-Responsive Janus Hollow Polydopamine Nanotubes. *Langmuir* **2022,** *38* (32), 9777-9789.

97. Barman, M.; Mahmood, S.; Augustine, R.; Hasan, A.; Thomas, S.; Ghosal, K., Natural halloysite nanotubes/chitosan based bio-nanocomposite for delivering norfloxacin, an anti-microbial agent in sustained release manner. *Int J Biol Macromol* **2020,** *162*, 1849-1861.

98. Dubey, R. S.; Rajesh, Y. B. R. D.; More, M. A., Synthesis and Characterization of SiO2 Nanoparticles via Sol-gel Method for Industrial Applications. *Mater Today-Proc* **2015,** *2* (4-5), 3575-3579.

99. Elkady, M.; Shokry, H.; El-Sharkawy, A.; El-Subruiti, G.; Hamad, H., New insights into the activity of green supported nanoscale zero-valent iron composites for enhanced acid blue-25 dye synergistic decolorization from aqueous medium. *J Mol Liq* **2019,** *294*.

100. Wang, Y. J.; Kai, Y.; Tong, L. F.; You, Y.; Huang, Y. M.; Liu, X. B., The frequency independent functionalized MoS2 nanosheet/poly(arylene ether nitrile) composites with improved dielectric and thermal properties via mussel inspired surface chemistry. *Appl Surf Sci* **2019,** *481*, 1239-1248.

101. Ali, R. M.; Elkatory, M. R.; Hamad, H. A., Highly active and stable magnetically recyclable CuFe2O4 as a heterogenous catalyst for efficient conversion of waste frying oil to biodiesel. *Fuel* **2020,** *268*.

102. Hamad, H. A.; Abd El-Latif, M. M.; Kashyout, A. B.; Sadik, W. A.; Feteha, M. Y., Study on synthesis of superparamagnetic spinel cobalt ferrite nanoparticles as layered double hydroxides by co-precipitation method. *Russ J Gen Chem+* **2014,** *84* (11), 2205-2210.

103. Cheng, Z. Q.; Wang, Z. W.; Wu, P. C.; Wang, Y. H.; Fu, J. W., Mass fabrication of oxygen and nitrogen co-doped 3D hierarchical porous carbon nanosheets by an explosion-assisted strategy for supercapacitor and dye adsorption application. *Appl Surf Sci* **2020,** *529*.

104. Lan, K.; Zhao, D. Y., Functional Ordered Mesoporous Materials: Present and Future. *Nano Lett* **2022,** *22* (8), 3177-3179.

105. Mekhamer, W. K., The colloidal stability of raw bentonite deformed mechanically by ultrasound. *J Saudi Chem Soc* **2010,** *14* (3), 301-306.

106. Chen, B.; Cao, Y. R.; Zhao, H. N.; Long, F. X.; Feng, X.; Li, J.; Pan, X. J., A novel Fe3+-stabilized magnetic polydopamine composite for enhanced selective adsorption and separation of Methylene blue from complex wastewater. *J Hazard Mater* **2020,** *392*.

107. Gupta, K.; Khatri, O. P., Fast and efficient adsorptive removal of organic dyes and active pharmaceutical ingredient by microporous carbon: Effect of molecular size and charge. *Chem Eng J* **2019,** *378*.

108. Qiu, H.; Lv, L.; Pan, B. C.; Zhang, Q. J.; Zhang, W. M.; Zhang, Q. X., Critical review in adsorption kinetic models. *Journal of Zhejiang University-Science A* **2009,** *10* (5), 716-724.

109. Inglezakis, V. J.; Balsamo, M.; Montagnaro, F., Liquid-Solid Mass Transfer in Adsorption Systems-An Overlooked Resistance? *Industrial & Engineering Chemistry Research* **2020,** *59* (50), 22007-22016.

110. Lagergren, S. K., About the theory of so-called adsorption of soluble substances. *Sven. Vetenskapsakad. Handingarl* **1898,** *24*, 1-39.

111. Ho, Y. S.; McKay, G., A comparison of chemisorption kinetic models applied to pollutant removal on various sorbents. *Process Saf Environ* **1998,** *76* (B4), 332-340.

112. Tan, K. L.; Hameed, B. H., Insight into the adsorption kinetics models for the removal of contaminants from aqueous solutions. *Journal of the Taiwan Institute of Chemical Engineers* **2017,** *74*, 25-48.

113. Zhang, J. F., Physical insights into kinetic models of adsorption. *Sep Purif Technol* **2019,** *229*.

114. Guo, X.; Wang, J. L., Comparison of linearization methods for modeling the Langmuir adsorption isotherm. *J Mol Liq* **2019,** *296*.

115. Feng, M. L.; Yu, S. C.; Wu, P. C.; Wang, Z. W.; Liu, S. H.; Fu, J. W., Rapid, high-efficient and selective removal of cationic dyes from wastewater using hollow polydopamine microcapsules: Isotherm, kinetics, thermodynamics and mechanism. *Appl Surf Sci* **2021,** *542*.

116. Weber, W. J.; Morris, J. C., Kinetics of Adsorption on Carbon from Solution. *Journal of the Sanitary Engineering Division* **1963,** *89*, 31-59.

117. Laing, I., The impact of effluent regulations on the dyeing industry. *Review of Progress in Coloration and Related Topics* **1991,** *21* (1), 56-71.

118. Ayawei, N.; Ebelegi, A. N.; Wankasi, D., Modelling and Interpretation of Adsorption Isotherms. *Journal of Chemistry* **2017,** *2017*.

119. Langmuir, I., The constitution and fundamental properties of solids and liquids Part I Solids. *J Am Chem Soc* **1916,** *38*, 2221-2295.

120. Freundlich, H., Über die Adsorption in Lösungen. *Zeitschrift für Physikalische Chemie 57U*, 385 - 470.

121. Temkin, M.; Pyzhev, V., Kinetics of ammonia synthesis on promoted iron catalysts. *Acta Physicochim Urs* **1940,** *12* (3), 327-356.

122. Dubinin M, M., The Equation of the Characteristic Curve of Activated Charcoal. *Dokl. Akad. Nauk. SSSR.* **1947,** *55*, 327-329.

123. Harkins, W. D.; Jura, G., Surfaces of solids XIII A vapor adsorption method for the determination of the area of a solid without the assumption of a molecular area, and the areas occupied by nitrogen and other molecules on the surface of a solid. *J Am Chem Soc* **1944,** *66*, 1366-1373.

124. Wang, J. L.; Guo, X., Adsorption isotherm models: Classification, physical meaning, application and solving method. *Chemosphere* **2020,** *258*.

125. Weber, T. W.; Chakravorti, R. K., Pore and Solid Diffusion Models for Fixed-Bed Adsorbers. *Aiche J* **1974,** *20* (2), 228-238.

126. Al-Ghouti, M. A.; Da'ana, D. A., Guidelines for the use and interpretation of adsorption isotherm models: A review. *J Hazard Mater* **2020,** *393*.

127. Wang, J.; Guo, X., Adsorption isotherm models: Classification, physical meaning, application and solving method. *Chemosphere* **2020,** *258*, 127279.

128. Akcay, M.; Ozcan, M., Application of the Freundlich and Polanyi Adsorption Potential Theories to the Adsorption of Alkylpyridines from Water Solution onto Activated Carbon. *Turkish Viiith National Symposium on Chemistry and Chemical Engineering, Vol 1* **1992,** *518*, 17-19.

129. Chabani, M.; Amrane, A.; Bensmaili, A., Kinetic modelling of the adsorption of nitrates by ion exchange resin. *Chem Eng J* **2006,** *125* (2), 111-117.

130. Zhou, Z. W.; Liu, R., Fe3O4@polydopamine and derived Fe3O4@carbon core-shell nanoparticles: Comparison in adsorption for cationic and anionic dyes. *Colloid Surface A* **2017,** *522*, 260-265.

131. Wang, C.; Yin, J.; Wang, R.; Jiao, T.; Huang, H.; Zhou, J.; Zhang, L.; Peng, Q., Facile Preparation of Self-Assembled Polydopamine-Modified Electrospun Fibers for Highly Effective Removal of Organic Dyes. *Nanomaterials (Basel)* **2019,** *9* (1).

132. Li, Q. Q.; Lv, C.; Xia, X. W.; Peng, C.; Yang, Y.; Guo, F.; Zhang, J. F., Separation/degradation behavior and mechanism for cationic/anionic dyes by Ag-functionalized Fe3O4-PDA core-shell adsorbents. *Front Env Sci Eng* **2022,** *16* (11).

133. Tran, H. N.; You, S. J.; Chao, H. P., Thermodynamic parameters of cadmium adsorption onto orange peel calculated from various methods: A comparison study. *Journal of Environmental Chemical Engineering* **2016,** *4* (3), 2671-2682.

134. Zhao, F.; Repo, E.; Yin, D.; Meng, Y.; Jafari, S.; Sillanpaa, M., EDTA-Cross-Linked beta-Cyclodextrin: An Environmentally Friendly Bifunctional Adsorbent for Simultaneous Adsorption of Metals and Cationic Dyes. *Environ Sci Technol* **2015,** *49* (17), 10570-80.

135. Attallah, O. A.; Al-Ghobashy, M. A.; Nebsen, M.; Salem, M. Y., Removal of cationic and anionic dyes from aqueous solution with magnetite/pectin and magnetite/silica/pectin hybrid nanocomposites: kinetic, isotherm and mechanism analysis. *Rsc Advances* **2016,** *6* (14), 11461-11480.